THE ROLE OF EXTRACELLULAR PROTEASES IN STROMAL-EPITHELIAL INTERACTIONS IN GASTRIC CANCER

Thesis submitted in accordance with the requirements of the University of Liverpool for the degree of Doctor in Philosophy by Sandhir Kandola

April 2014

ABSTRACT

Cancers of the upper gastrointestinal tract present at an advanced stage and carry a poor prognosis. Oesophageal and gastric tumours have a rich stroma composed of vascular cells, immune cells, and myofibroblasts, which promotes tumour growth, invasion and metastasis. In addition, mesenchymal stromal cells (MSCs) are recruited from the bone marrow to the tumour stroma; the mechanisms underpinning this have not yet been defined. Extracellular proteases play a role in cell migration, invasion, and cell signalling and are known to influence cancer growth in conflicting ways. Myofibroblasts present in normal tissue differ from those found in cancer. Cancer-associated myofibroblasts (CAMs) are known to modulate extracellular protease activity by secreting plasminogen activator inhibitor-1 (PAI-1), an inhibitor of the serine protease urokinase plasminogen activator, and matrix metalloproteinases (MMPs). This investigation studies the role of PAI-1 in gastric cancer and assesses the contribution of myofibroblast-derived MMPs to tumour growth. Finally, the role of chemerin in recruiting MSCs has been investigated.

The expression of PAI-1 in myofibroblasts was found to be higher than in gastric cancer cells. Overexpression of PAI-1 in gastric cancer cells resulted in decreased cell adhesion and decreased tumour growth in an *in vivo* subcutaneous xenograft model of gastric tumour growth.

The addition of gastric CAMs potentiated the growth of gastric cancer subcutaneous xenografts. This was not accounted for by differences in cell proliferation rate, apoptosis or final stromal content. Xenografts containing CAMs suppress the growth of a contralateral xenograft without CAMs, demonstrating that a long-range signal can be generated as a result of stromal-epithelial interactions.

MMP and cathepsin activity was compared between xenografts containing myofibroblasts to those without. MMP activity is increased in xenografts injected with CAMs, compared to those injected with myofibroblasts taken from normal stomach or those with gastric cancer cells alone. In an organotypic co-culture system, MMP inhibition resulted in a decrease in gastric cancer cell invasion.

The injection of fluorescently labelled MSCs injected resulted in homing of these cells to subcutaneous oesophageal tumours containing CAMs. Antagonism at the ChemR23 receptor inhibited this MSC homing to oesophageal xenografts containing CAMs.

This work emphasises the importance of assessing the contribution of specific proteases and their inhibitors in gastric cancer. The stroma is an important contributor to extracellular protease activity and myofibroblasts contribute both proteases and their inhibitors to the tumour microenvironment, resulting in the modulation of tumour growth and cell adhesion. MSCs are recruited to oesophageal tumours via a novel signalling pathway.

ACKNOWLEDGMENTS

Firstly I would like to thank the Wellcome Trust for providing the funding for this research. Their PhD programme here in Liverpool allowed me a broad choice of projects, enabling me to choose an area relevant to my future career and interesting to me. The University of Liverpool have provided me with academic support and I am grateful to them for facilities and infrastructure, without which I could not have completed this research.

Secondly I would like to thank my supervisors Profs. Andrea Varro and Graham Dockray for their invaluable guidance, support and advice during my time in the lab and writing this thesis. I truly believe we made a well-rounded team capable of facing both the excitements and the disappointments which inevitably characterise scientific research and I am grateful for their attentiveness and co-operation. I am grateful to our collaborator Dr. Nikolina Vlatković whose expertise and equipment were crucial to the project. The team at the Biological Services Unit were excellent and I am thankful for their assistance with many experiments. My many colleagues in the lab provided me with training, advice and company during an extremely enjoyable three years, and I am thankful for their support and friendship.

Finally I would like to thank Ajmir Kandola for designing a useful set of symbols and pictures for me to use in schematics. And last of all, I am grateful to Euan Green for his unwavering support during my foray into an unfamiliar field.

Table of Contents

CHAPTER 1: INTRODUCTION

1.1 Homeostasis and microenvironments

In 1865, Claude Bernard introduced the concept that the body maintains its internal environment in a stable state (1). This was later defined as homeostasis, the ability to maintain internal constancy under a variety of external conditions, for example the maintenance of a steady internal temperature in spite of external variations. Signals between neighbouring cells ('paracrine' signals) or between organs ('endocrine' signals) form a network of communication which enables cells of differing types and organs with differing functions to co-operate in maintaining homeostasis. Characterisation of the nature of the signals maintaining homeostasis began with the identification of the first hormone, secretin, which increases pancreatic secretion in response to increased acid in the duodenum in 1902 (2). Since then, many paracrine and endocrine signalling molecules, their corresponding receptors and intracellular signalling pathways have been identified, and their role in controlling cell growth determined.

In epithelia, the balance of cell proliferation and cell death, particularly in response to damage, involves interactions with underlying mesenchymal cells. This process is subverted in many common cancers (breast, prostate, colon, stomach) characterised by uncontrolled cell proliferation, invasion and metastasis and disruption to the homeostatic mechanisms controlling these processes. Solid tumours are composed

of the parenchyma (the neoplastic cells) and the stroma, the supportive network of connective tissue and cells surrounding epithelial cells. These cells are capable of preventing cancer initiation by suppressing uncontrolled cell growth. Once a tumour develops, the stroma can function to support tumour growth, invasion and metastasis. This thesis focuses on studies of the effect of stromal myofibroblasts on tumour growth in gastric cancer, and the contribution of extracellular proteases to stromal-epithelial signalling.

1.2 The cancer microevironment

In 1889, Paget noticed that breast cancer preferentially metastasised to specific sites independent of the anatomy, vascular supply and lymphatic drainage. He hypothesised that some tissues provided a favourable microenvironment for metastatic growth, an appropriate 'soil' for where the cancer 'seeds' establish and grow (3). This first evidence of how a microenvironment supports cell growth has since been extended to include events at the primary site (4), where cancer cells alter the behaviour of local stromal cells and *vice versa,* as well as recruiting other cell types.

In normal tissue there is a tight balance between cell proliferation and cell death, mediated by intercellular communication. Proteins such as integrins, E-cadherin and laminin facilitate cell-cell and cell-extracellular matrix (ECM) interactions in epithelia, creating a stable tissue structure and preventing neoplastic transformation (5).

Berenblum noted in 1949 that the skin suppresses damage caused by topical carcinogens, resulting in fewer tumours than expected after application of two carcinogenic agents (6). The addition of multipotent malignant teratocarcinoma cells to a mouse blastocyst results in the development of normal mosaic mice, showing that the embryonic microenvironment is capable of reprogramming the malignant cells to a non-malignant state (7).

In cancer, the microenvironment is altered by signals from tumour cells, changing the behaviour of surrounding cells and recruiting further cell types. The number and variety of cells present is similar to the temporary stromal reaction observed in response to inflammation, and such a comparison has labelled cancer as a 'wound that does not heal' (8). Indeed, when colon cancer cells are transplanted into wound granulation tissue, they show evidence of invasion (9). The cancer microenvironment is formed by the stroma, the cancer cells and the network of signalling molecules between these.

1.2.1 Components of the cancer stroma

In their updated review on the hallmarks of cancer, Hanahan and Weinberg emphasised the contribution of stromal cell types to the tumour microenvironment and the importance of studying stromal cell types as well as the neoplastic cells themselves (10). It is clear that during the process of tumorigenesis, signals from stromal cells aid the tumour to secure a blood supply for the tumour and acquire the ability to invade and metastasise (11). Tumours from different tissues of origin vary

in the amount and type of stroma they contain, for instance pancreatic tumours have a higher stromal content than other tumours and breast cancer stroma is particularly rich in fibroblasts. The stroma is composed of immune cells, vascular cells, the ECM, cancer-associated fibroblasts (CAFs) and mesenchymal stromal cells (MSCs) (Figure 1.1). CAFs and MSCs will be discussed in detail in the next sections.

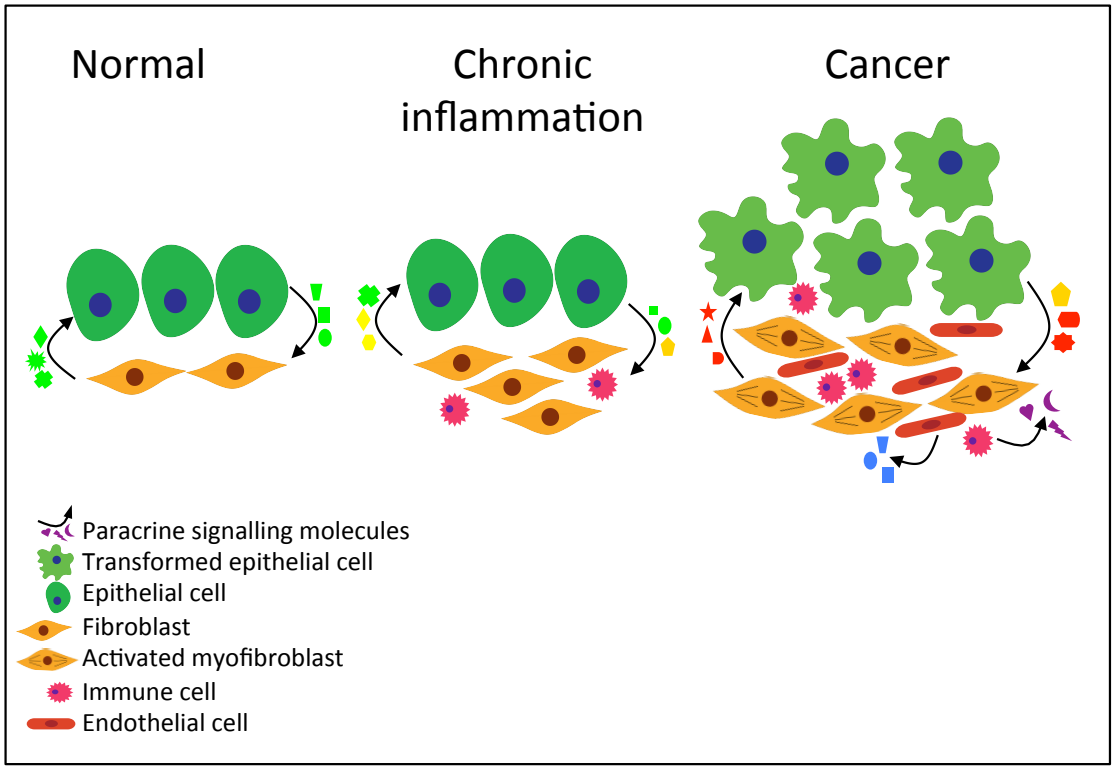

Figure 1.1 Components of the cellular microenvironment. In normal epithelial tissues, the cross-talk between tissue fibroblasts and epithelial cells contributes to the maintenance of normal tissue architecture. In chronic inflammation, fibroblasts increase and an immune reaction develops, changing the nature of the cell-cell communication. Finally in cancer, myofibroblasts with an 'activated' phenotype are present, as well as immune cells and endothelial cells. Stromal-epithelial signalling still takes place and the result of these signals is the promotion of cancer growth. In the normal gut, small numbers of subepithelial myofibroblasts are found and in tumours of the gastro-intestinal tract their numbers increase.

1.2.1.1 Immune cells

Cells from the immune system, many of which originate in the bone marrow, are recruited to tumours and secrete many signalling molecules, contributing to the paracrine signals in the tumour microenvironment. These cells were initially thought to attempt to suppress cancer growth, but it is now known that neutrophils, mast cells, B and T lymphocytes and macrophages all stimulate cell proliferation, invasion and metastasis (12,13). The pattern of immune cell infiltration resembles that of a wound or area of inflammation.

1.2.1.2 Vascular cells

A growing tumour requires a blood supply, as the capacity of interstitial fluid for oxygen diffusion is limited (14). The formation of blood vessels is a dynamic process adapting to changes in tissue oxygen demand. Endothelial cells form the walls of blood vessels and pericytes secrete vascular basement membrane; both cell types play an important role in angiogenesis. Lymphatic cells are also recruited and form a drainage system connecting to the local lymphatic supply, facilitating lymph node metastasis (15). A variety of cancer cell and stromal signals stimulate angiogenesis.

1.2.1.3 ECM

The ECM is composed of fibrillar proteins, glycoproteins and proteoglycans (16). A large component is collagen. It provides structural support and adhesion for cells as

well as acting as a reservoir of biologically active molecules. Different tissues have differing ECMs, providing contextual information to cells, aiding their ability to respond to extracellular signals (17). The ECM is a dynamic structure, undergoing constant synthesis and degradation appropriate to the tissue's circumstances.

Tumour-associated ECM differs from that of the pre-existing stroma in normal tissue (18). In cancer, vascular cells and fibroblasts synthesis ECM proteins (19). ECM remodelling takes place at the invasive front of a tumour, where protease activity and the abundance of ECM proteins are increased (20).

1.3 Myofibroblasts

1.3.1 Distribution and definition

Myofibroblasts are an important stromal cell type usually found rarely in normal tissues (except the gut) but commonly in many tumours. Gabbiani *et al* first identified myofibroblasts in tissues undergoing wound healing (21). These cells resembled fibroblasts but possessed contractile elements, making them able to play a role in scar contraction. These smooth muscle-like cells were then identified on the basis of alpha-smooth muscle actin (α-SMA) expression within the stroma of breast cancers (22). Since then, myofibroblasts have been identified in many solid tumours and their presence in large numbers, a 'desmoplastic stroma', confers a poor prognosis (23,24). Although in most normal tissues very few myofibroblasts are present, the normal gut contains a well-defined population of subepithelial

myofibroblasts (25). Gastric tumours are known to contain myofibroblasts (26), and high myofibroblast content is associated with a poor prognosis (27).

There is no specific immunohistochemical marker for myofibroblasts, although many have been proposed. α-SMA, although not exclusively expressed by myofibroblasts, remains an important marker (28). Other markers include tenascin-C (29), NG2 chondroitin suphate proteoglycan (30), podoplanin (31) and fibroblast-activated protein (32), as well as markers of mesenchymal cells such as vimentin (33). Myofibroblasts need also be negative for markers defining other cell types, such as epithelial cells (pancytokeratin). In 2008 DeWever *et al* proposed that a myofibroblast be defined on the basis of α-SMA expression in combination with at least three other markers (34). The present work identifies gastric myofibroblasts on the basis of α-SMA and vimentin positivity, in combination with desmin and cytokeratin negativity. Where these criteria have not been rigorously fulfilled the term cancer-associated fibroblast (CAF) will be used instead.

1.3.2 Origin of myofibroblasts

Myofibroblasts in wound healing are thought to arise from differentiation of fibroblasts found in normal tissue (35). In renal fibrosis (such as occurs in chronic hypertension) myofibroblasts originate both from transdifferentiation of tissue fibroblasts and to a lesser extent from bone marrow-derived cells (36). In cancer, however, the origin of myofibroblasts remains unclear. Some evidence suggests myofibroblasts arise from the transdifferentiation of fibroblasts (37), as well as from MSCs. Others have suggested that epithelial-mesenchymal transition (EMT) occurs,

making the cancer cells the source of myofibroblasts (38). In the pancreas, adipocytes, stellate cells and pericytes have all been proposed as precursors of myofibroblasts (39). In gastric cancer, evidence is accumulating that MSCs from the bone marrow are recruited to tumours and contribute to the myofibroblast population (40,41). However, recent findings suggest that *H. pylori* infection can cause the differentiation of fibroblasts into myofibroblasts (42). Many of the findings support the notion that myofibroblasts arise from a variety of sources, and that the myofibroblasts in a tumour comprise a heterogeneous population of myofibroblast subtypes.

1.3.3 Role of myofibroblasts in promoting cancer growth

In vitro studies have demonstrated that in gastric cancer CAFs promote and support tumour growth. Myofibroblasts from gastric cancers exhibit higher rates of proliferation and migration than myofibroblasts taken from normal stomach (43). Conditioned media (CM) from gastric CAFs or myofibroblasts increases the migration and invasion of gastric cancer cells (43, 44), in comparison to CM from fibroblasts/myofibroblasts taken from normal stomach (45). CM from CAFs harvested from the cancer-normal mucosa interface increased the proliferation of cancer cells (46).

In vivo xenograft co-injection studies using CAFs or myofibroblasts in combination with cancer cells have demonstrated the role of these cells in promoting tumour growth. Olumi *et al* showed in prostate cancer that CAFs potentiated the growth of both prostate cancer cells and when mixed with non-tumorigenic prostatic epithelial

cells, they caused their transformation and created *in vivo* tumours (47). Orimo *et al* showed that in breast cancer, the growth of cancer cells was enhanced by the addition of CAFs but not by fibroblasts harvested from normal breast tissue (48). Similar findings were obtained in studies in gastric cancer (43).

CAFs/myofibroblasts promote tumour growth by exerting an effect on a wide range of processes involved in the generation, maintenance, invasion and metastasis of many tumours. Studies in a mouse model of gastric cancer and in oesophageal cancer have shown that myofibroblasts stimulate angiogenesis (49,50). These cells are capable of transforming epithelial cells, stimulating them to produce xenografts *in vivo* where previously they did not (47). They stimulate the proliferation of cancer cells, as demonstrated in squamous cells from oral cancer (51), and they can be instrumental in instigating metastasis in colon cancer (52). They are involved in the suppression of the host-mediated immune response to a tumour (32). CAFs also promote tumour growth by remodelling the ECM into a more permissive environment for tumour growth (53).

1.3.4 Genetics of myofibroblasts

Although early studies indicated that the stromal cells within tumours harboured genetic mutations (54), these were based on paraffin-embedded tissue or did not isolate CAFs from other stromal components. Since then, one study failed to detect any substantial genetic alterations in CAFs (55) and another investigated pancreatic CAFs and found them to have normal allelotypes (56). In breast cancer, CAFs were shown to only rarely exhibit mutations in the p53 gene (57).

Evidence from gene expression studies shows that in gastric cancer the tumour stroma exhibits a distinctive expression profile compared with the stroma of non-malignant gastric mucosa (58). The differences in gene expression are unlikely to arise from somatic genetic mutations, but may occur as a result of epigenetic phenomena, such as changes in DNA methylation in the promoter region of a gene. Myofibroblasts from gastric cancer patients exhibit global hypomethylation, similar to the finding of hypomethylation in the epithelial cells of many carcinomas (59). In pancreatic CAFs, however, few genes are reactivated after treatment with a DNA methylation inhibitor, suggesting that there are few alterations in DNA methylation in these cells (60).

1.4 Mesenchymal Stromal Cells (MSCs)

Although many of the bone marrow-derived cells found in tumours belong to the immune system, recent evidence shows that another type of mesenchymal cell populates tumours. Xenograft experiments using a variety of cancer cells have shown that some CAFs in the tumours are derived from MSCs, and that the presence of these cells stimulates xenograft growth (61). In gastric cancer, the CAFs resemble the myofibroblasts found in normal gastric mucosa in the markers they express, but their biological behaviour is different. An experiment examining the fate of bone marrow-derived cells in patients with gastric cancer who previously received a gender-mismatched bone marrow transplant showed that bone marrow-derived

cells contribute to the stroma in gastric cancer (62). In a mouse model of inflammation-induced gastric cancer, it was thought that 20% of gastric CAFs were derived from the mesenchymal stromal cells in the bone marrow (41).

A population of spindle shaped clonogenic cells was first isolated from the bone marrow by Friedenstein in 1971 (63). Owing to their capacity for self-renewal and multipotency these cells were termed mesenchymal stem cells (64). It is now known that these cells actually comprise a mixed population, only a small proportion of which is self-renewing and multipotent, and the nomenclature was adjusted to mesenchymal stromal cells (MSCs) (65). These cells have mainly been isolated from the adult bone marrow (distinguishing them from embryonic stem cells), but they are also released into the circulation and recruited to tissues undergoing repair or renewal (66). Their physiological role in the bone marrow appears to be in the maintenance of the haematopoietic stem cell niche, responsible for generating the precursors of the cells which circulate in the blood (67).

There is no single defining characteristic or marker of an MSC. In 2006, a consensus was reached regarding the features which define a multipotent MSC. The cells must be plastic-adherent in culture. Expression of the surface markers CD105, CD73 and CD90 and absence of CD45, CD34, CD14, CD11b, CD79α, CD19 and HLA-DR are necessary. Finally, the cells must show capacity to differentiate into osteoblasts, adipocytes and chondroblasts *in vitro* (68). These criteria are however difficult to fulfil owing to variations in MSCs from different tissues of origin and from different species. More recent attempts at defining MSCs have included features from the

transcriptome, secretome and proteome (69). The term mesenchymal stem cell is now considered to only apply to those cells with a capacity for self-renewal and differentiation characteristics compatible with a multipotent state.

1.5 Stromal-epithelial signals

In cancer, the characterisation of intracellular signalling cascades within the cancer cells has increased dramatically, increasing the development of therapies targeting these processes. The paracrine heterotypic interactions occurring between stromal cells and epithelial cells remain poorly defined, leaving a gap in the understanding of extracellular processes, a potential source of therapeutic targets. Some examples of stromal-epithelial signals and their effects have been characterised, as illustrated in figure 1.2.

1.5.1 Chemerin

Chemerin is a protein first identified as upregulated in psoriatic skin (70). It is expressed in placenta, liver and adipose tissue. It is released as pro-chemerin into the circulation and is activated locally by proteolysis (71). Its binding to a G-protein coupled receptor known as ChemR23 is known to cause an increase in intracellular calcium (72) and cause ERK1/2 phosphorylation (73). This receptor is homologous to other chemoattractant receptors, raising suspicion that chemerin might act as a chemoattractant. Chemerin-mediated chemotaxis has been identified in leucocytes expressing ChemR23 (74).

Chemerin was thought to play a role in inflammation (75) and increased circulating chemerin is also found in obesity (76). Chemerin is overexpressed in oral squamous cell carcinomas (77). In melanoma, however, chemerin acts as a chemoattractant to natural killer (NK) cells, resulting in tumour suppression (78). The role of this poorly characterised molecule in long range stromal signalling will be discussed further in Chapter 6.

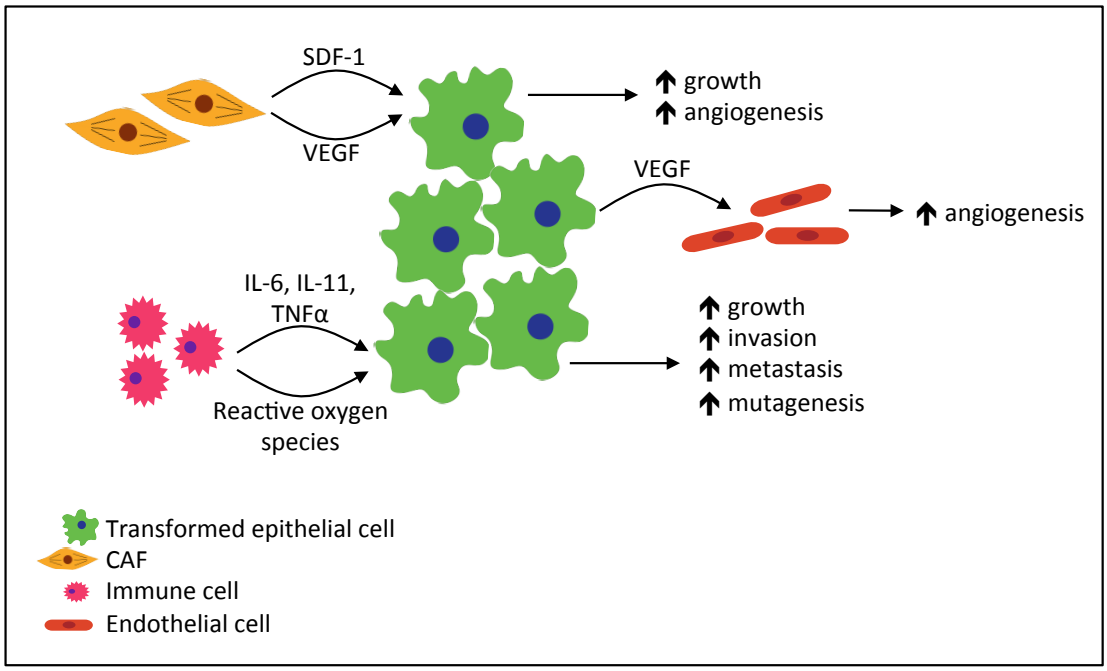

Figure 1.2 Stromal-epithelial signals and their effects. CAFs secrete stroma cell-derived factor-1 (SDF-1), which acts on tumour cells to increase growth (48). CAFs also secrete vascular endothelial growth factor (VEGF), which acts on endothelial cells and cancer cells, increasing angiogenesis (79). Cells from the immune system secrete a variety of chemokines, cytokines and growth factors, including IL-6, IL-11 and TNFα. These promote tumour growth in a variety of ways. The release of reactive oxygen species from these cells increases the likelihood of mutations in the cancer cells, accelerating the tumour's adaptation to the changing microenvironment (80).

1.7 Extracellular proteases

Extracellular proteases are enzymes released into the extracellular milieu capable of degrading other proteins. They have the effect of remodelling the ECM, the degradation of which is necessary in aiding tumour cells to migrate, invade and metastasise. Proteolysis also releases and activates growth factors, chemokines and cytokines, making extracellular proteases key players in the tumour microenvironment.

There are 570 proteases known in humans, involved in diverse processes (81). There are six families of proteases: metallo-, serine, aspartate, threonine, cysteine and glutamic, named according to the component of their active site. The three extracellular systems relevant to this investigation are the urokinase plasminogen activator (uPA) system (a family of serine proteases), the matrix metalloproteinases (MMPs), and cathepsins (a family of cysteine proteases).

1.7.1 uPA system

The uPA system is an important extracellular proteolytic system. uPA is activated on binding to the uPA receptor (uPAR), a cell membrane-anchored protein, which means that proteolytic activity is localised to the cell membrane (82). Upon activation uPA cleaves plasminogen to produce plasmin, a powerful protease with an

important role in fibrinolysis. In tumours, however, the ability of plasmin to cleave proteins in the ECM releases cytokines and growth factors and is a driver of tumour growth. Plasminogen activator-inhibitor-1 (PAI-1) functions as the main inhibitor of uPA by binding to the uPA-uPAR complex, resulting in its internalisation by the cell in a low-density lipoprotein (LDL) dependent manner (83) (Figure 1.3).

PAI-1 is a 52kDa glycoprotein first characterized in bovine endothelial cells (84). It forms part of the uPA system by acting as the main physiological inhibitor of uPA. It circulates in plasma, is stored in platelets and is expressed in a variety of cell types including endothelial cells, fibroblasts and hepatocytes (85). PAI-1 can exist in an active (inhibiting proteolysis) state or a latent state (86). Circulating PAI-1 is bound to vitronectin. The mouse and human proteins share 82% amino acid homology (87) (88). Genetically modified mice lacking the PAI-1 gene develop to term and exhibit a mild hyperfibrinolytic state (89). They also demonstrate increased haemorrhagic gastric lesions in response to ethanol or indomethacin (90). In humans, PAI-1 may make a more significant contribution to the prevention of clot degradation as humans lacking PAI-1 exhibit episodes of haemorrhage (91).

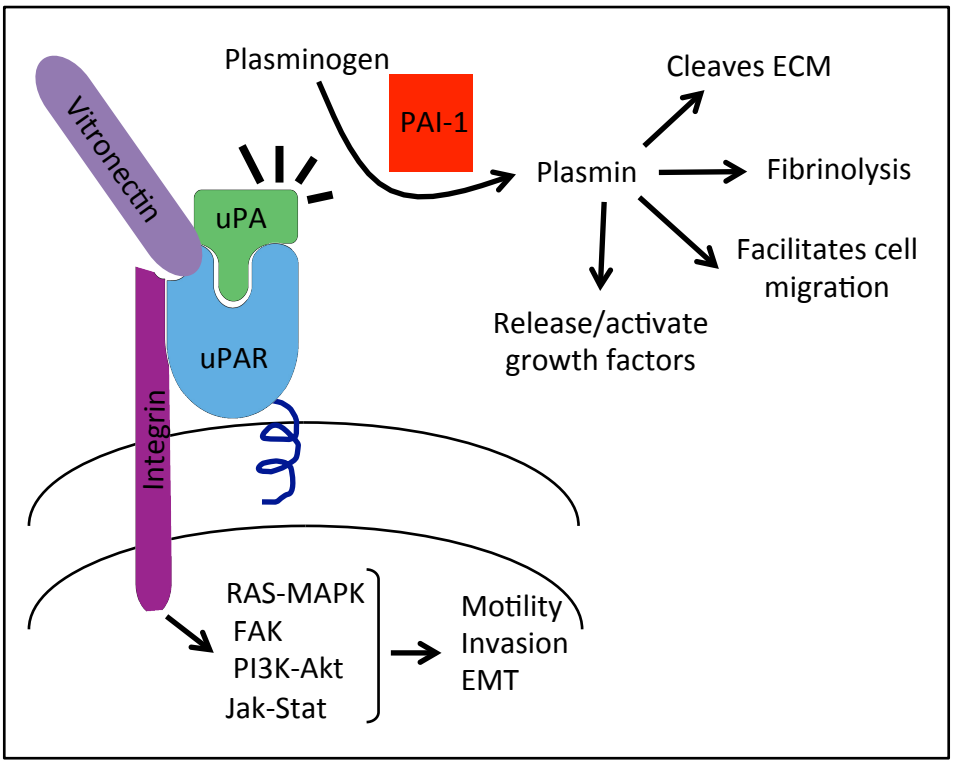

Figure 1.3 Interactions between uPA, uPAR and PAI-1. uPA binds to the cell membrane-anchored uPAR, catalysing the conversion of plasminogen to plasmin. PAI-1 inhibits this process, preventing plasmin activation and the consequent proteolytic processes which contribute to tumour growth and invasion. uPAR can orchestrate intracellular signalling through its interaction with cell membrane-spanning integrins, causing an increase in cell motility, invasiveness and epithelial-to-mesenchymal transition (EMT). uPAR also interacts with vitronectin, providing anchorage to the ECM.

In addition to binding to uPA-uPAR complexes, when unbound PAI-1 has a high affinity for vitronectin, an ECM protein (92). Vitronectin mediates intracellular signalling by interacting with cell membrane-spanning integrins. PAI-1 competes with integrins for binding to vitronectin and this is independent of its ability to inhibit uPA (93). uPAR also interacts with vitronectin, enhancing cell adhesion by creating a connection between a membrane-anchored protein and the ECM. PAI-1 is able to compete with uPAR for vitronectin binding (94) (Figure 1.4).

Although an extracellular molecule, secreted PAI-1 is capable of exerting an influence on intracellular signalling, causing changes in cell adhesion and proliferation. This effect seems to be unrelated to its role in the inhibition of proteolysis. In fibroblasts PAI-1 inhibited insulin-induced protein kinase B phosphorylation (an intracellular process) by preventing the integrin-vitronectin interaction necessary for this. This resulted in decreased cell migration (95). PAI-1 activated the intracellular JAK/STAT pathway in a variety of cells and this resulted in increased cell migration. This effect was dependent on the presence of a functional LDL receptor-related protein (LRP) (96) (Figure 1.4).

Intracellular PAI-1 also affects cell behaviour. In pulmonary fibroblasts, intracellular PAI-1 knockdown results in an increase in caspase-3 mRNA, showing that PAI-1 has a role in the inhibition of apoptosis (97).

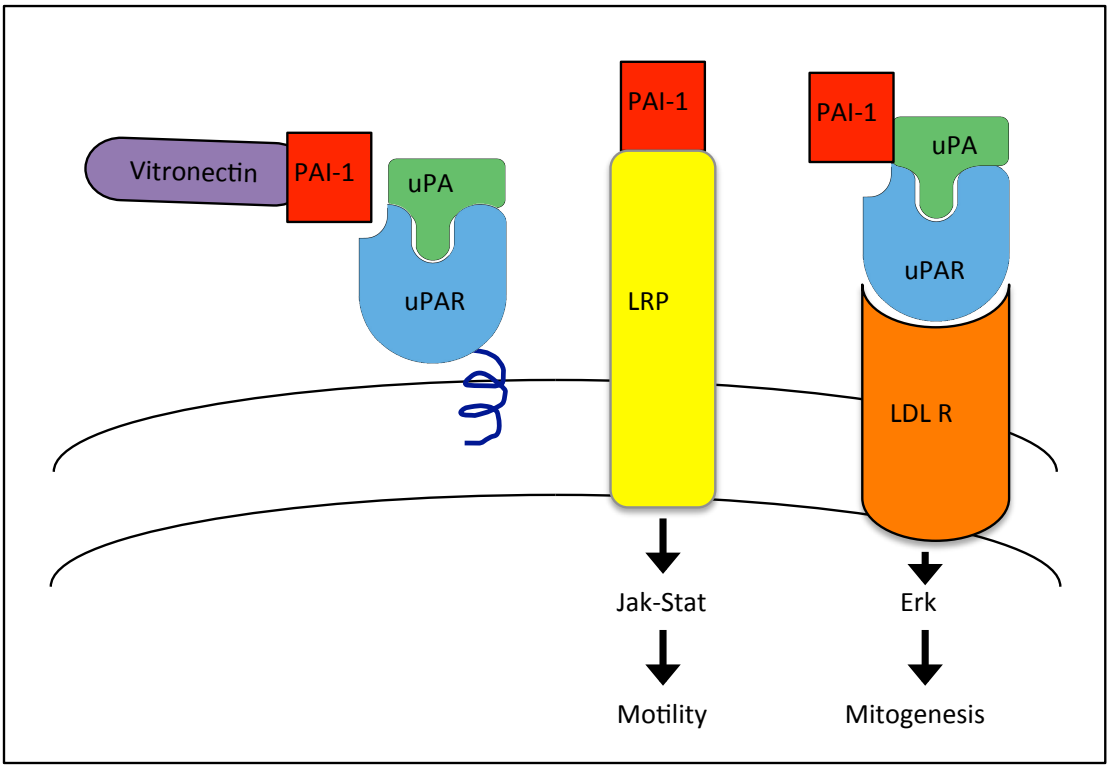

Figure 1.4 Protease-independent actions of PAI-1. PAI-1 interacts with vitronectin, preventing uPAR from binding and causing loss of anchorage to the ECM. PAI-1 increases cell motility by stimulating intracellular signalling in an LDL-dependent manner. Binding of PAI-1 to the uPA-uPAR complex stimulates mitogenesis through an interaction with the LDL receptor.

Based on its role in protease inhibition, it might be predicted that PAI-1 offers a protective role in cancer, by preventing the degradation of the ECM necessary for local tumour invasion and release of tumour cells into the circulation. Indeed, there are *in vitro* data to suggest that this is the case. PAI-1 prevents uPA-dependent invasion of lung cancer cells into an amnion cell membrane (98). PAI-1 promoted cell adhesion of human myogenic cells in a dose-dependent manner (99). *In vivo* this may also be the case, as a study using PAI-1 overexpressing fibrosarcoma cells showed reduced metastasis formation from tumours overexpressing PAI-1 (100).

However, many studies have described evidence that conflicts with these findings, suggesting that PAI-1 may also promote tumour growth, invasion and metastasis. For example, when PAI-1 is added to tumour cell cultures, it inhibits apoptosis, showing that it contributes to cell survival in cancer (101). Evidence from clinical samples of gastric cancer reveals that high PAI-1 expression is associated with a poor prognosis (102, 103, 104). In an *in vivo* model of gastric cancer, knockdown of PAI-1 decreased peritoneal metastases, showing that PAI-1 plays an important role in tumour dissemination (105).

1.7.2 MMPs

MMPs are a family of 24 zinc binding endopeptidases either secreted as soluble enzymes or bound to the cell membrane, first discovered by Gross and Lapiere (106). Their shared structure consists of a prodomain, a catalytic domain and, usually, a

haemopexin-like domain (not present in MMP-7), connected to the catalytic domain by a hinge region (Figure 1.5). Intracellularly, the protein has a preprodomain which directs it to the endoplasmic reticulum for processing. The prodomain contains a Cys residue which interacts with the zinc-binding domain, maintaining the inactive state. Cleavage of the prodomain separates the Cys residue from the active domain, activating the enzyme. The catalytic domain contains the active site. The haemopexin-like domain mediates interaction with tissue inhibitors of metalloproteinases (TIMPs), binds cell surface molecules and interacts with substrate molecules. MMPs have a role in diverse processes including embryogenesis (107), wound healing (108) and angiogenesis (109). MMP inhibition occurs through TIMPs (110) and in plasma, MMPs are inhibited by α2-macroglobulin (111).

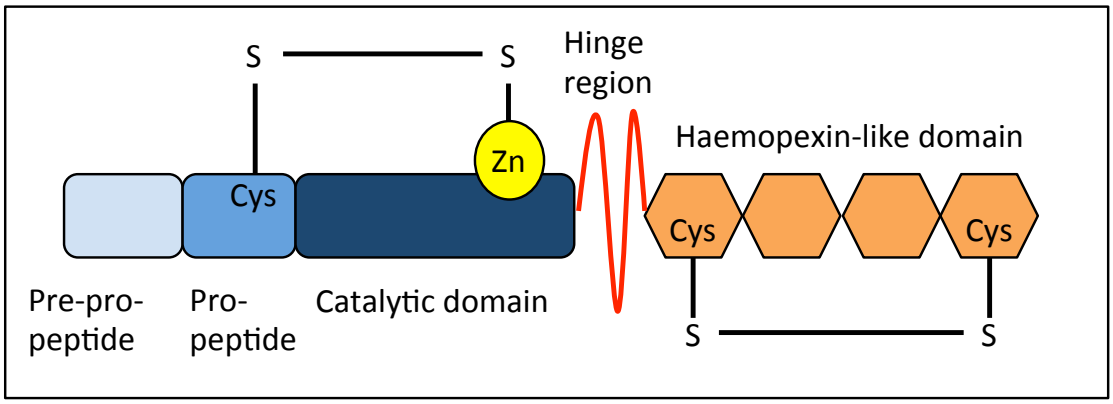

Figure 1.5 Structure of MMPs. MMPs share a common structure, with minor modifications to this according to which class of MMP they are from. MMPs all have a pre-pro-peptide which targets the protein to the endoplasmic reticulum for post-translational processing. After being secreted, cleavage of the prodomain results in activation of the MMP as the Cys residue is separated from the active domain. The catalytic domain's active site contains a zinc ion. A hinge region connects the catalytic domain to a haemopexin-like domain, which is responsible for binding to substrate molecules, TIMPs and cell-surface receptors.

Tumours often express a variety of MMPs which may activate each other and together create a cascade of proteolytic activity (Figure 1.6) or may individually play roles in specific process. The earliest evidence suggested that MMPs, through their ability to degrade ECM, aided tumour invasion and cell migration. Liotta *et al* first showed that the metastatic potential of cancer cells was proportional to their ability to degrade the basement membrane (112). Evidence from mouse models of breast cancer confirmed that overexpression of MMPs caused tumours to develop and invade (113,114,115). In gastric cancer, MMP-7 was shown to play a role in the migration of cancer cells *in vitro* (116) and *in vivo*, MMP-7 deficient mice developed fewer colonic tumours than their MMP-7-expressing counterparts (117).

This prompted the rapid development of small molecule MMP inhibitors, which although promising in *in vitro* assays, were not successful in clinical trials. This failure was due to a variety of reasons. Some trials were discontinued due to severe musculoskeletal side effects. Others noticed that patients in the treatment group experienced poorer survival or an increase in metastases compared with those in the placebo group (118). In gastric cancer, however, the results showed some promise as the use of a MMP inhibitor increased the survival of patients with inoperable disease (119).

Further research into MMPs demonstrated that these proteins exert wider effects than was previously thought, and that these may not necessarily involve proteolysis. MMP-9 is capable of providing growth signals through its interaction with E-Cadherin and the epidermal growth factor receptor, leading to ovarian cancer metastasis

(120). MMP-7 is capable of disrupting apoptosis by cleaving the Fas ligand on the surface of cells, diminishing the effect of doxorubicin chemotherapy (121). Furthermore, it has now been shown that MMP-9 can stimulate cell migration in a proteolysis-independent manner (122). MMP-12 exerts antimicrobial effects, again through a mechanism which is independent of proteolysis (123). This shows that the role MMPs extends beyond ECM degradation and that some effects are not due to proteolysis.

1.7.2.1 MMPs in stroma

The majority of MMPs are not usually secreted in healthy tissue, with the exception of MMP-7, which is expressed constitutively in most epithelia (124). MMP expression typically increases in response to injury, disease or inflammation.

It is clear that MMPs play an important role in the extracellular milieu and there is abundant evidence showing that the stroma is an important source of MMPs. Fibroblasts in particular have been shown to secrete a variety of MMPs, including MMP-1 (125) and MMP-3 (115). The production of MMPs by fibroblasts can be stimulated by paracrine signals from cancer cells, highlighting the importance of reciprocal interaction in this system (126). Tumour-associated macrophages are also implicated in MMP production (127). Mast cell degranulation results in the release of proteases (128) and when this process is inhibited, this results in the inhibition of tumour growth (129). Neutrophils are thought to be the primary source of MMP-8 (130). Vascular cells such as endothelial cells and pericytes are not implicated in the

production of MMPs but MMPs nevertheless contribute to the control of angiogenesis, as the cleavage of pro- or anti-angiogenic factors by these proteases can result in their activation or degradation (131).

The impact of stromal MMPs is demonstrated in breast cancer, where the presence of microinvasion in ductal carcinoma *in situ* samples is associated with MMP-13 expression in stromal fibroblasts (132). In xenograft studies, the tumour-promoting effect of fibroblasts can be diminished by the inhibition of MMPs, either by the addition of TIMPs or the administration of synthetic MMP inhibitors (133).

1.7.2.2 MMPs in gastric cancer

In gastric cancer, expression of various MMPs has been associated with poor prognosis, advanced cancer stage and short survival. MMP-9 protein expression by immunohistochemistry and mRNA expression by qPCR is correlated with short survival (134,135). MMP-9 increases gastric cancer cell invasion in response to gastrin stimulation (136). MMP-1 expression is correlated with lymph node spread (137), with poor prognosis and presence of metastases (138). MMP-7 has also been proposed as an independent prognostic marker in gastric cancer (139).

It is now known that in gastric cancer, MMPs are expressed both by cancer cells and by stromal cells. MMP-7 is unusual in that it is expressed by gastric cancer cells (140). Ohtani *et al* showed that in colon and gastric cancer, MMP-1 was expressed on the surface of stromal cells such as macrophages and fibroblasts (141). MMP-2 is

expressed by fibroblasts in gastric cancer (142). Stromal MMP expression may play a role in stromal-epithelial signalling, enabling intercellular communication within the tumour. Higher concentrations of serum MMP-9 are associated with a denser stromal reaction in the primary tumour, which is associated with a poor prognosis (143). MMP-1 expression in gastric fibroblasts can be induced by treatment with CM from cancer cells, showing that MMP expression is regulated by stromal-epithelial interactions (144). MMP-7 expression by gastric cancer cells stimulates myofibroblast proliferation (145).

One of the major risk factors for the development of gastric cancer is *H. pylori* infection (see below). This infection has been shown to stimulate expression of MMPs in the stomach (116,146). The increase in MMP-7 in *H. pylori* infection stimulates myofibroblast proliferation, demonstrating that stromal changes may even precede the development of neoplasia (147).

It is clear that MMPs are involved in tumour progression owing to their ability to facilitate ECM degradation. In gastric cancer, it appears that MMP expression is correlated with advanced tumour stage and short survival. Stromal MMP expression has been demonstrated although the effect of stromal-derived MMPs remains to be determined in gastric cancer. With increasing evidence that MMPs are cancer and situation specific, it will be interesting to see which MMPs are particularly important in gastric cancer.

1.7.2.2 Imaging MMPs

Many of the clinical trials assessing MMP inhibitors failed to demonstrate an effect on tumour burden, which was assessed using conventional imaging modalities such as computed tomography. MMP inhibitors are cytostatic agents, so a reduction in tumour volume may not necessarily result although the activity of the tumour could have changed significantly. There is therefore a need for alternative methods of assessing tumour burden. The use of conventional clinical imaging techniques in combination with the development of new MMP-sensing probes has shown promise. The first fluorogenic MMP substrate was used in 2001 by Bremer *et al* (148). Positron emission tomography has also been used in the detection of MMP activity (149). A gadolinium-related MMP-sensitive probe has been developed for use with magnetic resonance imaging (150). With increasing resolution, these techniques will enable the assessment of biochemical processes within the tumour, allowing the effect of new drug compounds to be measured.

1.7.3 Cathepsins

Cathepsins are a family of 11 proteins, all with a conserved active site composed of histidine and cysteine residues (151). They are synthesised as inactive precursors and are activated in the acidic environment of the lysosome. Historically, their role was thought to be in the terminal degradation of proteins within the lysosome but more recently they have been implicated in a larger variety of intracellular and extracellular processes.

Cathepsin expression in many tumours correlates with a poor prognosis (152). In the RIP1-Tag-2 mouse model of pancreatic cancer many of the cathepsins are upregulated in the tumours (153). In humans, cathepsin E is expressed in the stomach and in signet cell carcinomas (154). Cathepsin B activity is increased in a genetically engineered mouse model of gastric cancer (155). Proteomic work has identified that cathepsin S is upregulated in gastric cancer cell lines and knockdown of this protein results in decreased gastric cancer cell migration and invasion (156).

These extracellular protease systems interact with one another by cleaving members of another family of enzymes (Figure 1.6). For instance, plasmin stimulates the activation of MMP-3 (157). uPA is implicated in the activation of MMP-9 (158) and interacts with cathepsin B (159). Extracellular protease systems are key players in the network of stromal-epithelial signals and investigation of these will shed insight into the most important paracrine signals in gastric cancer.

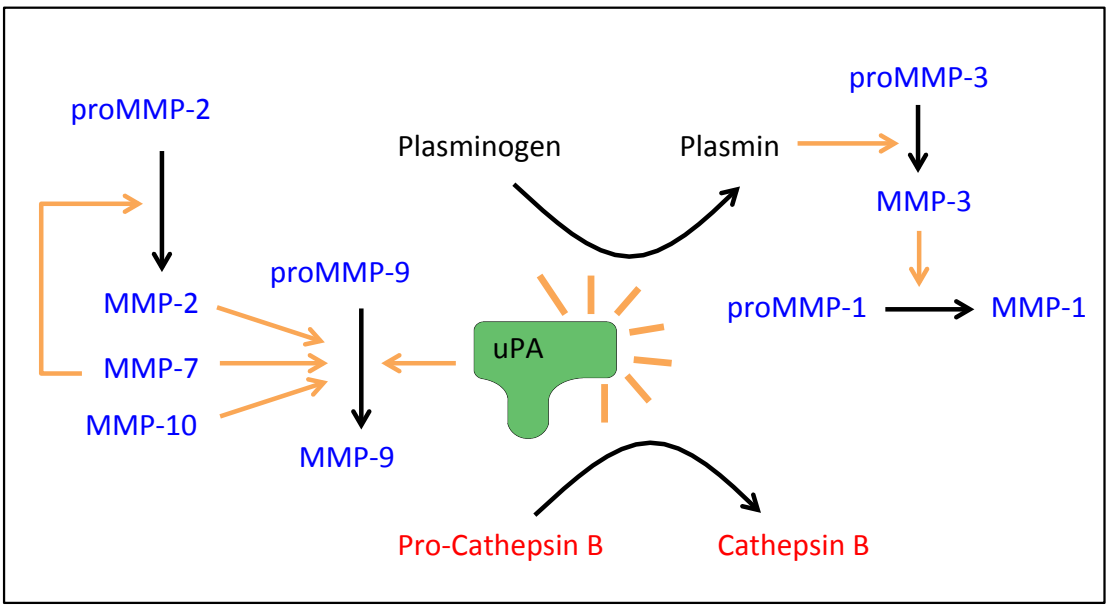

Figure 1.6 Interactions between extracellular protease systems. The MMPs form a cascade of extracellular protease activity by mutual activation. The uPA system plays a central role in the enhancement of proteolysis as uPA activates MMP-9 and cathepsin B, and plasmin activates MMP-3.

1.5 The stomach

The stomach is structurally divided into five areas (Figure 1.7**A**). The majority of gastric cancers occur in the corpus and antrum. The stomach wall is composed of four layers (Figure 1.7**B**). The level of invasion of the primary tumour through the wall of the stomach is used in the staging of gastric cancer (Table 1.1).

The gastric epithelium secretes enzymes, acid and hormones involved in digestion and protection against infection. The secretion of proteolytic enzymes and lipases commences the process of digestion. The digestive enzymes in the stomach function optimally at low pH. The secretion of acid by the gastric epithelium creates an environment hostile to pathogens, enabling the stomach to protect against food-borne pathogens. The production of a mucous layer protects the gastric epithelium from the acidic stomach contents. The gastric epithelium is also capable of absorbing water and ethanol. The secretion of intrinsic factor is necessary for the absorption of vitamin B_{12}. The gastric epithelium has invaginations known as gastric pits and at the base of these the gastric glands produce the acid, enzymes and hormones crucial to the normal functioning of the stomach (Figure 1.8).

It was thought that the gastric epithelium was renewed by a population of stem cells located in the isthmus of gastric glands (160). Recent evidence suggests that another population of cells located in the base of gastric glands is capable of acting

as a reserve of stem cells increasing epithelial cell renewal in response to tissue damage (Figure 1.8) (161). It is thought that dysregulation of stem cell renewal is an important contributing factor in the development of gastric cancer and stem cells may represent a therapeutic target (162).

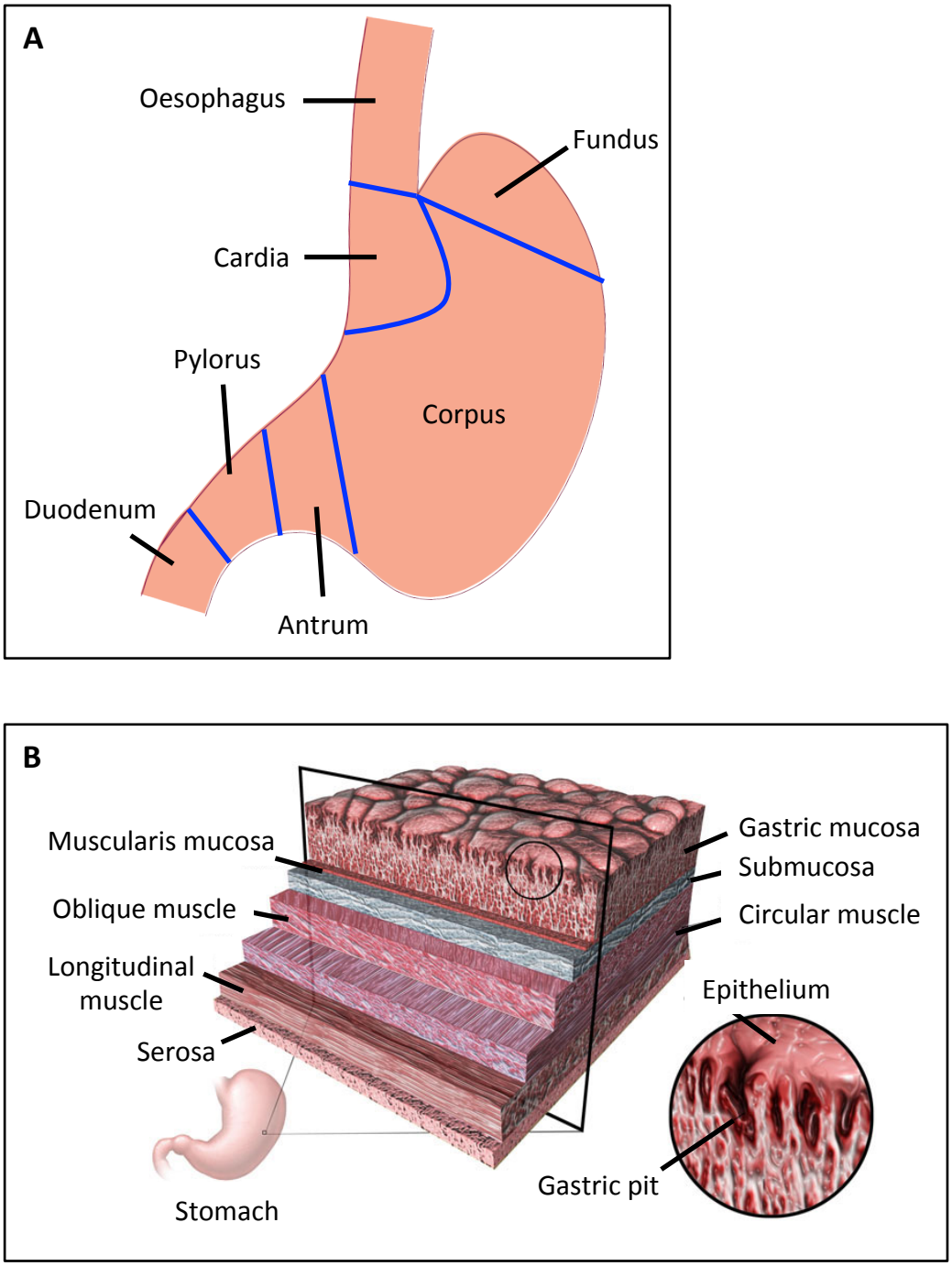

Figure 1.7 The Stomach. A, The five regions of the stomach: fundus, corpus, antrum, cardia and pylorus. **B,** Layers of the stomach wall from inner to outer: mucosa, submucosa, muscularis propria (containing circular, oblique and longitudinal muscle) and serosa (which is continuous with the visceral peritoneum).

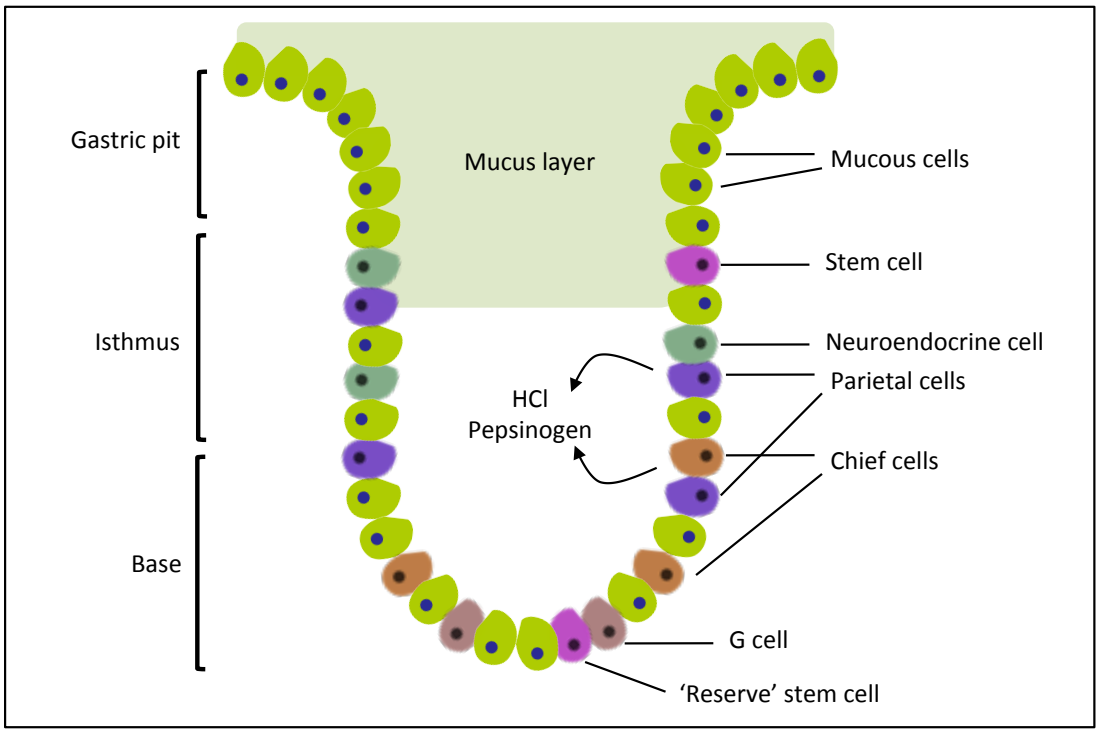

Figure 1.8. **Schematic illustrating a gastric pit and gland with the cell types involved in gastric epithelial function.** The epithelium of the fundus and corpus of the stomach has invaginations known as gastric pits. Gastric pits are lined with mucous cells, which secrete the protective layer of bicarbonate-rich mucus which covers the gastric epithelium. The base of gastric pits opens into gastric glands, which contain cells responsible for the secretion of gastric enzymes and acid and for renewal of the epithelium. Parietal cells secrete hydrochloric acid and intrinsic factor (necessary for the absorption of vitamin B_{12} in the terminal ileum). Chief cells secrete pepsinogen which is converted to pepsin (an important digestive enzyme) in the presence of hydrochloric acid. G-cells secrete gastrin, which acts on neuroendocrine cells to stimulate histamine release, which acts on parietal cells to increase acid production. Gastrin also stimulates gastric motility. Neuroendocrine cells also secrete other hormones such as serotonin.

1.6 Gastric cancer

1.6.1 Epidemiology of gastric cancer

In the UK, the incidence of gastric adenocarcinoma is 16 per 100,000 for men and 8 per 100,000 for women. It is the ninth most commonly diagnosed cancer in males and the fourteenth most common in females (163). Tumours of the corpus and antrum are decreasing but adenocarcinomas of the gastric cardia are increasing, in parallel with the increase in these tumours in the distal oesophagus (164). The five-year survival rate for gastric cancer was reported to be 17% in 2011, which is low when compared to survival from other cancers such as breast and colon (165).

Worldwide there are geographical variations in the incidence of gastric cancer. These seem to be related to the variation in the incidence of risk factors for the disease, diet and *H. pylori* infection. The highest incidence occurs in Eastern Asia at 42 per 100,000 and the lowest in Southern Africa at 2 per 100,000 (166). Stomach cancer is the second commonest cause of cancer-related death worldwide (167).

1.6.2 Classification of gastric cancer

Gastric adenocarcinoma represents more than 95% of malignant stomach tumours, the rest being accounted for mostly by lymphomas and leiomyosarcomas. Histological classification of these tumours is based on Lauren's classification, where the two main subtypes are intestinal or diffuse (168). The intestinal type is more frequently associated with *H. pylori* infection, while the diffuse type affects females

and young patients more frequently. The TNM (tumour, nodes, metastasis) staging system is used to assess the extent of the primary tumour's local invasion, its spread to lymph nodes and the burden of metastatic disease (Table 1.1).

Primary tumour (T)	T0: no evidence of primary tumour T1: tumour invades lamina propria or muscularis mucosa (T1a) or submucosa (T1b) T2: tumour invades muscularis propria T3: tumour penetrates subserosal connective tissues without invasion of serosa T4: tumour invades serosa (T4a) or adjacent structures (T4b)
Lymph node status (N)	N0: no metastasis to lymph nodes N1: metastasis in 1-2 regional lymph nodes N2: metastasis in 3-6 regional lymph nodes N3: metastasis in 7 or more regional lymph nodes
Metastasis (M)	M0: no distant metastasis M1: distant metastasis

Table 1.1 TNM staging system for gastric cancer showing the staging of disease based on the extent of the primary tumour, the spread to lymph nodes and any metastatic disease (169).

1.6.3 Management of gastric cancer

The only curative procedure for gastric cancer is surgical resection, involving either a total or partial gastrectomy. This is sometimes combined with adjuvant or neo-adjuvant chemotherapy (170). Surgery is most successful if the tumour is confined to the mucosa or submucosa, but only a small percentage of tumours are still at this early stage at the time of diagnosis. More than 50% of patients have locally advanced or metastatic disease at presentation (171). In this setting, chemotherapy and radiotherapy are used to prolong survival by months or in the palliative setting, to alleviate symptoms of metastatic disease or from local recurrence (172).

1.6.4 Aetiology of gastric cancer

Correa *et al* proposed in 1975 that chronic inflammation of the gastric mucosa led to gastric atrophy, causing intestinal metaplasia and eventually leading to neoplasia over decades (173). Until the discovery of *H. pylori* by Marshall and Warren in 1984 (174), the cause of gastric inflammation was thought to be environmental. It is now known that *H. pylori* infection increases the risk of gastric cancer (175). Other patients at risk of gastric cancer include those who have undergone a partial gastrectomy or vagotomy and those with chronic atrophic gastritis (176). This is thought to be related to chronic inflammation and hypochlorhydria. Like many other cancers, the incidence of gastric cancer increases with age (162). A diet rich in preserved or pickled foods was thought to be associated with a higher risk of gastric cancer due to their high nitrosamine content. Recent evidence suggests that high

dietary nitrates and nitrites may not necessarily cause gastric cancer (177). Cigarette smoking increases the risk of developing gastric cancer by nearly two-fold (178).

In some cancers, a multi-step sequence of carcinogenesis has been characterised involving the accumulation of genetic lesions resulting in phenotypic changes, for example the adenoma-carcinoma sequence in colon cancer (179). In gastric cancer, however, there is histopathological and molecular heterogeneity that precludes the identification of a common sequence (180). Loss of expression of certain genes is associated with gastric cancer. Germ-line mutations in the *CDH1* gene (encoding E-Cadherin) predispose to a hereditary form of gastric cancer (181). Loss of expression of the transcription factor RUNX3 in gastric cancer cells is associated with gastric cancer formation and progression (182). Mutations of p53, an event common to many cancers, occur in up to 70% of gastric cancers, with a wide distribution of these mutations throughout the gene (183).

1.6.4.1 H. pylori

H. pylori is a gram-negative bacillus which chronically infects the gastric mucosa. Infection increases the risk of developing gastric cancer (176). It is a genetically diverse organism, and infection with strains positive for the CagA pathogenicity island are particularly associated with higher grades of inflammation and the highest risk of cancer (184). *H. pylori* activates Wnt signalling in gastric epithelial cells, causing cell cycle disruption (185). Infection activates stromal fibroblasts, increasing the myofibroblast content in the stomach wall (42, 147). Increased epithelial MMP-7 expression in *H. pylori* may contribute to epithelial cell proliferation by increasing the

availability of myofibroblast-derived growth factors (147). *H. pylori* stimulates PAI-1, uPA and uPAR expression in gastric epithelial cells, stimulating epithelial cell proliferation (186).

1.6.5 Mouse models of gastric cancer

In gastric cancer, the use of mice as model organisms requires caution, as there are important differences in gastric anatomy between mice and humans. For instance, the mouse fundus is lined with squamous epithelium rather than glandular. Mice rarely spontaneously develop gastric cancer, so early models attempted to increase the likelihood of a cancer developing by administering chemical carcinogens such as nitrosamines (187). With the discovery of *H. pylori* and its effect on gastric carcinogenesis, the focus shifted to mimicking the effects of this bacterium on gastric mucosa. Few strains of *Helicobacter* infect the mouse stomach, with the notable exception of *H. felis*, where infection results in a similar progression from inflammation, to atrophy, metaplasia, dysplasia and finally neoplasia as is seen in *H. pylori* infection in humans (188). However, *H. felis* lacks the *cagA* gene responsible for causing ulcers in humans, so the mechanisms by which it causes inflammation are almost certainly different from those in humans.

Genetically engineered mice have struggled to replicate human gastric cancer. Gastric cancer is a genetically heterogeneous disease, making it difficult to replicate the disease by mutating one or two genes. Early genetically engineered models mutated genes not known to be associated with gastric cancer, such as the SV40 T antigen (189), and the resulting lesions did not follow the sequence of development

commonly observed in gastric cancer. INS-GAS mice (where the insulin promoter has been inserted upstream of the coding region for gastrin leading to hypergastrinaemia due to expression in pancreatic β-cells) develop gastritis and metaplasia which is accelerated by *H. felis* infection (190). The H/K-ATPase-IL-1β mouse (over-expressing IL-1β in the stomach) also mimics human gastric cancer, and IL-1β mutations have been identified in gastric cancers (191).

Genetically engineered mouse models have the advantage of working in a system with an intact host response including the immune reaction. However, as they are developed from a single genetic lesion they fail to replicate the complexity and variety of lesions in gastric cancer.

Human cells taken from gastric cancers can be used in mouse models if they are injected into strains of mice lacking in components of the immune system. Nude athymic mice are lacking in mature T cells, but retain B cells, dendritic cells and granulocytes. They have increased natural killer cells and macrophages. NOD/SCID mice are more profoundly immunodeficient and lack both B and T cells.

Injection of cells subcutaneously is quick, technically simple and results in tumours which are easy to monitor. However, the subcutaneous tissue will not fully replicate the characteristics of the tissue of origin. Orthotopic implantation of tumours is more invasive, time-consuming and technically challenging. Often the site is difficult to monitor without the use of *in vivo* imaging. These tumours mirror the behaviour

of the original tumour more accurately and in many cases an orthotopic model is the only way to replicate the pattern of metastasis seen in the human disease.

Xenografts created with the use of human cell lines show a poor correlation with the response to therapy of the primary disease (192). The use of primary cells in xenograft experiments increases the correlation between the xenograft's response to therapy and that of the primary tumour (193). *In vivo* modelling of stromal-epithelial interactions will be discussed in the next section.

1.8 Modelling stromal-epithelial interactions

The first insights in the investigation of stromal-epithelial interactions came from the field of developmental biology, where reciprocal signalling between mesenchyme (which later becomes stroma in the adult) and epithelium results in the activation differentiation programs and the development of tissues and organs. An early example of this was the finding that stromal-epithelial interactions were necessary in directing the morphogenesis of the male or female urogenital system in response to sex hormones (194). The cancer stroma is composed of cells of mesenchymal origin, and similarities in behaviour were noted between the mesenchyme in development and the stroma in cancer (195).

1.8.1 In vitro models

Since the first attempts at cell culture in the nineteenth century (196) this technique has become established as the fastest and easiest way to study cell behaviour. Primary cells (those harvested from tissues or organs) undergo senescence after a few passages, limiting their long-term use. This can be circumvented by immortalisation of the cells using viruses. The present investigation used MKN45 cells, which are derived from a poorly differentiated metastatic gastric adenocarcinoma (197). AGS cells were also used; these are derived from a gastric adenocarcinoma (198). Although normal fibroblast cell lines exist, they are not of gastric origin so this study used primary gastric myofibroblasts harvested from gastric adenocarcinoma tissue.

Defining the signals between stromal and epithelial cells begins with the examination of the range of secreted proteins in the medium of cells. Studying the response of cells to treatment with conditioned media from another cell type is useful in determining the effect of stromal-epithelial interactions. However, two-dimensional cell monolayers do not accurately replicate *in vivo* cell morphology and this system does not allow the study of short-range or short-lived signals, for which direct cell-cell contact may be necessary.

Organotypic cultures are three-dimensional co-culture systems where cells are re-aggregated into an organ-appropriate architectural arrangement and embedded within a synthetic basement membrane. There is evidence to show that matrix attachment is necessary for the maintenance of cell differentiation and cell polarity

(199). These systems were first developed in the 1980s (200) and are now used to assess the response to drug treatment (201). It is important to remember that although good *in vitro* models of tumorigenic processes (proliferation, invasion, migration) do exist, some aspects of tumorigenesis such as metastasis cannot be modelled *in vitro*.

1.8.2 In vivo models

In vivo modelling of stromal-epithelial interactions poses a particular challenge. In genetically modified models of gastric cancer the stroma arises from the host mouse. Comparison of any stromal reaction therefore relies on similarities between the mouse immune response, vasculature and recruitment of myofibroblasts and those of humans. Additionally, the use of genetically modified mice has proven challenging owing to the lack of organ-specific promoters allowing the targeting of stromal genes. The role of the stromal TGF- type II receptor was however elucidated by creating a conditional knockout in mouse fibroblasts (202). In xenograft models, stromal cells can be co-injected with the cancer cells (48), enabling a degree of control over stromal composition. The use of immunocompromised animals for this purpose limits the analysis of the immune reaction to the tumour.

1.9 *In vivo* imaging

1.9.1 History of imaging

For many years microscopy has provided a foundation for much of cell and tissue biology. However, conventional microscopy is limited by a visualisation depth of 10µm, necessitating sectioning prior to examination. Transparent organisms such as *C. elegans* or monolayers of cells can be inspected whilst alive, and consequently have become popular model systems. The reason for the limited depth of focus is the high light scattering seen in the visible, UV and near infra-red parts of the electromagnetic spectrum as photons are most able to interact with cellular components at these wavelengths (203). Light scattering creates image blur, and the more scattering events occur, the poorer the image quality. Confocal microscopy partially overcomes this problem, and extends the depth of imaging to hundreds of µm in some tissues. It achieves this by taking into account the average angle by which photons are scattered and calculates the distance a photon travels before its direction of travel is no longer related to its original direction of travel (204).

The need for thin sections of tissue had largely precluded the use of microscopy in live animals until laser scanning confocal microscopy and two-photon microscopy reduced light scattering further, enabling the visualisation of virtual tissue sections in intact tissues. This allowed microscopy to be used *in vivo* in an unperturbed environment, with tissue penetration reaching up to a few mm. These techniques have been used to examine the activity of fluorescent proteins, probes and dyes (205).

Imaging deeper than a few mm in tissue required further approaches to reduce light scattering. Tissues can be treated with chemicals to minimize the scattering of photons, but this is toxic to cells and therefore only appropriate for post-mortem examination (206). The reduction in scattering does, however, make it possible to image specimens by measuring the transillumination of light through them and processing of these data using 3D reconstruction algorithms to create 3D images. This is known as optical tomography.

1.9.2 Fluorescence Molecular Tomography (FMT)

Improvements in imaging methods which account for photon diffusion beyond a few mm in combination with the development of optical reporters of biological processes have allowed the visualisation of deeper tissues and whole organs. At these depths, light in the visual spectrum is absorbed by melanin and haemoglobin and there is a high degree of photon scattering. Beyond wavelengths longer than 1100nm, however, light absorption by water precludes adequate signal detection. This makes the most favourable window for animal tissue imaging between 600 and 1000nm. Fluorescence molecular tomography (FMT) combines optical tomography with fluorescence, taking advantage of the low light scattering and tissue absorption experienced in the 600-800nm range. It uses data obtained from the optical illumination of a specimen over many different angles and combines this to build a quantitative 3D representation of the fluorescence from a reporter, illuminating the surface using point light sources and different mathematical models of photon behaviour than optical tomography (207) (Figure 1.9). This technique permits

imaging of biological processes such as protease activity through the use of activatable fluorochromes. These injectable molecules mimic the protease substrate and upon cleavage by the enzyme of interest, emit light in the near infra-red spectrum (208). In order to improve the resolution of FMT, data obtained from this technique can be combined with more detailed anatomical information from a different imaging modality, such as computed tomography (CT) (209) or magnetic resonance imaging (MRI) (210).

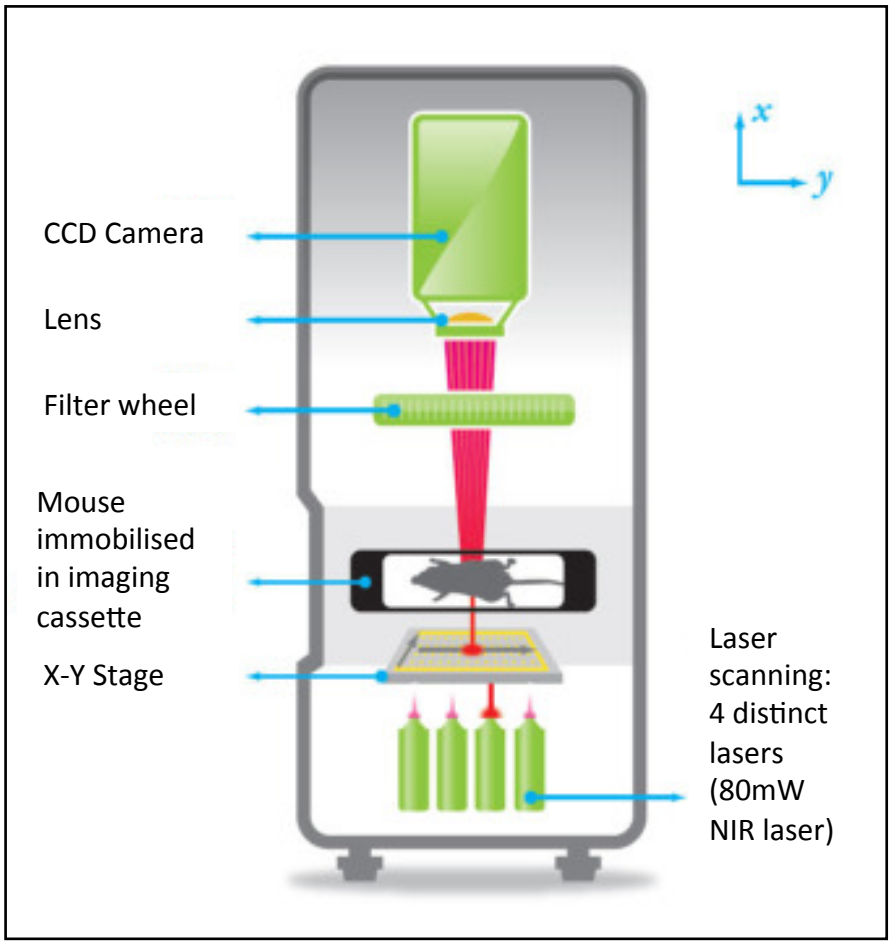

Figure 1.9 FMT imaging. The anaesthetised mouse is immobilised in the imaging cassette. Light is directed at the animal from different projections and the signal is detected by the charge-coupled device (CCD) camera from multiple points. Paired absorption and fluorescence acquisition data are normalised according to algorithmic models of photon transport in tissue.

The appeal of harnessing red-shifted fluorescent proteins for *in vivo* imaging applications has led to intense research into the development of more intensely fluorescent proteins in the far-red range. This has proved to be challenging, due to difficulties with poor light intensity, insufficiently red-shifted emission spectra and detrimental effects on cell viability following transfection. Using site-directed and random mutagenesis, proteins such as mCherry and mPlum have been altered further to shift their excitation and emission peaks beyond 600nm (211). E2-Crimson was created in this manner from the red fluorescent protein dsRed Express2 (212).

The main advantage of FMT is its ability to detect fluorescent reporters of cellular processes and track fluorescent cells at a variety of wavelengths, enabling the visualization of multiple processes simultaneously. Other imaging modalities, such as CT and MRI, do not have such varied reporters and are limited to reporting anatomical features. Combined with positron emission tomography (PET) CT can highlight areas of high glucose uptake using the radiotracer fluorodeoxyglucose. MRI can also estimate local blood flow, which in the brain can highlight areas of activity. These represent the only visualisations of cellular processes in widespread clinical use. Emerging clinical applications of FMT include mapping the lymphatic spread of tumours, accurate identification of tumour margins and as an adjunct to endoscopic or radiological imaging to improve the diagnostic yield (213).

1.10 Overview of the present study

This investigation focuses on the role of myofibroblasts in gastric cancer. These cells are known to produce PAI-1 (214), an inhibitor of the serine protease urokinase plasminogen activator (uPA), as well as MMPs (215). An *in vivo* subcutaneous xenograft model of stroma-stimulated tumour growth has been developed together with an *in vitro* 3D organotypic culture modelling myofibroblast-stimulated cancer cell invasion; together these were used to assess the contribution of extracellular proteases. Finally, the recruitment of MSCs to oesophageal xenografts was assessed and the role that chemerin-ChemR23 signalling plays in this process was studied using a ChemR23 antagonist.

1.11 Aims

1. To characterise the expression of PAI-1 in gastric cancer cells and myofibroblasts and create cancer cells overexpressing PAI-1
2. To create an *in vivo* model of stromal-epithelial signalling, and characterise the contribution of myofibroblasts to tumour growth.
3. To compare MMP and cathepsin activity in xenografts containing myofibroblasts to those without.
4. To assess the effect of a ChemR23 antagonist on recruitment of MSCs to oesophageal xenografts containing myofibroblasts.

CHAPTER 2: MATERIALS AND METHODS

2.1 Materials

2.1.1 Cell culture

AGS and MKN45 gastric cancer cell lines were obtained from the American Type Culture Collection (Manassas, VA, USA) and RIKEN (Tsukuba, Ibaraki, Japan) respectively. OE21 oesophageal squamous carcinoma cells were from American Type Culture Collection. Human MSCs were from Lonza (Castleford, UK). Dulbecco's Modified Eagle's Medium (DMEM), antibiotic-antimycotic solution, non-essential amino acid solution, penicillin-streptomycin solution, erythrosin B and trypsin-EDTA 0.25% were obtained from Sigma (Poole, UK). The MycoAlert^{TM} Kit was purchased from Lonza. Fetal bovine serum (FBS) was obtained from Perbio (Cheshire, UK). Phosphate-buffered saline (PBS) was from Invitrogen (Paisley, UK).

2.1.2 Xenografts

Male 6-week old nude mice (BALB/c nu/nu) were purchased from Charles River (Wilmington, MA, USA). Heparin sodium 1000units/1ml vial was obtained from the Royal Liverpool Hospital. Isoflurane for general anaesthesia was from O'Neill Medicalia (Liverpool, UK).

2.1.3 Fluorescence molecular tomography

ProSense 750 FAST™, Cat B 750 FAST™ and MMPSense 750 FAST™ were obtained from Perkin Elmer (Cambridge, UK). CellVue® Claret and PKH67 green fluorescent cell linker mini-kits were purchased from Sigma. E2-Crimson plasmid was from Clontech (Saint-Germain-en-Laye, France). CCX832 in corn oil and vehicle were gifts from ChemoCentryx (Mountain View, CA, USA).

2.1.4 Immunofluorescence

Bovine serum albumin (BSA) and donkey serum were obtained from Jackson Immuno Research Laboratories (Suffolk, UK). Vectashield with or without 4',6-diamidino-2-phenylindole (DAPI) was purchased from Vector laboratories (Peterborough, UK). Novocastra mouse monoclonal anti-human vimentin intermediate filament antibody was from Leica Biosystems (Newcastle-upon-Tyne, UK). Guinea pig polyclonal anti-vimentin antibody was from Fitzgerald Industries (North Acton, MA, USA). NaCl and HEPES (4-(2-hydroxyethyl)-1-piperazineethanesulfonic acid) were from Sigma. Triton-X-100 was obtained from Sigma. Paraformaldehyde (PFA) was from Agar Scientific (Stansted, UK). Cryo-M-Bed and Cryospray were obtained from VWR Jencons (Lutterworth, UK). Thermo scientific microscope slides with polysine adhesion and cork discs were purchased from Fisher Scientific (Loughborough, UK). Sucrose was purchased from Sigma.

2.1.5 EdU

The EdU Click-It® kit was purchased from Invitrogen.

2.1.6 Adhesion assays

PBS containing $CaCl_2/MgCl_2$ was purchased from Invitrogen. Crystal violet, H_2SO_4 and NaH_2PO_4 were from Sigma. Human vitronectin from human plasma was obtained from BD Biosciences (San Jose, CA, USA).

2.1.7 Transfection of MKN45 cells

TransFast™ transfection reagent cationic lipid was obtained from Promega (Madison, WI, USA). Calbiochem G418 sulphate was purchased from Merck KGaA (Darmstadt, Germany). Human PAI-1 overexpressing plasmid was a gift from Prof. Rod Dimaline, University of Liverpool. Cloning cylinders were from Sigma.

2.1.8 Scratch migration assays

Calbiochem recombinant human mutant plasminogen activator inhibitor-1 was from Merck KGaA.

2.1.9 Boyden chamber migration assays

BD Control Cell Culture Inserts were purchased from BD Biosciences. Diff-Quick staining kit was obtained from Dade Behring Inc. (Glasgow, DE, USA).

2.1.10 PAI-1 ELISA

The Imubind Tissue PAI-1 ELISA kit was purchased from American Diagnostica (Stamford, CT, USA).

2.1.11 RNA extraction, reverse transcription and qPCR

The RNase-Free DNase set and the RNeasy Mini Kit were from Qiagen (Manchester, UK). Precision 2x real time PCR master mix with or without SYBRgreen was from PrimerDesign, (Southampton, UK). RNAsin, dNTPs, oligoDT and AMV reverse transcriptase were obtained from Promega. Primers and probes were obtained from Eurogentec (Liege, Belgium).

2.1.11 Organotypic co-cultures

Collagen Type 1 Rat Tail extracted from rat tail tendons was obtained from Millipore (Billerica, MA, USA). BD Matrigel™ Basement Membrane Matrix was purchased from BD Biosciences. Stainless steel mesh was purchased from Bracon (Etchingham, UK). Gauze was a gift from Jag Dhanda, University of Liverpool, UK. Glutaraldehyde 25%, 10 x DMEM and NaOH were obtained from Sigma. Calbiochem MMP-2 Inhibitor I and MMP-3 Inhibitor IV were from Millipore.

2.1.11 Luciferase promoter-reporter assays

A Dual-Luciferase® Reporter Assay System was purchased from Promega. PMA (phorbol 12-myristate-13-acetate) was from Sigma.

2.2 Methods

2.2.1 Culture of gastric cancer cell lines

MKN45 and AGS cells were cultured in DMEM containing 10% v/v FBS, 2% v/v Antibiotic-Antimycotic, 1% v/v Penicillin-Streptomycin in 5% CO_2 at 37°C. Medium was changed every 48-60 h. At confluence, cells were washed in PBS twice and trypsinised using 0.25% w/v trypsin-EDTA until they were fully detached (4-8 min). Viable cells were counted using a haemocytometer by preparing a 50:50 mixture of cell suspension and Erythrosin B.

Media were tested for mycoplasma using the Lonza MycoAlert^{TM} kit according to the maufacturer's instructions and found to be negative.

Conditioned medium (CM) was prepared by plating 1.5 x 10^6 cells in a 75cm^2 flask. After 24 h, cells were washed twice in PBS, 15ml of serum-free (SF) medium was added, collected 24 h later and centrifuged. Supernatants were either used immediately or frozen at -80°C for use in subsequent experiments.

OE21 and MSC cell lines were maintained and harvested by J. Dinesh Kumar.

2.2.2 Primary gastric myofibroblasts

Human gastric myofibroblasts were derived from samples obtained peri-operatively at resection of 12 gastric tumours at the Department Surgery, University of Szeged, Hungary.

Patients were aged 39-84 and 64% were male. Tissue was taken from the tumour itself (from which CAMs were derived) and adjacent normal tissue located at least 5cm from the tumour margin (from which ATMs were derived). Data on patient demographics, TNM staging, tumour classification and patient survival are detailed in Table 2.1. Myofibroblasts were also derived from deceased transplant donors with no gastric pathology (NTMs). Immunohistochemical staining revealed spindle-shaped α-SMA positive cells and the morphology, architecture and number of these had been scored. All tumours had increased numbers of myofibroblasts and distorted architecture. Myofibroblasts were prepared as previously described (43). This work was approved by the Ethics Committee of the University of Szeged, Hungary.

Both native (*in situ*) and cultured myofibroblasts were positive for α-SMA and vimentin and negative for desmin and cytokeratin. Myofibroblasts were used from passages 3 to 12 in *in vitro* assays; for *in vivo* work myofibroblasts were used from passages 3 to 7.

Primary gastric myofibroblasts were cultured in DMEM containing 10% v/v FBS, 2% v/v Antibiotic-Antimycotic, 1% v/v Penicillin-Streptomycin and 1% non-essential amino acids in 5% CO_2 at 37°C. Medium was changed every 48-60 h. At confluence cells were washed in PBS twice and trypsinised using 0.25% w/v trypsin-EDTA until cells were fully detached (5-10 minutes). Cells were counted using a haemocytometer. CM from myofibroblasts was prepared in the same manner as for AGS and MKN45 cells as detailed above.

Oesophageal CAMs were derived from samples obtained peri-operatively at resection of 4 squamous carcinoma at the Department Surgery, University of Szeged, Hungary and were

prepared as previously described (43). Myofibroblasts were maintained and harvested by J. Dinesh Kumar.

Patient No.	Age	Gender	Survival (months)	Tumour Staging	Tumour Location	Lauren Classification	Adjacent Tissue
1	72	M	53	pT1N0M0	antrum corpus border	medullar (non-Lauren)	intestinal metaplasia, atrophy
2	82	M	3	pT4N2M0	antrum	intestinal	intestinal metaplasia, chronic gastritis
3	65	F	5	pT4N4M1	antrum corpus border	mixed	chronic gastritis
4	49	F	22	pT3N1M0	antrum corpus border	diffuse	chronic gastritis
5	76	M	25	pT1N0M0	antrum	intestinal	intestinal metaplasia, chronic gastritis
6	77	M	>38	pT2aN0M0	antrum	intestinal	intestinal metaplasia, chronic gastritis
7	76	M	15	pT4N2M0	antrum	intestinal	intestinal metaplasia, atrophy, chronic gastritis
8	72	M	39	pT3N1M0	corpus	mixed	chronic gastritis
9	84	F	>31	pT3N0M0	antrum corpus border	intestinal	chronic gastritis
10	59	F	17	pT3N2M0	antrum and corpus	diffuse	chronic gastritis
11	51	M	9	pT1N3M0	antrum corpus border	mixed	chronic gastritis
12	67	M	>39	pT3N1M0	antrum	intestinal	chronic gastritis
13	39	F	31	pT4N2M0	antrum corpus border	intestinal	no adjacent tissue
14	54	M	>48	pT2aN0M0	antrum corpus border	diffuse	no adjacent tissue

Table 2.1. Age, gender, post-operative survival (>, alive at time of submission), tumour staging, tumour localisation, tumour classification, and pathology assessment of tissue taken adjacent to the tumour, for patients used to provide gastric CAMs and ATMs.

2.2.3 Cell preparation for xenograft experiments

Cells were cultured as described above. After trypsinisation, cells were centrifuged and re-suspended in 10ml PBS. Viable cells were counted using a haemocytometer and aliquots (containing the appropriate cell number) prepared for injection. If cells were to be co-injected (e.g. MKN45 cells + myofibroblasts) they were mixed at this stage. Aliquots were then centrifuged for 7 min at 800 xg and re-suspended in an appropriate volume of PBS, so that an injection corresponded to 100µl of cell suspension.

MSCs were labelled separately with CellVue® Claret Fluorescent Cell Linker and with PKH67 Green Fluorescent Cell Linker kit. They underwent fluorescence-activated cell sorting. In preparation for IV injection, cells were trypsinised and counted. Aliquots were prepared such that 7.5 x 10^5 CellVue® Claret-labelled cells and 7.5 x 10^5 PKH67 Green-labelled cells were combined and re-suspended in 100µl of PBS, which was injected IV into the mice. This work was performed by J. Dinesh Kumar.

2.2.4 Xenograft studies in nude mice

Male 6-week old nude mice (BALB/c nu/nu, Charles River, Wilmington, MA) were acclimatized for 1 week prior to subcutaneous injection of cancer cells with or without primary human gastric or oesophageal myofibroblasts, suspended in 0.1ml PBS. For gastric cancer experiments, 1 x 10^5 MKN45 cells, with or without 5 x 10^4 gastric myofibroblasts, were used unless otherwise indicated. For oesophageal cancer experiments, 1 x 10^6 OE21 cells with or without 5 x 10^5 oesophageal myofibroblasts were used. Following injection, the weight and general condition of the mice were monitored daily. Tumours were

measured in two dimensions three times per week using external callipers. Estimated tumour volumes were determined using the two longest measurements of these in the modified ellipsoid formula

Tumour volume = ½(ab^2)

where *a* = longest diameter and *b* = shortest diameter.

Animals were culled using a *Schedule 1* method once the mean diameter of the tumour reached 1.2 cm, or alternatively if there were any signs of tumour ulceration or if the animal lost more than 20% of its body weight, in accordance with guidelines from the British Journal of Cancer (216).

Post-mortem, the tumours were dissected and fixed in 4% w/v PFA in PBS for 1 h. Tumours were then halved and one half transferred to 20% w/v sucrose in PBS after which it was embedded in Cryo-M-Bed and frozen onto cork discs using Cryospray; sections (5 - 10µm) were cut on a cryostat and mounted using Vectashield containing DAPI for direct visualisation. The remaining slides were stained by immunofluorescence or using EdU as detailed below. After 24 h the other half of the tumour was transferred to 70% v/v ethanol and processed into paraffin blocks by the Department of Pathology, School of Veterinary Science, University of Liverpool.

2.2.5 Fluorescence molecular tomography (FMT)

All FMT and IV tail vein injections were carried out under general anaesthesia. Mice were placed in a box filled with oxygen and an increasing concentration of isoflurane. At a

respiratory rate of 60-100/min isoflurane was decreased to maintenance levels and the mouse transferred to an imaging cassette. Oxygen and isoflurane were delivered to the mouse during FMT imaging, which lasted 2-4 min/mouse. For IV tail vein injections anaesthesia was administered through a nose cone. Mice were allowed to recover on a heat pad until moving independently when they were transferred to their cages.

a) Identification of E2-C labelled cells

Validation of E2-C-labelled MKN45 cells was performed by imaging 100µl droplets of MKN45 E2-C and MKN45 cells of varying concentrations suspended in PBS and comparing to droplets containing PBS only.

Subcutaneous xenografts containing MKN45E2-C cells were established as described above. When a mouse was approaching an endpoint (mean diameter >1.2cm, early signs of ulceration, weight loss approaching >20% of starting weight), FMT imaging at 635nm under GA was carried out.

b) MSC homing assay

Subcutaneous xenografts were established as described above. When a mouse was approaching an endpoint (mean diameter >1.2cm, early signs of ulceration, weight loss approaching >20% of starting weight), baseline FMT imaging at 680nm under GA was carried out. Animals received a subcutaneous injection of 125µl CCX832 (2mg/ml) or vehicle 24 h prior to and at the time of IV MSC injection. Tail vein injections of 7.5 x 10^5 MSCs

labelled with CellVue® Claret Fluorescent Cell Linker kit combined with 7.5 x 10^5 MSCs labelled with PK67 Green Fluorescent Cell Linker kit (cells were labelled and selected by flow cytometry or by fluorescence microscopy by J. Dinesh Kumar) were performed under GA. FMT imaging at 680nm under GA was then carried out at 6 and 24 h post injection.. Animals were culled 24 h post injection and tissue processed as described above. The images were processed using TrueQuant software. PKH67-labelled cells were identified in frozen sections using the FITC filter on a Zeiss Axioplan-2 microscope (Zeiss vision, Welwyn Garden City, UK).

c) Quantification of MMPSense 750 FAST™, ProSense 750 FAST™ and CatB 750 FAST™ activity

Subcutaneous xenografts were established as described above. When a mouse was approaching an endpoint (mean diameter >1.2cm, early signs of ulceration, weight loss approaching >20% of starting weight), baseline FMT imaging at 750nm under GA was carried out. MMPSense 750 FAST™, ProSense 750 FAST™, and CatB 750 FAST™ (100µl) were injected IV (tail vein), and after 6 and 24 h further FMT imaging at 750nm was carried out under GA and the animal then culled. Images were processed using TrueQuant software.

2.2.6 Immunofluorescence

a) Tissue sections

Frozen sections were thawed by immersion in distilled water for 30 seconds. Sections were transferred to 50% v/v ethanol for 10 min followed by 75% v/v ethanol for 10 min. The ethanol was rinsed off by repeated immersion in distilled water. Sections were covered in 10% v/v donkey serum in PBS for 30 min at room temperature to decrease non-specific binding of the secondary antibody. This was then removed and the sections incubated in primary antibody (Table 2.1) diluted in 1% w/v BSA in PBS overnight at 4°C in a humidified chamber. The sections were then washed sequentially with 0.14M NaCl, 0.5M NaCl and 0.14M NaCl for 5 min each. Sections were then incubated in an appropriate secondary antibody (Table 2.1) diluted in 10mM HEPES at room temperature in darkness. This was washed off with 3 5 min PBS washes. Slides were mounted with Vectashield containing DAPI.

b) Cultured cells

MKN45, MKN45 E2-C cells and MKN45 E2-C PAI-1 cells (1 x 10^4 per well) were plated onto coverslips in 24-well plates in FM. 24 h later they were washed twice in PBS and fixed for 30 min in 4%w/v PFA in PBS. Cells were then washed 4 times in PBS. Permeabilisation was carried out by incubating cells in 0.3%w/v BSA 0.2%v/v Triton X-100 in PBS (PBT) for 30 min. Cells were then washed twice in PBS and incubated in 5%w/v BSA in PBS for 30 min. Cells were washed twice in PBS and blocked in 10%v/v donkey serum for 30 min. After washing twice in PBS cells were incubated in primary antibody (Table 2.2) diluted in PBS at 4°C overnight in a humidified chamber. Cells were then washed sequentially in 0.14M, 0.5M and 0.14M NaCl for 10 min each and incubated in secondary antibody (Table 2.2) diluted in 10mM HEPES for 1 h at room temperature in the dark. Cells were washed 3 times in PBS and coverslips were mounted in Vectashield containing DAPI.

Primary antibody	**Dilution**	**Supplier**	**Secondary antibody**	**Dilution**	**Supplier**
Anti-vimentin (non species-specific) (Guinea pig)	1/200	Fitzgerald, MA, USA	FITC-conjugated donkey anti-guinea pig	1/400	Jackson, PA, USA
Anti-vimentin (human vimentin V9 filament) (Mouse)	1/400	Leica Biosystems, Newcastle-upon-Tyne, UK	TXR-conjugated donkey anti-mouse	1/400	Jackson, PA, USA
Anti-PAI-1 (Rabbit)	1/200	Santa Cruz, Heidelberg, Germany	FITC-conjugated donkey anti-rabbit	1/400	Jackson, PA, USA

Table 2.2 Primary and secondary antibodies used for immunofluorescence experiments on frozen tissue sections and on cultured cells.

2.2.7 EdU cell proliferation assay

a) Cultured cells

MKN45, MKN45E2-C cells and MKN45 E2-C PAI-1 cells (1 x 10^5) were plated on coverslips in 24-well plates in FM. After allowing them to adhere overnight, the cells were washed in PBS 3 times and incubated in SF medium. Cells were washed in PBS 24 h later and fresh SF medium was added. After 24 h, EdU was added to a final concentration of 10µM. Two hours following EdU addition cells were fixed in 4% w/v PFA in PBS for 30 min, washed twice with 3% w/v BSA in PBS and then twice in PBS. Permeabilisation was carried out by incubating cells in 0.5% v/v Triton X-100 in PBS for 20 min. Cells were then washed twice in 3% w/v BSA in PBS, incubated for 30 min in the dark with Click-It™ reaction cocktail and washed with 3% w/v BSA in PBS followed by PBS. DNA staining was carried out by incubating cells in 2µg/ml Hoechst 33342 in PBS for 30 min in the dark. Finally cells were washed twice in PBS and coverslips were mounted with Vectashield. EdU positive nuclei in 5 fields were quantified as a proportion of the total number of nuclei and the mean taken. Cells were visualized with a Zeiss Axiovert microscope and images acquired with a Hamamatsu 480-80 CCD camera with Axioplan software.

b) In vivo

One hour prior to sacrifice mice received an IP injection of 0.2ml EdU (2 mg/ml in PBS; equivalent to 400µg/mouse). Tissues were processed post-mortem as described above. Frozen tumour sections were thawed by immersion in distilled water for 30 sec. Click-It™ reaction cocktail was applied to sections and they were incubated in the dark for 30 min. Sections were then washed 3 times in PBS and mounted with Vectashield containing DAPI.

2.2.8 Adhesion assays

MKN45, MKN45 E2-C cells and MKN45 E2-C PAI-1 cells (1 x 10^5 per well) were plated in quadruplicate on 24 well plates in FM. After 45 min at 37°C, 5% CO_2 cells were washed 3 times with PBS containing $CaCl_2$/$MgCl_2$ and stained using 0.2% w/v crystal violet in 50% v/v ethanol for 5 min on a shaker. Cells were solubilized by incubation in a 50:50 mixture of 0.1M NaH_2PO_4, pH4.5 and ethanol for 5 min on a shaker at room temperature and 100µl of the solution transferred to a 96-well plate for determination of absorbance at 550nm using a Spectracount (Packard, CT, USA) plate reader. Blank controls (no cells) were subtracted. The mean absorbance at 550nm was reported. Assays were also performed on vitronectin-coated plates. These were prepared by making a 250ng/ml solution of vitronectin in PBS and adding 0.25ml of this to each well of a 24-well plate. After 90 min the wells were washed in PBS twice and the plate stored at 4°C until required.

2.2.9 Transfection of MKN45 cells with vectors for hPAI-1 and E2-Crimson (E2-C)

MKN45 cells (3 x 10^6 per 10cm dish) were allowed to adhere overnight. DNA (15µg) was vortexed with 5ml warmed SF medium. For cells co-transfected with E2-C and PAI-1 encoding vectors the DNA sample was composed of 50% E2-C and 50% PAI-1 DNA. TransFast™ (45µl) was added to the SF medium-DNA mixture and vortexed. The mixture was left at room temperature for 15 min. FM was removed from the cells and the SF medium-DNA-TransFast™ mixture added. The dish was incubated at 37°C, 5% CO_2 for 1 h. FM (5 ml) containing 20% FBS was then added. After 48 h the medium was removed and replaced with FM containing 1.5mg/ml G418 (selection medium). This was replaced every 48-72 h until colonies appeared. Fluorescent colonies were marked following examination

of the cells under the Texas red (TXR) filter on a Leica DMIRE2 microscope (Leica Microcsope Systems GmbH, Wetzlar, Germany) and images captured with a Hamamatsu Orca ER camera (Hamamatsu photonics, Hamamatsu City, Japan). Colonies were then cloned using cloning cylinders. The colonies were washed twice in PBS and cloning cylinders placed over the marks. Trypsin-EDTA (50µl, 0.25% v/v) was added to each cylinder and the plate incubated at 37°C, 5% CO_2 for 10 min. FM (200µl) was added to each cylinder and the contents transferred to a 5cm diameter dish filled with 5ml selection medium. This was replaced every 48-72 h until colonies appeared. Once again, red colonies were marked and cloned as described above. The procedure was repeated until all colonies growing in the 5cm diameter plate appeared red. At this point, colonies were allowed to grow to confluence and cultured in selection medium for 5 passages (Figure 2.1). Flasks of cells were regularly examined under the microscope and cells validated in the FMT equipment as described in 2.2.5b. qPCR was performed on MKN45 E2-C PAI-1 cells to assess PAI-1 mRNA expression (see 2.2.13-15). Immunofluorescent staining for PAI-1 was carried out on MKN45 E2-C PAI-1 cells (see 2.2.6b).

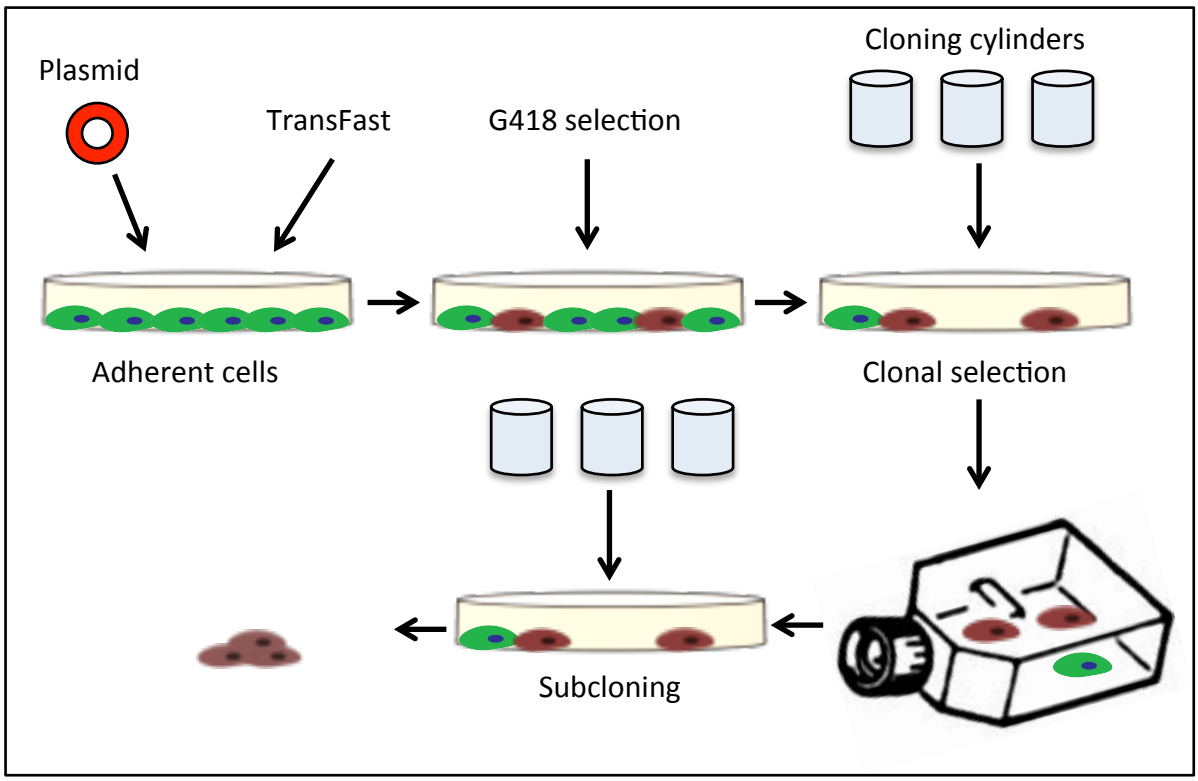

Figure 2.1. Schematic of the process of creating stably transfected MKN45 cells. MKN45 cells were transfected with an E2-C plasmid alone or in combination with a human PAI-1 overexpressing plasmid. Transfected cells were selected for using FM containing G418 and emerging colonies visualised under a TXR filter. Further rounds of subcloning took place until a uniform population of cells had developed.

2.2.10 Scratch migration assays

MKN45, MKN45 E2-C cells and MKN45 E2-C PAI-1 cells (1.5 x 10^6 per well) were grown to confluence in 6-well plates. The medium was removed and a vertical scratch wound made in the cell monolayer using a 10µl pipette tip. Wells were then washed 3 times with PBS and SF medium containing 50nM human recombinant PAI-1 was added. Baseline images at fixed points along the scratch were acquired. The cells were then incubated at 37°C, 5% CO_2 for 16 h. For MKN45 cells, the distance across the wound was measured at 10 fixed points at time 0 and after 16 h. Assays were performed in triplicate and the mean result calculated.

2.2.11 Boyden chamber migration assays

BD Control Cell Culture inserts and companion plates were used (BD Biosciences). These are composed of inserts with a base made of a membrane with 8µm pores and a companion plate where putative modulators of cell migration can be added. The inserts were filled with a suspension of 2.5 x 10^4 AGS or CAM14 cells in SF medium. The wells in the companion plate were filled with 0.75ml SF medium with or without the treatment (e.g. 50nM recombinant human PAI-1). The inserts were then transferred onto the wells of the companion plate (Figure 2.2). This was incubated for 22 h at 37°C, 5% CO_2. Non-migrated cells were scrubbed off with a cotton-tipped swab. Migrated cells were then stained using Diff-Quik™. The inserts were transferred sequentially through the staining solutions every 2 min and then rinsed in distilled water. Once dry, the membrane was excised and mounted on immersion oil. Migrating cells were counted at x 10 magnification in 5 fields per membrane and the mean calculated.

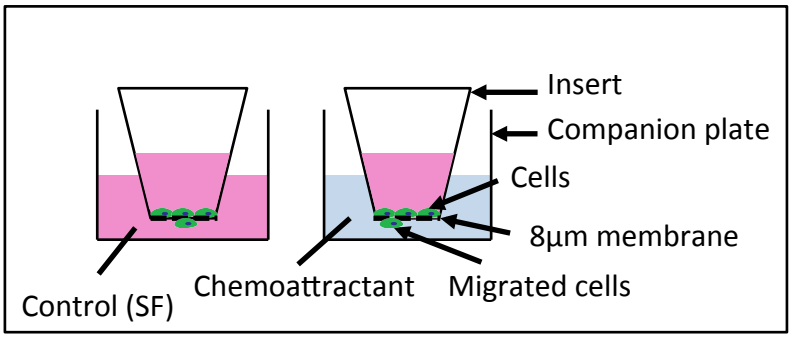

Figure 2.2. Schematic of Boyden chamber migration assay. AGS cells were seeded onto a membrane with 8µm pores. Putative chemoattractants (e.g. PAI-1) were added to the wells in the companion plate and the number of cells which migrated through the pores was compared to the SF control.

2.2.12 PAI-1 ELISA

Imubind Tissue PAI-1 ELISA kits (American Diagnostica) were used to assay PAI-1 in CM. PAI-1 standard, control or sample (100 μl) was added to wells in the precoated microtest strips and incubated overnight at 4°C in a humidified chamber. Wells were washed 4 times in wash buffer and then incubated with 100μl of detection antibody for 1 h at room temperature. Wells were washed 4 times with wash buffer and then incubated with 100μl of diluted enzyme conjugate for 1 h at room temperature, washed with wash buffer 4 times and then incubated for 20 min after the addition of 100μl of substrate solution. The enzymatic reaction was stopped by the addition of 50μl 0.5N H_2SO_4 and the absorbance at 450nm read on a Spectracount plate reader (Packard). Background signal was subtracted from the sample values. Samples were assayed in duplicate and the mean taken. A standard curve was generated using recombinant PAI-1 and the concentration in the samples determined by reference to this.

2.2.13 RNA extraction for qPCR

Cancer cells or CAMs (1.5×10^6) were plated in 10cm diameter dishes and incubated at 37°C, 5% CO_2. Cells were then trypsinised, counted and RNA extracted after 24 h treatment with SF medium or CM. RNA extraction was performed using the Qiagen RNeasy Mini kit according to the manufacturer's instructions, with the lysate homogenized by passage through a blunt 20G needle at least 5 times. On-column DNase digestion was performed to eliminate contamination by genomic DNA. RNA yield was quantified on a NanoDrop spectrophotometer (Labtech, Uckfield, UK).

2.2.14 Reverse transcription for qPCR

All cDNAs were prepared using 4μg RNA. RNA was combined with oligoDT and heated to 70°C for 5 min to achieve RNA/primer annealing. The RNA/primer mixture was combined with AMV reverse transcriptase, RNAsin and dNTPs in AMV buffer and incubated at 42°C for 1 h.

2.2.15 qPCR for hPAI-1

Real time PCR was carried out in an ABI7500 thermocycler (Applied Biosystems, Warrington, UK). For PAI-1 Precision FAST 2x real time PCR master mix with SYBRgreen was used. For GAPDH (the reference gene) Precision FAST 2x real time PCR master mix was used with 5'-FAM, 3'-TAMRA double dye probes. Primers and intron-spanning probes were designed using Primer Express v3.0 software (Applied Biosystems, Warrington, UK) by Prof Rod Dimaline (Table 2.3).

All assays included a no template control and a standard curve, which was developed using serial dilutions of cDNA template corresponding to the relevant gene amplicon, ligated into pGEM-T Easy (Promega). For all assays the correlation coefficient of the slope of standard curve was greater than 0.97 and the PCR amplification efficiency was between 90–110% (calculated from the log-linear part of the standard curve as being between -3.6 and -3.1). For PAI-1 assays the dissociation curve was examined and found to contain a single narrow peak. Each sample was assayed in triplicate and PAI-1 mRNA abundance was determined based on expression relative to GAPDH.

Primer/Probe	Sequence
hGAPDH probe	CGT CGC CAG CCG AGC CAC A
hGAPDH forward	GCT CCT CCT GTT CGA CAG TCA
hGAPDH reverse	ACC TTC CCC ATG GTG TCT GA
hPAI 1 probe	AGT TCA ACT ATA CTG AGT TCA CCA CGC CCG
hPAI 1 forward	TGC CCA TGA TGG CTC AGA
hPAI 1 reverse	GCA GTT CCA GGA TGT CGT AGT AAT G

Table 2.3. Primers and probes used in qPCR experiments. PAI-1 and GAPDH (as the reference gene) were assayed.

2.2.16 Organotypic co-cultures

The protocol was adapted from a previously described organotypic co-culture system (217). Gels were prepared by mixing 350µl Matrigel™, 350µl collagen, 100µl 10 x DMEM solution, 100µl FBS and 5 x 10^5 myofibroblasts suspended in 100µl FM, leading to a final gel volume of 1ml. Treatments were applied to the gel at appropriate concentrations. Reagents, tubes and pipettes were cooled on ice to facilitate handling of the Matrigel™ and collagen. The resulting 1ml solutions were transferred to wells of a 24-well plate and allowed to polymerise at 37°C for 30 min. FM (1ml/well) was then added to the top and left overnight at 37°C. The next day, FM was aspirated and 2 x 10^6 MKN45 cells suspended in 100µl of FM were added dropwise to the top of the gel, and the gel incubated overnight at 37°C. The following day gels were removed from the 24-well plate and transferred to the top of collagen-coated gauze squares resting on steel grids in 6-well plates. The steel grids allowed the gel to sit 5mm higher than the bottom of the well. FM (with treatments as appropriate) was added to the bottom of the well until it reached the undersurface of the steel grid, allowing the epithelial layer to remain at an air-liquid interface (Figure 2.3). Medium was replaced every 2 days and the gels incubated at 37°C throughout. After 2 weeks, gels were bisected and fixed in 4% PFA in PBS for 24 h. They were then transferred to 70% ethanol and embedded in paraffin for histology by the Department of Pathology, School of Veterinary Science, University of Liverpool and the Department of Cellular Pathology, Royal Liverpool University Hospital. Quantification of the invasive front of MKN45 cells was performed using ImageJ software.

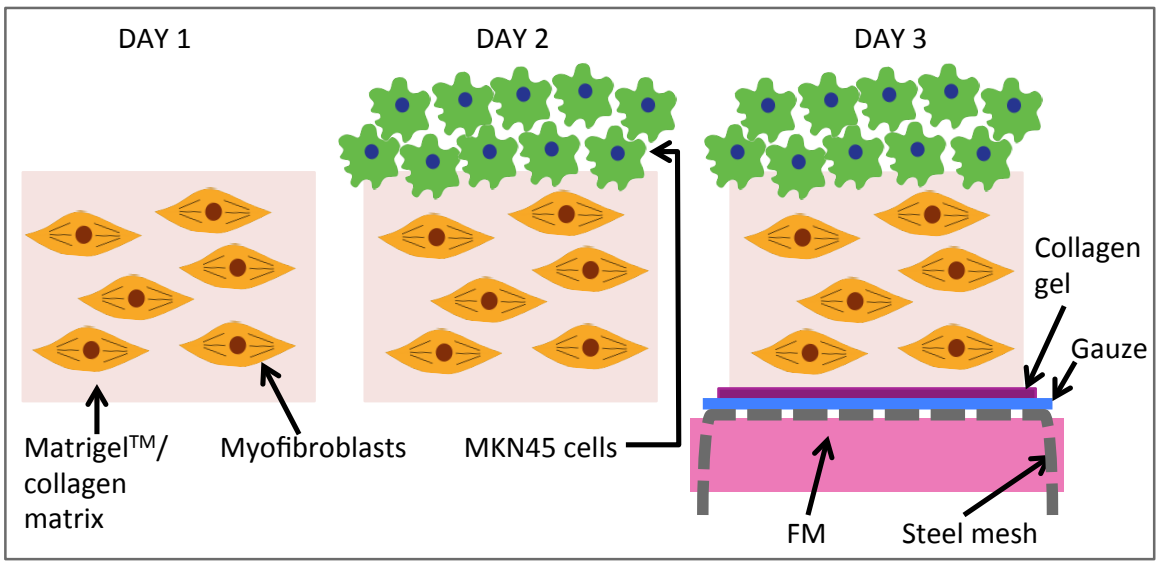

Figure 2.3. Schematic showing the process of creating the 3-D organotypic co-culture system. Myofibroblasts were seeded into a Matrigel/collagen matrix and left overnight. MKN45 cells were added to the top and left overnight. On day 3, the gel culture was transferred to an air-liquid interface. This was achieved by placing the gel on top of a collagen-soaked gauze on a steel mesh platform. FM was then added to the level of the gauze and replaced every 48 hours for 2 weeks.

2.2.17 Luciferase promoter-reporter assays

A PAI-1-luciferase promoter-reporter construct was generated using a 4.5kb fragment of the human PAI-1 promoter generated by PCR of human genomic DNA and cloned into the firefly luciferase reporter construct pXP2 as previously described (183). AGS cells (2 x 10^5 per well) were plated into wells of a 6-well plate in FM and allowed to adhere overnight. The following day, cells were washed in PBS 3 times and cells were co-transfected with PAI-1-luc (0.25ng/well) and a constitutively active *Renilla* luciferase reporter (phRL-SV40, 0.5ng/well) by TransFast™ (see 2.2.9) in SF medium for 1 h. After transfection 2ml of FM were added to each well and 24 h later cells were washed 3 times in PBS. Cells were then incubated in SF medium or CM for 6 h. SF medium containing 100nM PMA, which is known to stimulate PAI-1 expression (218), was used as a positive control (Figure 2.4). Cells were washed in PBS, 500µl/well of lysis buffer was added and the plate was placed on a shaker for 30 min. Lysates (20µl) were transferred to a tube and luciferase activity was measured using a dual luciferase reporter assay on a Lumat LB9507 luminometer (Berthold Technologies, Redbourne, Herts, UK) according to the manufacturer's instructions. Assays were performed in duplicate and the mean result calculated. Results were normalized to *Renilla* activity.

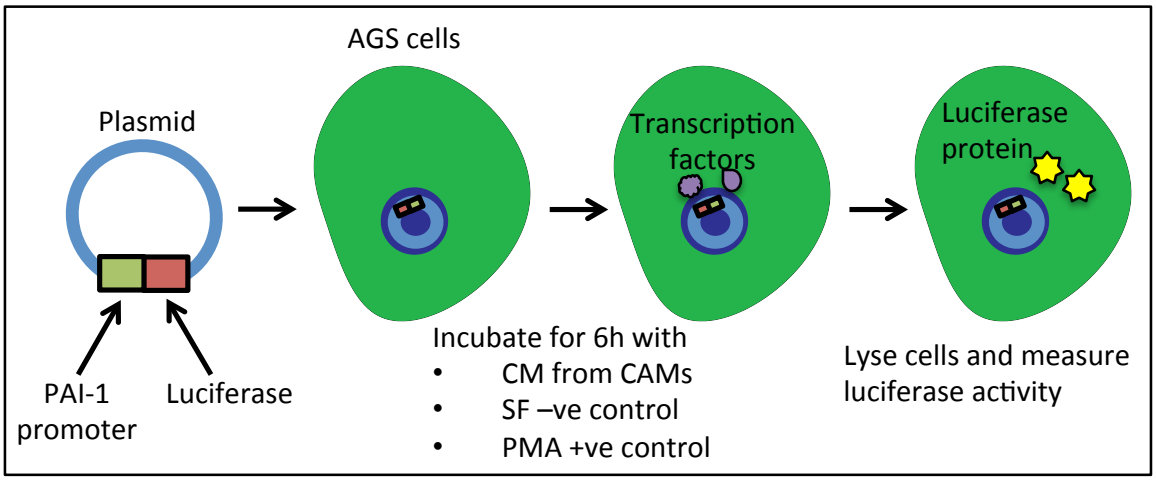

Figure 2.4. Schematic illustrating principle of the luciferase promoter-reporter assay. A plasmid encoding a region of the human PAI-1 promoter and luciferase was transfected into AGS cells. These were then incubated with SF control, putative stimulators of PAI-1 transcription (e.g. CM) and PMA as a positive control. If transcription factors bound to the PAI-1 promoter, luciferase was transcribed and translated. Luciferase activity was measured in a luminometer.

2.2.18 Statistics

Results are expressed as mean ± standard error of the mean (SE) unless otherwise stated. Student's t-test and one-way analysis of variance (ANOVA) were used to determine the significance of results with significance defined as $p=<0.05$, unless otherwise stated. Vertical lines represent SE and horizontal lines with asterisks denote statistical significance unless otherwise stated. Graphs and statistics were produced using GraphPad Prism version 5.0 software.

CHAPTER 3: PAI-1 EXPRESSION IN GASTRIC CANCER CELLS AND MYOFIBROBLASTS

3.1 Introduction

Members of the uPA system are known to play a role in carcinogenesis and frequently overexpression of these proteins is associated with a more invasive phenotype and a poor prognosis (219). The role of PAI-1, however, remains unclear as it acts both as a promoter of carcinogenesis as well as a protective factor (220). In gastric cancer, the role of PAI-1 also remains poorly defined although there is evidence to show that PAI-1 is overexpressed (221). It is unclear whether high PAI-1 expression in gastric cancer is stromal or epithelial and this study aims to define PAI-1 expression in gastric myofibroblasts compared with two gastric cancer cell lines, AGS and MKN45. The effect of PAI-1 overexpression on the *in vitro* and *in vivo* behaviour of gastric cancer cells was then assessed in an effort to characterise the role of PAI-1 in gastric cancer.

Stromal-epithelial signalling relies on the release of soluble mediators capable of affecting the behaviour of neighbouring cells. The stimulus for increased PAI-1 expression in stomach has not been demonstrated and this study has examined the role of soluble mediators released from myofibroblasts and gastric cancer cells in modulating PAI-1 expression. PAI-1 is a secreted molecule and is known to affect cell

migration and invasion *in vitro* (222). This study examined the effect of PAI-1 on gastric cancer cell and myofibroblast cell behaviour.

3.1.1 Aims

1. To determine the relative abundance of PAI-1 in gastric cancer cells and myofibroblasts.
2. To study the effect of soluble mediators produced by cancer cells or myofibroblasts on PAI-1 expression.
3. To create fluorescently labelled, PAI-1 over-expressing, MKN45 cells in order to examine the effect of PAI-1 over-expression on cancer cell behaviour *in vitro* and *in vivo.*

3.2 Methods

Cell culture was performed as detailed in 2.2.1-2. Boyden chamber migration assays were described in 2.2.11. Preparation of samples and qPCR was described in 2.2.13-15. PAI-1 ELISA was carried out as outlined in 2.2.12. Luciferase assays were described in 2.2.17. Transfection of MKN45 cells was described in 2.2.9. Immunofluorescence was carried out as detailed in 2.2.6b. Scratch migration assays were performed as in 2.2.10. EdU incorporation assays were performed as outlined in 2.2.7a. Cell adhesion assays were described in 2.2.8.

3.2.1 PAI-1 ELISA

CM from CAM1, CAM11 and CAM14 was prepared as described in 2.2.1 using CM from 1.2 x 10^7 MKN45 cells in 12ml SF medium and collected 24 h later. The Imubind Tissue PAI-1 ELISA kit (American Diagnostica, Stamford, CT) was used according to the manufacturer's instructions.

3.2.2 Organotypic invasion assay

MKN45, MKN45 E2-C cells and MKN45 E2-C PAI-1 cells were added dropwise to the top of gels seeded with CAM4 on day 2 as described in 2.2.16.

3.2.3 Subcutaneous xenografts

MKN45, MKN45 E2-C cells and MKN45 E2-C PAI-1 cells (5 x 10^5 per mouse) were injected subcutaneously in the left flank as described in 2.2.4.

3.3 Results

3.3.1 Increased expression of PAI-1 in CAMs compared with cancer cells.

In order to establish the relative expression of PAI-1 in gastric cancer cells and myofibroblasts, mRNA abundance was determined by qPCR and secreted PAI-1 protein was quantified by ELISA of CM. Expression of PAI-1 mRNA was higher in CAMs (CAM1, CAM11 and CAM14) than in AGS cells (Figure 3.1**A**). Moreover, the concentration of PAI-1 in media from these CAMs was higher than in MKN45 cell media (Figure 3.1**B**).

To determine whether stromal-epithelial interactions influenced PAI-1 expression, CAMs (CAM1, CAM11 and CAM14) were treated with CM from MKN45 or AGS cells and the effect on PAI-1 mRNA abundance was quantified by qPCR (Figure 3.1**C**). PAI-1 expression in CAMs did not change significantly in response to CM from MKN45 cells. Treatment with CM from AGS cells resulted in a 1.3-fold increase in PAI-1 mRNA abundance, although this did not reach statistical significance. As an alternative approach, the expression of a PAI-1-luc promoter reporter construct transfected into AGS cells was examined. In transfected AGS cells treated with CM from myofibroblasts (3 NTMs or CAMs 3, 4, 10, 11 and 14) there appeared to be a decrease in PAI-1-luc expression compared with control, but this did not achieve statistical significance (Figure 3.1**D**). These data suggest that soluble factors derived from cancer cells or myofibroblasts do not affect PAI-1 transcription or expression.

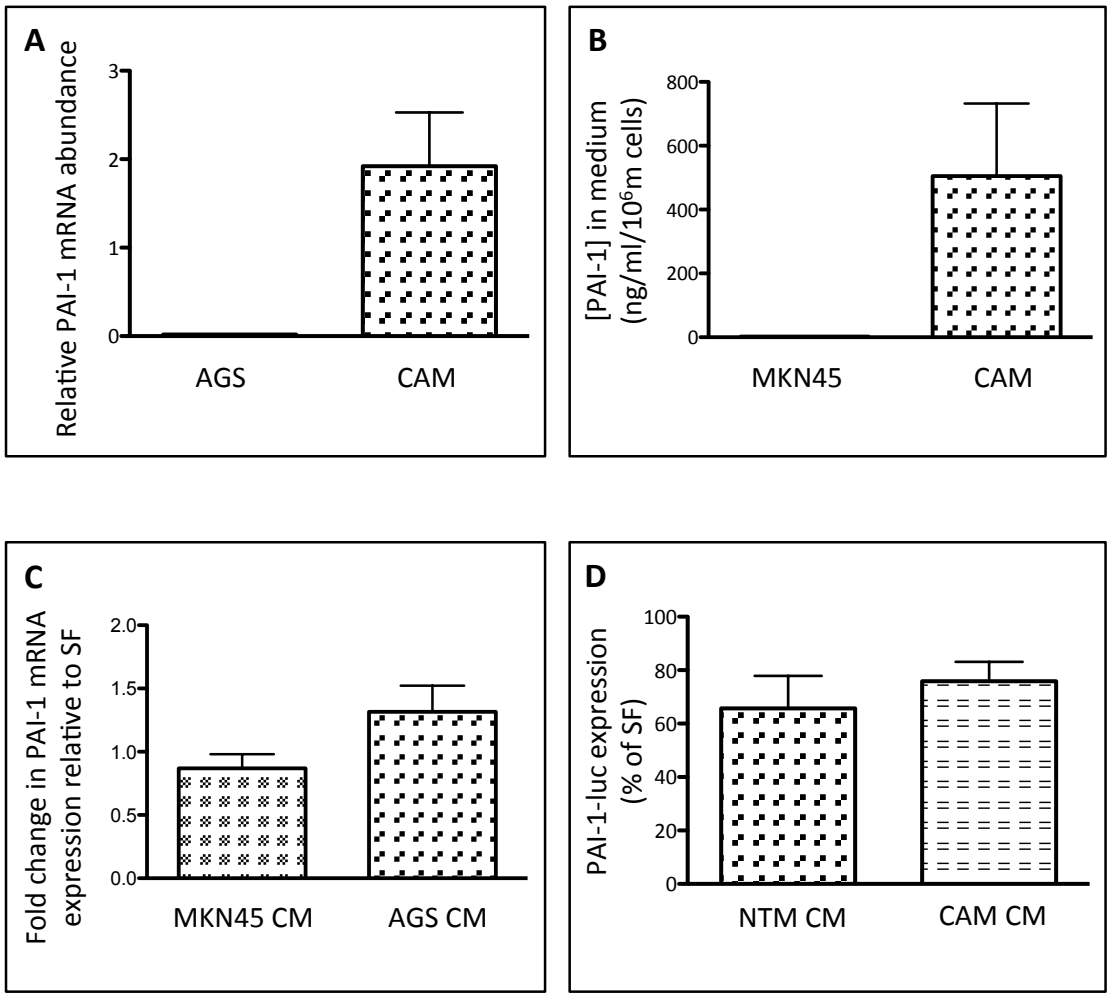

Figure 3.1. Increased expression of PAI-1 in CAMs compared with cancer cells. A, PAI-1 mRNA expression determined by qPCR and expressed relative to GAPDH mRNA expression is elevated in CAMs (n=3 independent lines) compared to AGS cells. **B,** Higher concentrations of secreted PAI-1 assessed by ELISA in the medium of CAMs (n=3 independent lines) compared to MKN45 cells, normalised to cell number. **C,** PAI-1 mRNA expression in CAMs 1, 11 and 14 is not significantly changed in response to CM from gastric cancer cell lines. PAI-1 mRNA abundance relative to GAPDH mRNA is expressed as a fold change compared to SF medium. **D,** PAI-1-luc expression in AGS cells is unchanged in response to CM from NTMs (n=3 independent lines) and from CAMs (n=4 independent lines). The mean of 2-3 experiments is shown.

3.3.2 PAI-1 suppresses migration of AGS cells and CAMs but stimulates migration of NTMs.

In order to investigate the effect of PAI-1 on the migration of cancer cells and myofibroblasts, PAI-1 was added to the bottom well in Boyden chamber assays. AGS cells were used for these experiments, as MKN45 cells do not exhibit transwell migration in this type of assay. Addition of 50nM of human recombinant PAI-1 almost completely suppressed migration of AGS cells (Figure 3.2**A**). Similarly PAI-1 suppressed migration of CAM14 cells, although in this case the reduction was approximately 50% of that in SF medium (Figure 3.2**B**). However, when NTMs were used in the assay, PAI-1 had the opposite effect, stimulating cell migration 6-fold (Figure 3.2**C**).

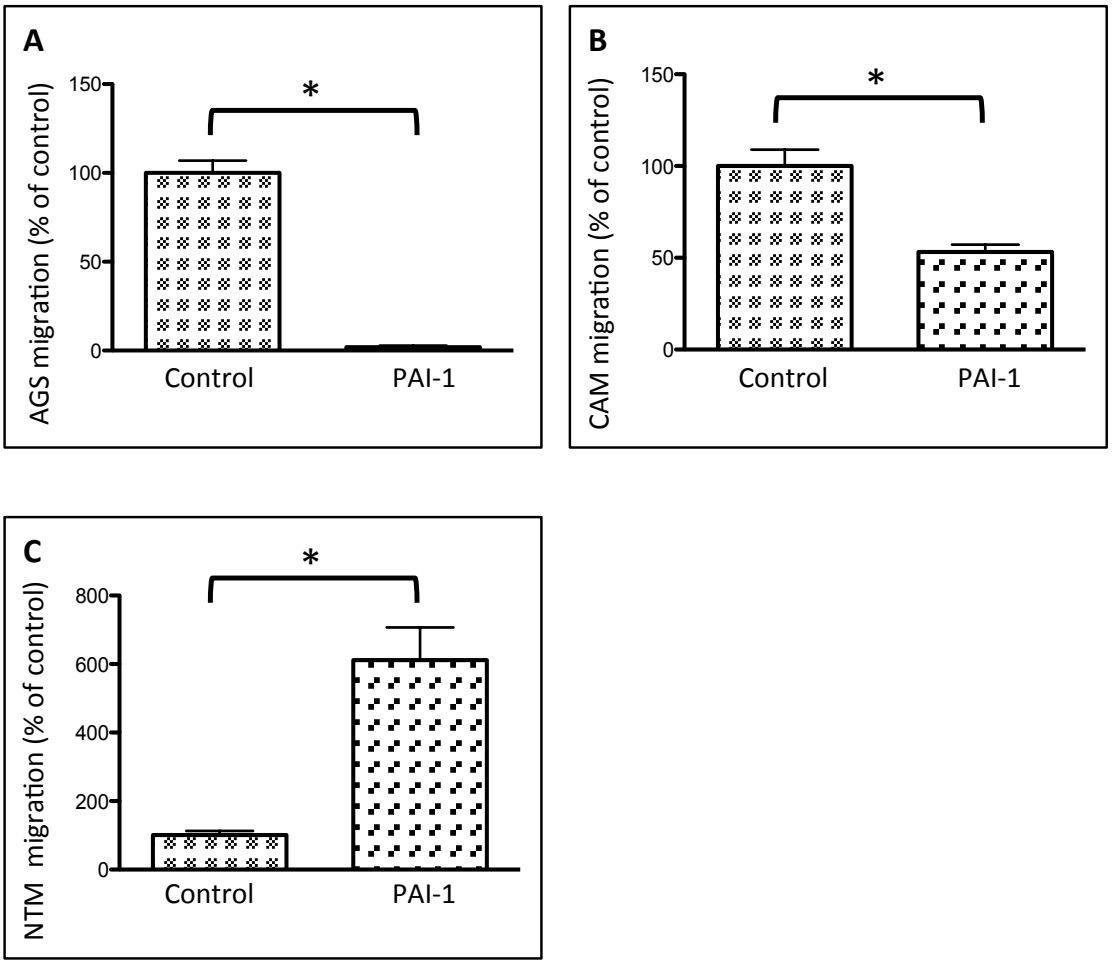

Figure 3.2. PAI-1 suppresses migration of AGS cells and CAMs but stimulates migration of NTMs. A, Recombinant human PAI-1 (50 nM) suppresses cell migration in AGS cells in a Boyden chamber assay expressed relative to control (SF medium: mean ± SE, 105 ± 7 cells per field). **B,** PAI-1 suppresses cell migration in CAM14 cells in a Boyden chamber assay relative to control (119 ± 5 cells per field). **C,** PAI-1 stimulates migration of NTMs relative to SF control (196 ± 17 cells per field). The mean of 3 experiments is shown.

3.3.3 MKN45 E2-C cells can be visualised by fluorescence microscopy and using FMT.

MKN45 E2-C cells were visualised in culture under a TRITC filter. The intensity of fluorescence was heterogeneous within the cell population but the majority of cells appeared red (Figure 3.3**A**). Varying concentrations of cells were suspended in droplets of PBS and these were visualised using FMT, in the 635nm channel (Figure 3.3**B**). The droplet containing the highest number of cells exhibited the highest fluorescence. Untransfected MKN45 cells exhibited fluorescence comparable to PBS containing no cells (data not shown).

In vivo, xenografts composed of MKN45 cells transfected with E2-C (with or without PAI-1) were more fluorescent than those composed of MKN45 cells alone (Figures 3.4 and 3.5). The 15-120-fold increase in fluorescent signal due to the transfection of E2-C shows that it is possible to grow and quantify fluorescent xenografts. In order to eliminate any changes in fluorescent signal owing to differences in tumour size, animals were imaged when the tumours reached comparable sizes. No significant difference was observed in tumour volume at the time of imaging in this experiment (Figure 3.4**D**), although differences in the rate of tumour growth due to the overexpression of PAI-1 were observed as described in 3.3.4.

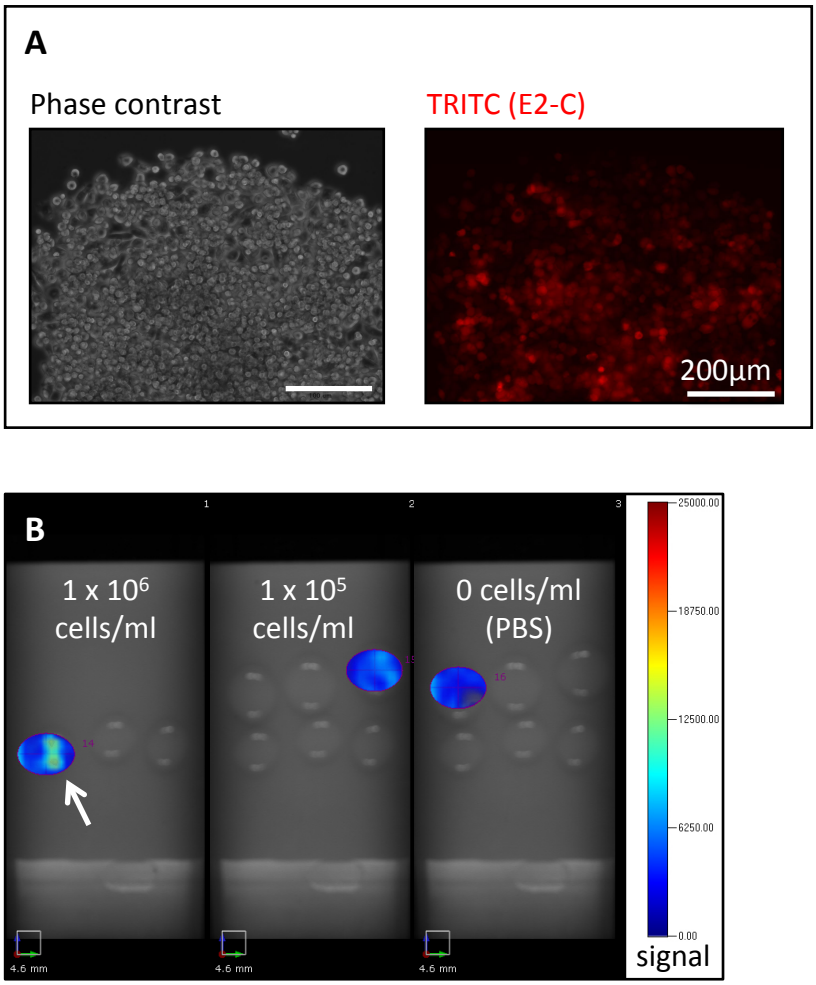

Figure 3.3. MKN45 E2-C cells can be visualised by fluorescence microscopy and using FMT. A, Representative images of MKN45 E2-C cells in culture viewed under phase contrast microscopy (left) and under fluorescence microscopy (right). **B,** Representative images of droplets of MKN45 E2-C cells imaged using FMT demonstrates higher fluorescence in the droplet containing the highest concentration of cells (arrow).

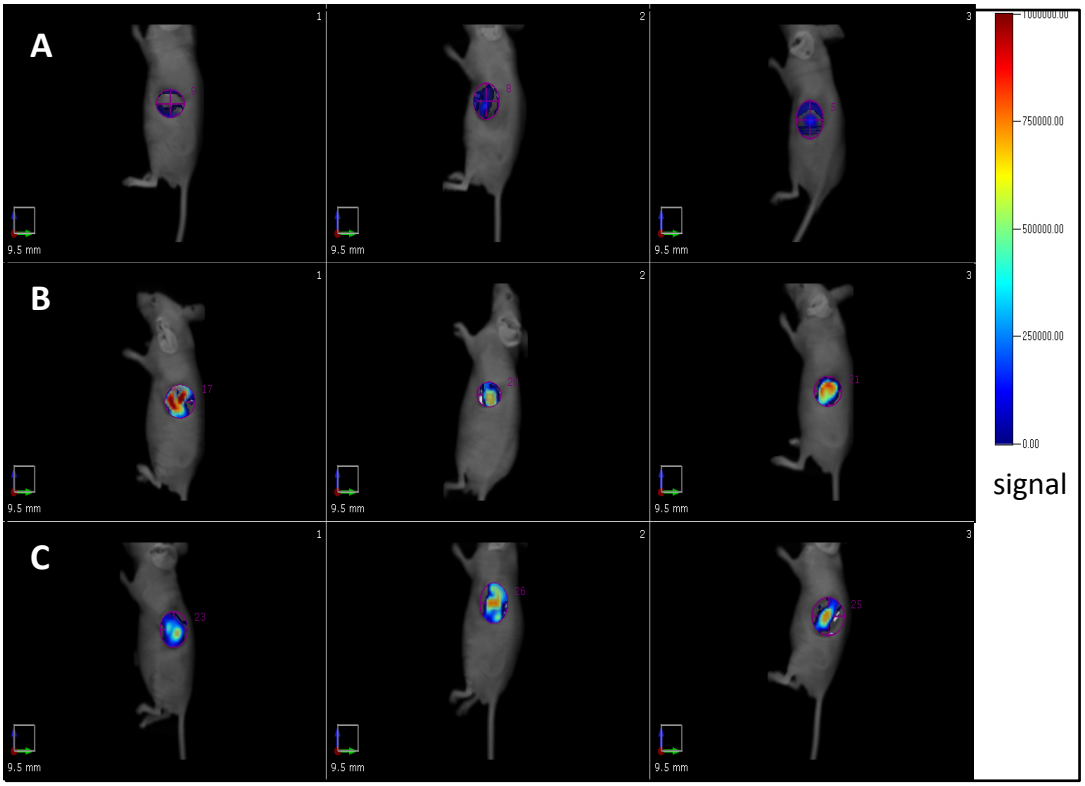

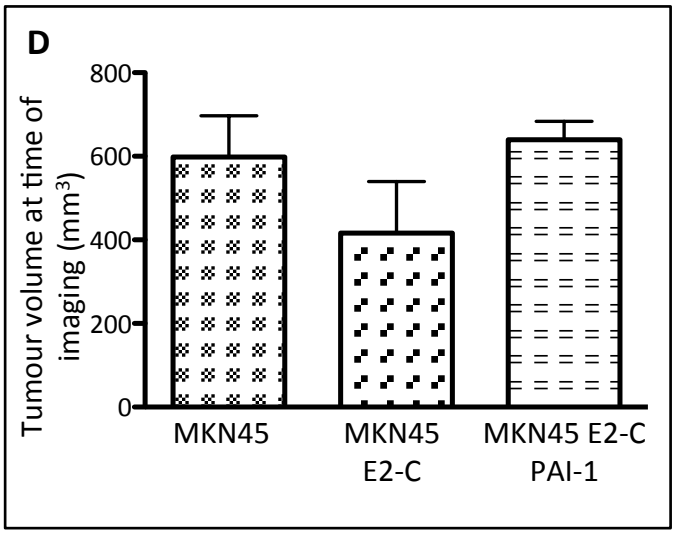

Figure 3.4. Xenografts composed of MKN45 E2-C cells fluoresce at 635nm and this is captured by FMT. A-C, Representative FMT images at 635 nm of subcutaneous xenografts composed of MKN45 cells (**A**), MKN45 E2-C cells (**B**) and MKN45 E2-C PAI-1 cells (**C**) demonstrating higher signal in the xenografts composed of cells transfected with E2-C. **D,** Tumours did not have significantly different volumes at the time of imaging. Mean results from 4-5 animals are shown; results were not statistically significantly difference by one-way ANOVA.

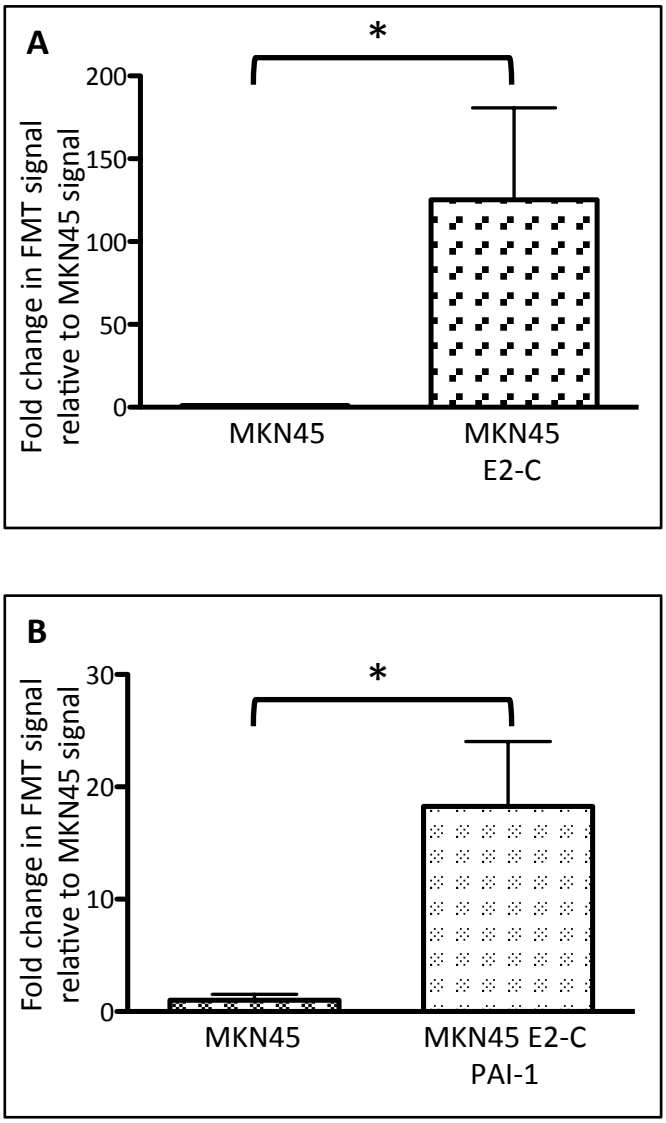

Figure 3.5. Subcutaneous xenografts transfected with E2-C cells fluoresce at 635nm. A, Quantification of FMT signal in MKN45 E2-C xenografts (right) relative to MKN45 xenografts (left). **B,** Quantification of FMT signal in MKN45 xenografts (left) compared to MKN45 E2-C PAI-1 xenografts (right). Mean results from 4-5 animals are shown; horizontal bars denote statistical significance at $p<0.05$ by Mann-Whitney test.

3.3.4 Transfection of MKN45 cells with a PAI-1 over-expressing plasmid results in higher PAI-1 expression

As MKN45 cells normally express low amounts of PAI-1 the consequences of over-expressing PAI-1 were studied as a model for elucidating the role of PAI-1 expression in gastric cancer cells. This approach made it possible to study MKN45 cell function in response to increased autocrine PAI-1 without the influence of other soluble mediators secreted by myofibroblasts. Thus MKN45 cells were stably transfected with either the fluorescent protein E2-C alone or in combination with PAI-1. Transfection with E2-C enabled colonies composed of transfected cells to be identified and selected under the microscope (and was also used as a marker in subsequent xenograft studies). As expected, MKN45 E2-C PAI-1 cells exhibited higher PAI-1 mRNA expression than their MKN45 E2-C counterparts (Figure 3.6**A**). Moreover, immunofluorescence for PAI-1 in MKN45 E2-C PAI-1 cells demonstrated more intense fluorescence than either MKN45 cells or MKN45 E2-C cells (Figure 3.6**B**).

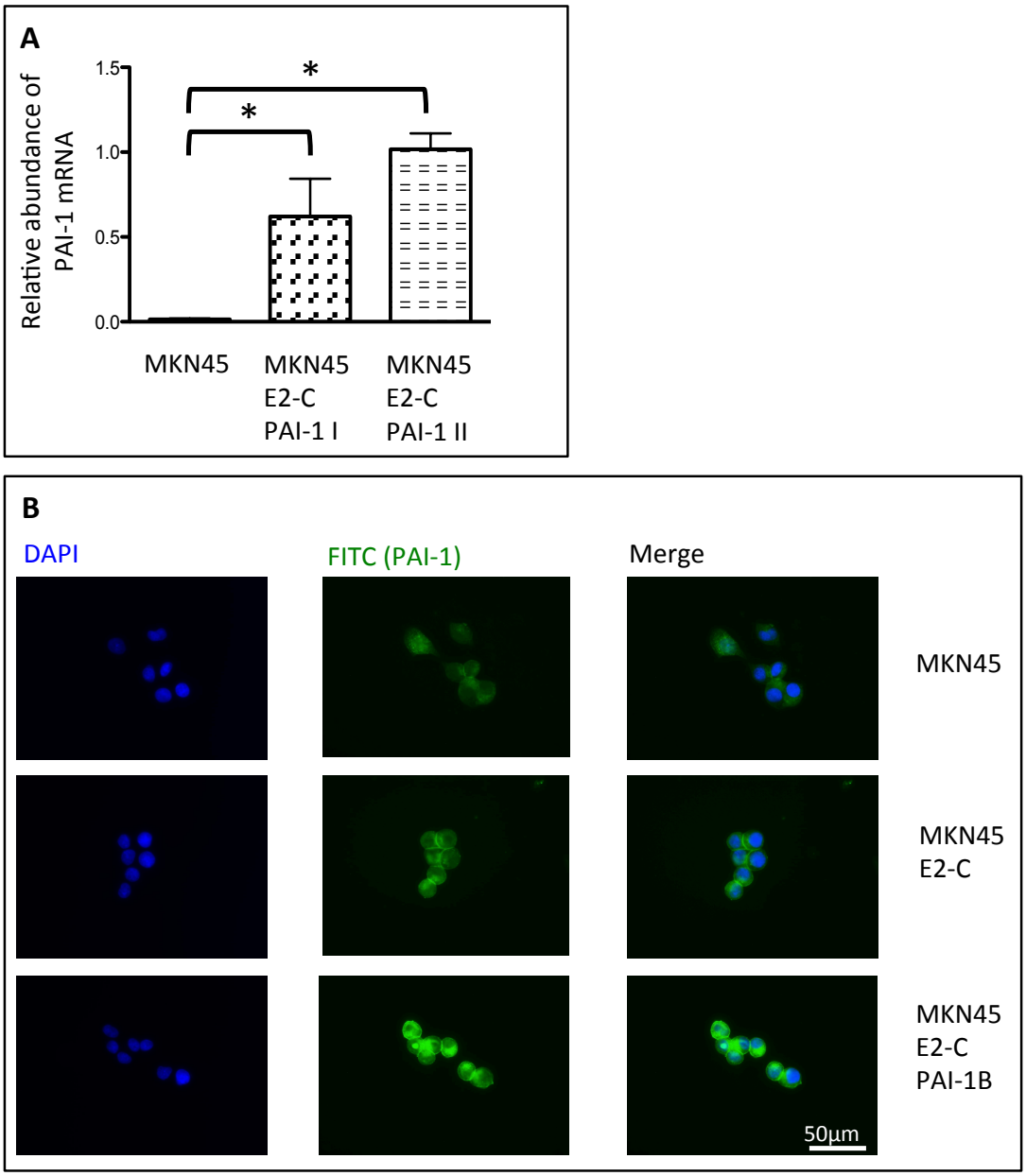

Figure 3.6. Transfection of MKN45 cells with a PAI-1 overexpressing plasmid results in higher PAI-1 expression. A, PAI-1 mRNA expression is elevated in 2 separate transfections (I and II) of human PAI-1 plasmid into MKN45 cells. The mean of 3 experiments is shown. **B,** Representative immunocytochemistry images showing higher intensity PAI-1 staining in MKN45 E2-C PAI-1 cells (bottom row) compared to control MKN45 cells (top row) or MKN45 E2-C cells (middle row). Left panels show nuclear staining with DAPI, centre panels show PAI-1 localisation using FITC-labelled secondary antibody, right panels show merged images.

3.3.5 Transfection with PAI-1 has no effect on cell migration.

The effect of PAI-1 overexpression on cell migration was assessed using scratch migration assays (Figure 3.7**A**). Comparison of MKN45 E2-C cells with MKN45 E2-C PAI-1 cells showed no significant difference in migration in SF medium or in FM (Figure 3.7**B**).

3.3.6 Transfection with PAI-1 has no effect on cell proliferation.

The effect of PAI-1 overexpression on cell proliferation was examined using EdU incorporation assays (Figure 3.8**A**). Comparison of proliferation in MKN45 E2-C cells with MKN45 E2-C PAI-1 cells showed no significant difference in proliferation (Figure 3.8**B**).

3.3.7 Transfection with PAI-1 decreases cell adhesion and this is inhibited by vitronectin.

The effect of overexpression of PAI-1 in MKN45 cells on cell adhesion was assessed using an *in vitro* assay of cell adhesion. Transfection of PAI-1 resulted in decreased cell adhesion (Figure 3.9**A**). However, when the assay was performed on vitronectin-coated plates, PAI-1 overexpressing cells exhibited increased adherence (Figure 3.9**B**).

3.3.8 Transfection with PAI-1 has no effect on invasion in an organotypic assay.

In order to assess cell invasion in a system which reflects the three-way interaction of cancer cells, myofibroblasts and extracellular matrix which occurs *in vivo*, an

organotypic co-culture system was developed (see chapter 5). Overexpression of PAI-1 in MKN45 cells did not affect invasion into the gel layer seeded with myofibroblasts after 2 weeks (Figure 3.10**A**).

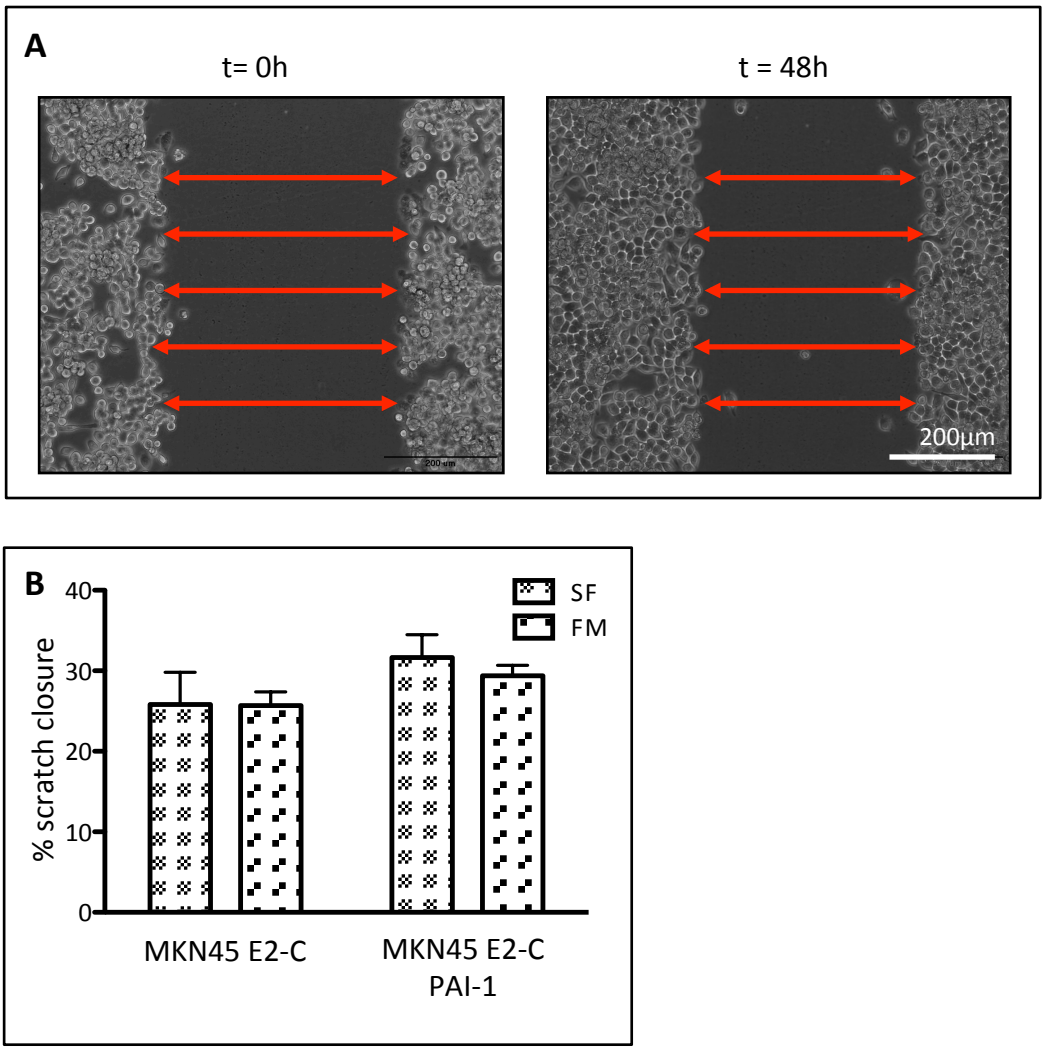

Figure 3.7. Transfection with PAI-1 has no effect on cell migration. A, Representative example illustrating the method for quantification of scratch migration assays; the mean percentage scratch closure across 10 measurements of scratch width (red arrows, 5 points shown) per well after 48 h was determined. **B,** Cell migration in serum-free media (SF) or in full media (FM) is not significantly different in MKN45 E2-C cells (left) and MKN4545 E2C PAI-1 cells (right) by transfection with PAI-1. The mean of 3 experiments is shown.

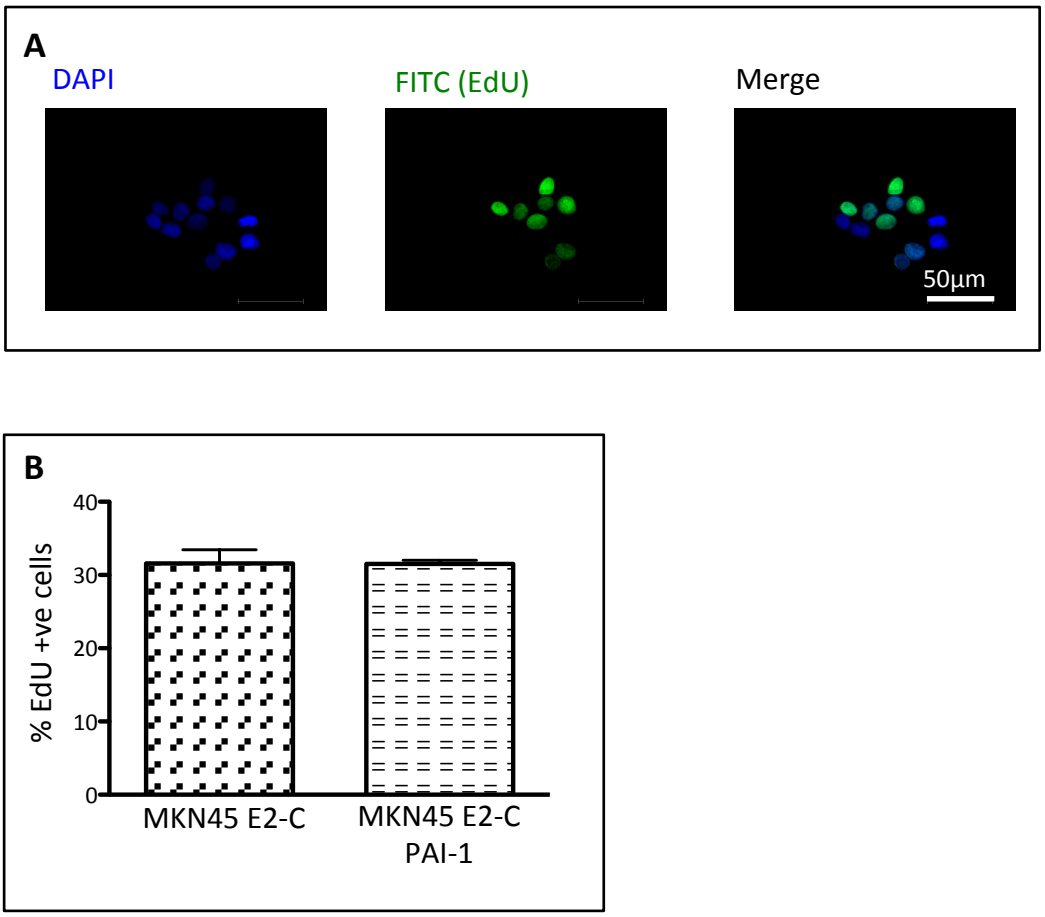

Figure 3.8. Transfection with PAI-1 has no effect on cell proliferation. A, Representative images showing EdU incorporation; quantification is performed by calculation of the percentage of EdU positive nuclei. **B,** Cell proliferation is not significantly different in MKN45 E2-C cells (left) and MKN4545 E2C PAI-1 cells (right). The mean of 3 experiments is shown.

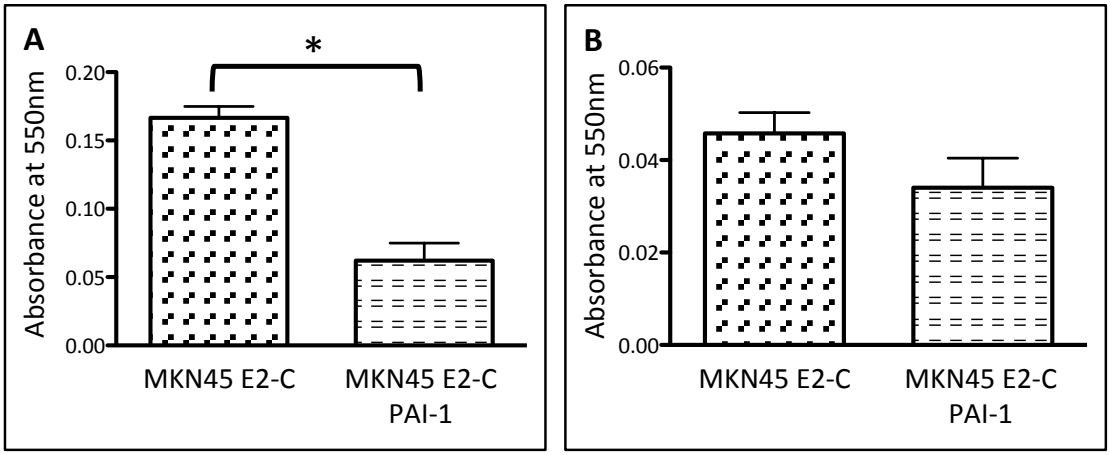

Figure 3.9. Transfection with PAI-1 decreases cell adhesion and this is inhibited by vitronectin. A, Adhesion is significantly lower in MKN45 E2C PAI-1 cells (right) compared with MKN45 E2C cells (left). **B,** Adhesion is not significantly different in MKN45 E2-C cells (left) and MKN45 E2C PAI-1 cells (right) if the assay is performed on vitronectin-coated plates. The mean of 3 experiments is shown.

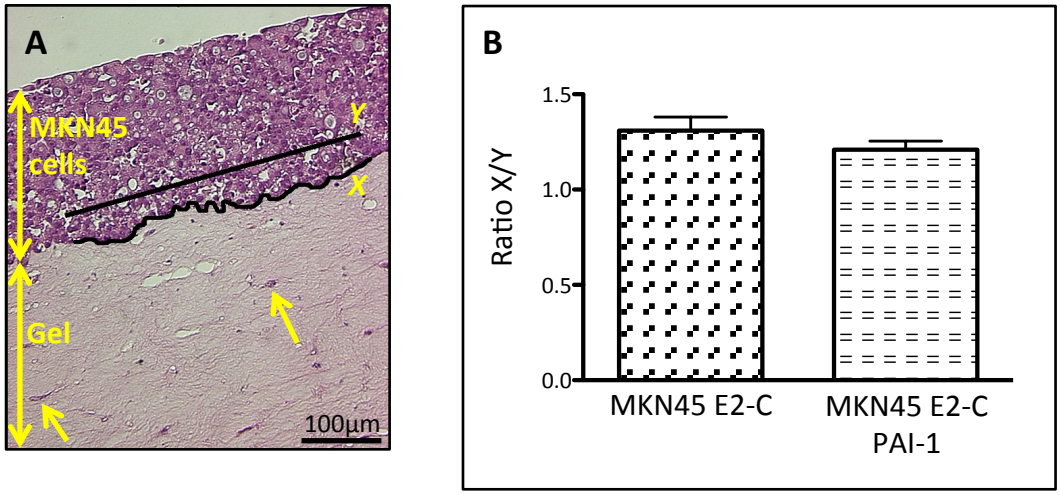

Figure 3.10. Transfection with PAI-1 has no effect on invasion in an organotypic assay. A, Representative image of an organotypic culture, showing calculation of invasion using the ratio of length of a line drawn along the interface between cells and the gel (***X***) to the length of a straight line (***Y***). Arrows indicate myofibroblast nuclei within the gel. **B,** Invasion in an organotypic culture is not significantly different in MKN45 E2-C cells (left) and MKN45 E2C PAI-1 cells (right). Results from 3 experiments are shown.

3.3.9 Transfection with PAI-1 increases in vivo tumour growth

To examine the effect of PAI-1 overexpression on *in vivo* tumour growth subcutaneous xenografts were established in BALB/c nu/nu mice. MKN45 cells overexpressing PAI-1 grew to a larger volume than those transfected with E2-C alone (Figure 3.11**A**).

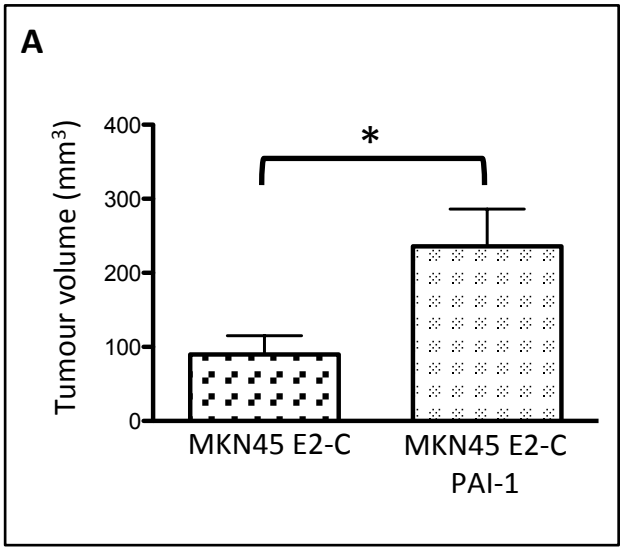

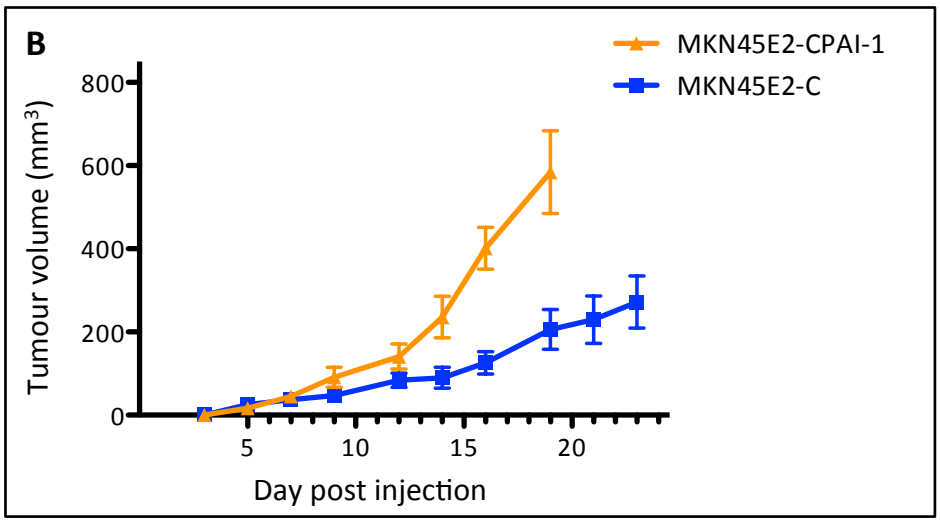

Figure 3.11. Transfection with PAI-1 increases *in vivo* tumour growth. A, In a subcutaneous xenograft model in BALB/c nu/nu mice, MKN45 cells transfected with PAI-1 exhibited higher tumour volume at day 14 compared with MKN45 E2-C cells. **B,** Increased tumour growth of xenografts composed of MKN45 E2-C PAI-1 cells compared to MKN45 E2-C cells. Results from 4-5 animals are shown.

3.4 Discussion

The results in this chapter show that CAMs are the principal source of PAI-1 in a model of stromal-epithelial interaction in gastric cancer. The use of CM has shown that soluble mediators from one cell type do not affect PAI-1 expression in the other type. PAI-1 exhibited differing effects on cell migration; it suppressed the migration of AGS cells and CAMs but enhanced migration of NTMs. Interestingly, when PAI-1 was overexpressed in MKN45 cells this did not alter cell proliferation, migration or invasion but did decrease cell adhesion and *in vivo* in a xenograft model there was increased tumour growth.

Two different gastric cancer cell lines exhibited low expression of PAI-1. *In vivo*, however, there is a well-recognised link between PAI-1 overexpression in gastric cancer cells and disease progression (102). To model this experimentally, MKN45 cells overexpressing PAI-1 were therefore generated in an attempt to recapitulate increased PAI-1 expression in a cell-autonomous manner. It is possible that the PAI-1 secreted by PAI-1 overexpressing MKN45 cells differs in activity compared with PAI-1 secreted endogenously. Although the use of gastric cancer cell lines has allowed us to use a homogenous cell population, it is important to understand that cell lines are prone to genotypic and phenotypic drift during continuous culture and that this may mean they no longer possess the same characteristics of the tissue of origin.

The experimental approach to study cell migration involved scratch migration assays and Boyden chambers. Scratch migration assays study cell movement into an empty space in 2 dimensions, while Boyden chambers measure a chemotactic response as cells migration along a concentration gradient. Scratch wound assays can be used for both MKN45 and AGS cells, but MKN45 cells do not migrate in Boyden chambers. The organotypic co-culture system replicates more accurately the movement of tumour cells *in vivo*, by modelling the interactions between cancer cells, myofibroblasts and extracellular matrix. Regardless of the experimental approach used to study cell movement, no difference in cell migration was observed as a result of PAI-1 overexpression.

The EdU proliferation assay allows studies of those cells in a population that are in the S-phase of the cell cycle. It is worth stressing that this does not necessarily represent tumour growth which reflects the balance of cell proliferation and cell death. This investigation did not examine apoptotic cells which would merit further work in the future. Nevertheless *in vivo* in a xenograft model, the PAI-1 over-expressing cells were associated with increased tumour growth. Taking the two observations together, it would appear that the link between PAI-1 and tumour growth is not directly attributable to increased cancer cell proliferation.

In gastric cancer, high PAI-1 expression has been shown to be a marker of advanced tumour stage (104), although not all studies are in agreement (223,224). This may arise from differences in the methods of quantification and the source of PAI-1 studied. Some studies have examined PAI-1 expression in the tumour tissue by

ELISA, although this approach does not distinguish between PAI-1 of cancer or stromal cell origin (104,221). Others have visualised PAI-1 expression by immunohistochemistry and only quantified staining in the cancer (epithelial) cells (220). In other cancers, PAI-1 expression has been localized to the stroma (225), the epithelial cells (226) or to both the stromal and epithelial compartments (227). Our data show high PAI-1 expression in cultured stromal cells and low expression in cultured cancer cells. Interestingly, there was no evidence for cross-talk between cancer cells and myofibroblasts with respect to control of PAI-1 expression. Moreover, although PAI-1 expression in MKN45 E2C PAI-1 cells remained relatively low compared with myofibroblasts, it was still sufficient to enhance tumour growth *in vivo*.

The uPA system is part of a cascade of extracellular proteases capable of exerting effects on cell migration, adhesion and invasion. When activated by binding to uPAR, uPA cleaves its main substrate plasminogen, which in turn cleaves proteins in the ECM, releasing growth factors and MMPs, and triggers the fibrinolytic cascade. This promotes cell detachment, migration and invasion (215,228). PAI-1 is the main physiological inhibitor of uPA, and it is able to suppress cell migration and invasion by inhibiting proteolysis (229). PAI-1 is also able to interact with integrins, vitronectin and lipoprotein receptor-related protein 1 (LRP-1) (230), which enables it to influence intracellular signalling cascades which in turn lead to a range of uPA-independent effects on cell behaviour, which may be in opposition to those occurring as a result of decreased extracellular proteolysis. The net influence of PAI-

1 both in experimental and in clinical conditions is therefore presumably the result of a balance between uPA-related and uPA-independent interactions.

We did not show any effect of PAI-1 overexpression on cell migration. In the literature, reports about the role of PAI-1 in cell migration are conflicting (231,232). PAI-1 overexpression would be predicted to decrease cell migration through its ability to suppress proteolysis, but even when it does, the mechanism may not be uPA-dependent (233).

An example of PAI-1's uPA–independent effects lies in its interaction with vitronectin. Vitronectin is a component of the extracellular matrix capable of binding both to PAI-1 (92) and uPAR (234). This interaction enhances the activity of PAI-1 by stabilizing its active conformation, leading to more effective inhibition of proteolysis. Its binding to uPAR stabilizes the cell's connection to the ECM, making it less able to de-adhere.

Our results show in the presence of vitronectin, the decreased adhesion of PAI-1 overexpressing cells was partially reversed. This is in agreement with published data, where stable transfection of PAI-1 enhanced vitronectin binding and increased cell adhesion (235). It may be that when the adhesion assay is performed on vitronectin, the cell membrane-associated uPAR binds to it, keeping the cell anchored to the extracellular matrix and therefore less able to de-adhere. Without vitronectin however, we observed a decrease in cell adhesion when PAI-1 was overexpressed in cancer cells. PAI-1 has previously been shown to decrease cell

adhesion by its ability to disrupt the interaction between uPAR and integrins when it is bound to the uPA-uPAR complex (236). It remains uncertain whether or not this effect contributes to the *in vivo* finding that PAI-1 overexpression resulted in increased xenograft growth. In particular, xenograft growth is influenced by a number of factors we have not studied *in vitro*, including the role of other stromal cells (such as endothelial cells and inflammatory cells) and the response of tumours to hypoxia or acidosis.

The present results illustrate the complexity of PAI-1 in gastric cancer. Even so, the data indicate that PAI-1 expressing cancer cells promote tumour growth *in vivo* and this provides a basis for further study. In this context it is important to note, however, that there are multiple pathways involving extracellular proteolysis in cancer that remain only partially characterised. Similarly, the interactions between myofibroblasts and cancer cells *in vivo* are still incompletely understood. In both cases, it is apparent that these limitations restrict interpretation of studies on the role of PAI-1 in cancer. Subsequent studies therefore sought to address these issues.

3.5 Conclusions

1. The main source of PAI-1 in cultured cells derived from gastric cancers is the CAM.
2. CAM and cancer cell-derived soluble mediators do not alter PAI-1 expression.

3. Overexpression of PAI-1 in MKN45 cells does not alter cell migration, proliferation or invasion. PAI-1 overexpression results in decreased cell adhesion and enhances xenograft growth (Figure 3.12).

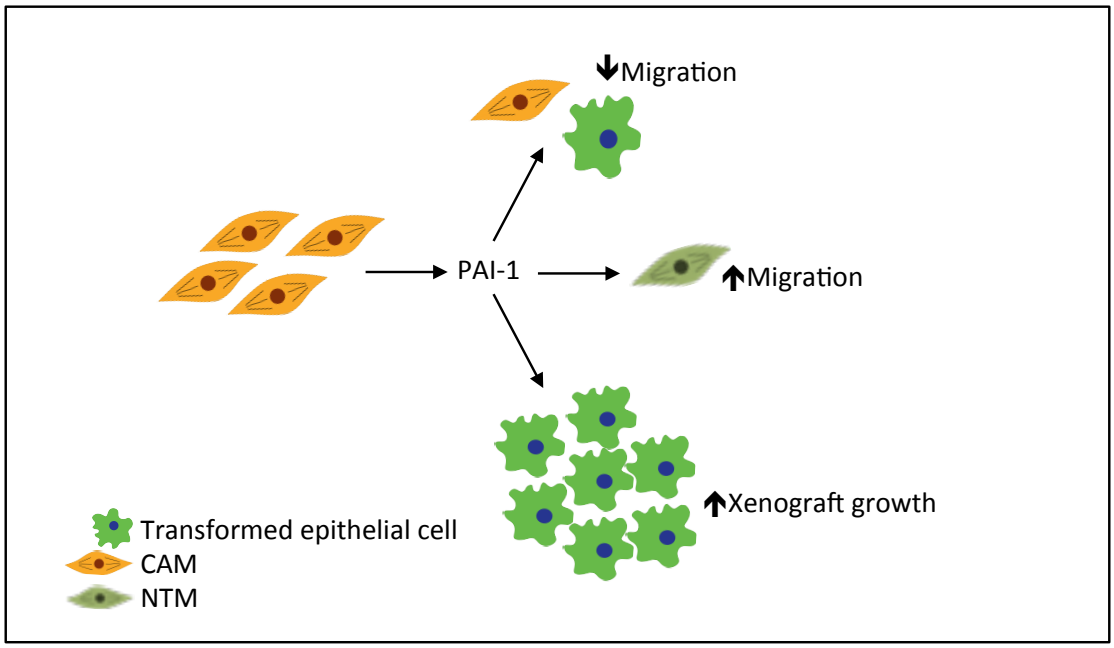

Figure 3.12. Conflicting effects of PAI-1 in gastric cancer. In gastric cancer, PAI-1 is secreted by CAMs. PAI-1 decreases the migration of gastric cancer cells and CAMs but stimulates migration of NTMs. Overexpression of PAI-1 in xenografts enhances tumour growth.

CHAPTER 4: LOCAL AND DISTANT EFFECTS OF MYOFIBROBLASTS ON TUMOUR GROWTH

4.1 Introduction

Myofibroblasts stimulate tumour growth in a variety of cancers (237). Indeed, in gastric cancer evidence from a subcutaneous xenograft study has shown that the addition of CAMs to cancer cells resulted in a larger tumour (43). The effect of myofibroblasts from normal gastric tissue or from tissue adjacent to the tumour has not yet been firmly established and this study extended the model of myofibroblast-stimulated xenograft growth to include NTMs and ATMs.

Myofibroblasts in tumours are thought to arise from the transformation of tissue fibroblasts, from epithelial-to-mesenchymal transition of cancer cells or from the influx of mesenchymal stromal cells from the bone marrow (34). This study further characterised the origin of myofibroblasts in gastric cancer xenografts with the use of species-specific staining and fluorescent labelling of cancer cells.

Little is known of the systemic effect a tumour has on the host organism. Molecules released into the circulation affect a distant organ's ability to host metastatic cells (238) or instruct the bone marrow to release cells which are then incorporated into the tumour (239). The contribution of stromal cells to the systemic effect of a

tumour remains unknown and this study begins to examine the effect of stromal-epithelial interaction on the growth of a distant tumour.

4.1.1 Aims

1. To develop and characterise a subcutaneous MKN45 xenograft system capable of revealing the effect of myofibroblasts on tumour growth.
2. To determine the effect of CAMs, ATMs and NTMs on xenograft growth.
3. To study the effect of long-range interactions between tumours.

4.2 Methods

4.2.1 Cell culture

Primary gastric myofibroblasts, MKN45 cells and AGS cells were cultured as described in 2.2.1-2.

4.2.2. Subcutaneous xenografts

Cell preparation was conducted as in 2.2.3. Aliquots of cancer cells were prepared in 100µl PBS and injected subcutaneously. When MKN45 cells were injected in combination with myofibroblasts, 1 x 10^5 cells and 5 x 10^4 myofibroblasts were used. The two cell types were mixed, centrifuged, re-suspended in PBS and administered as a single injection. For AGS cells, 5 x 10^6 AGS cells with or without 2.5 x 10^5 myofibroblasts were used. Tissues were harvested as described in 2.2.4.

4.2.3 Haematoxylin and Eosin (H&E) staining

Tissues were paraffin-embedded and processed for H&E staining by the Department of Pathology, School of Veterinary Science, University of Liverpool.

4.2.4 Immunohistochemistry

Sections were stained for Ki-67, cleaved caspase-3 and αSMA by the Department of Cellular Pathology, Royal Liverpool University Hospital. A field of fixed dimensions was superimposed on an area of the section containing cancer cells (rather than

necrotic or ulcerated areas, or areas of inflammatory infiltrate) and this was scored on a 4-point scale (0 = no staining, 1 = <10% cells positive, 2 = 10-50% cells positive, 3 = 50-90% cells positive, 4 = >90% cells positive).

4.2.5 Immunofluorescence

Frozen sections of tumour tissue and mouse stomach were processed for immunofluorescence as described in 2.2.6a.

4.3 Results

4.3.1 Tumour size is proportional to the number of MKN45 cells administered.

In order to generate xenografts of an appropriate volume over a suitable length of time animals were injected with varying numbers of MKN45 cells and the resulting xenograft volumes followed over time. The same experiment was performed with AGS cells but subcutaneous injections of up to 5 x 10^6 cells yielded no tumours. Animals were also injected with CAMs alone and again no tumours resulted.

Animals injected with 5 x 10^6 MKN45 cells developed visible tumours earlier and exhibited faster tumour growth compared to smaller numbers of cells (Figure 4.1**A**). At a given time point tumour volume was directly proportional to the number of injected cells (Figure 4.1**B**). However, animals with a high tumour burden experienced significant weight loss and in two cases this necessitated sacrifice.

Injections of fewer MKN45 cells resulted in slower tumour growth and consequently longer animal survival. The yield of tumours was decreased but where tumours did develop, their growth was more consistent. The reasons for sacrifice in these animals were tumour dimensions or ulceration.

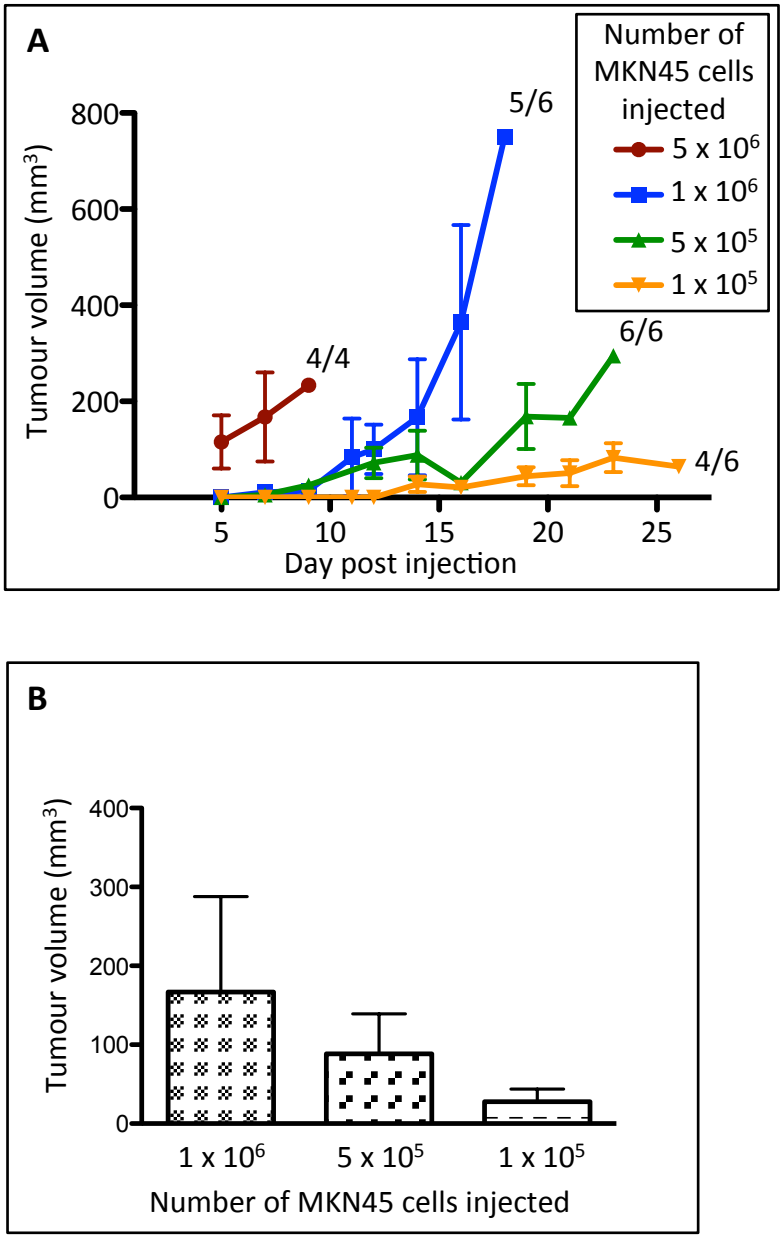

Figure 4.1. Tumour size is proportional to the number of MKN45 cells injected. A, Use of higher MKN45 cell number at subcutaneous injection resulted in faster tumour growth and earlier sacrifice of the mouse. Fractions denote the proportion of subcutaneous injections which eventually yielded a tumour. **B,** Tumour volume on day 14 is directly related to MKN45 cell number. Mean results from 4-6 animals are shown.

4.3.2 Myofibroblasts enhance xenograft growth.

The addition of myofibroblasts to MKN45 cells stimulated tumour growth. Addition of NTMs, CAMs and ATMs all potentiated tumour growth to the same extent (Figure 4.2**A**). The tumour yield per injection was also improved by the addition of myofibroblasts, as only 2/5 injections produced a tumour when 1 x 10^5 MKN45 cells were injected alone, whereas in combination with myofibroblasts this increased to 5/5 in all but one myofibroblast type (Figure 4.3). This experiment was repeated using AGS cells with CAMs but this did not yield any visible or palpable tumours.

The use of CAM/ATM paired samples allowed comparison of myofibroblasts from the same patient. In the case of patient 9, ATMs potentiated tumour growth to a greater extent than CAMs (Figure 4.2**B**). However, when myofibroblasts from patient 11 were used, the CAMs and ATMs enhanced tumour growth to a similar degree (Figure 4.2**C**).

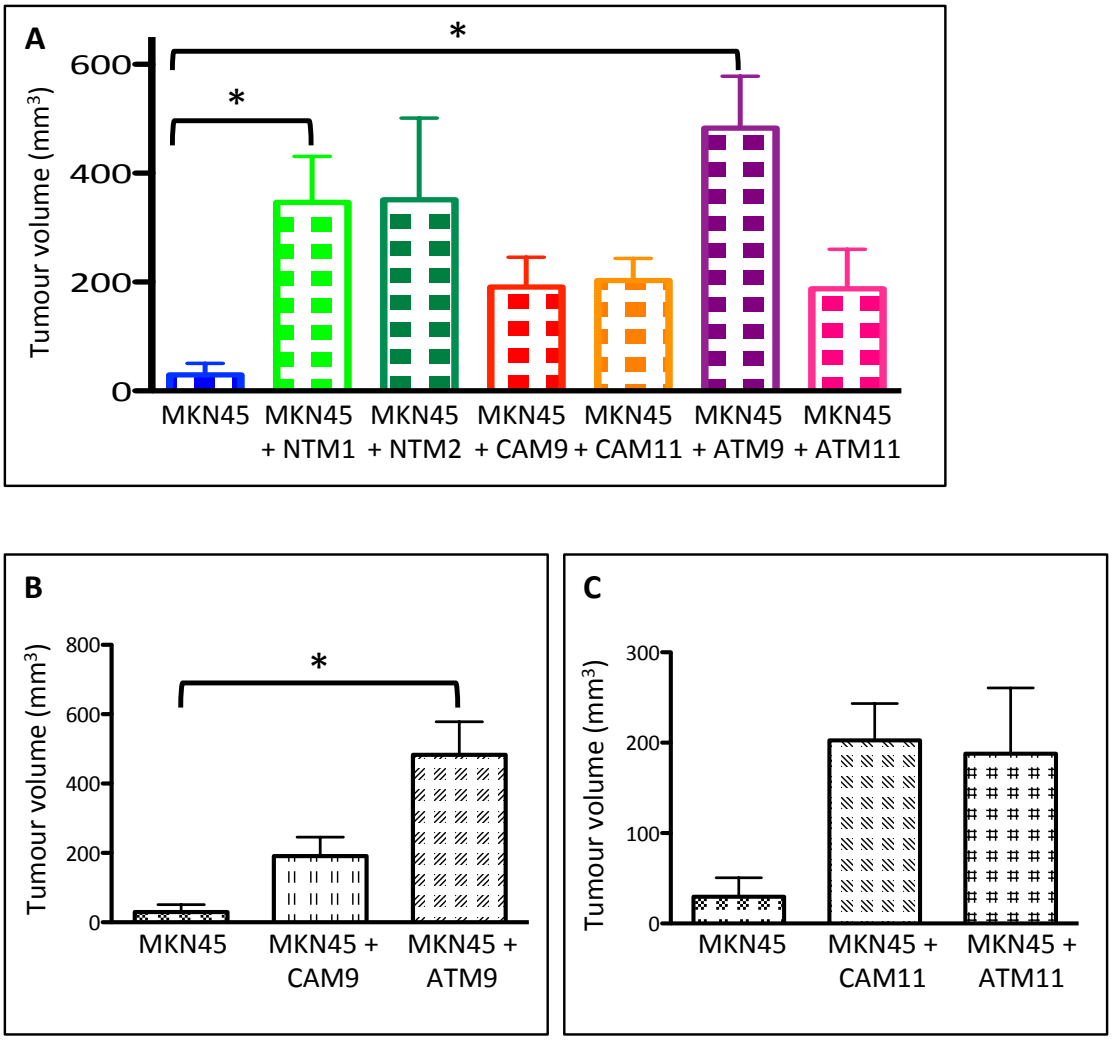

Figure 4.2. Myofibroblasts enhance xenograft growth. **A,** Tumours containing 1 x 10^5 MKN45 cells with 5 x 10^4 NTMs, CAMs or ATMs all achieve a larger tumour volume on day 23 than those composed of 1 x 10^5 MKN45 cells alone. Results from two CAMs with their corresponding ATMs and two NTMs are shown, 5 animals per group. **B,** ATM9 potentiates tumour growth more than CAM9, as shown by tumour volume on day 23. Mean results from 5 animals are shown; horizontal bars represent statistical significance by Kruskal-Wallis test with Dunn's post-hoc comparison. **C,** CAM11 and ATM11 potentiate tumour growth to the same extent, as tumours of similar volumes develop by day 23. Mean results from 5 animals are shown.

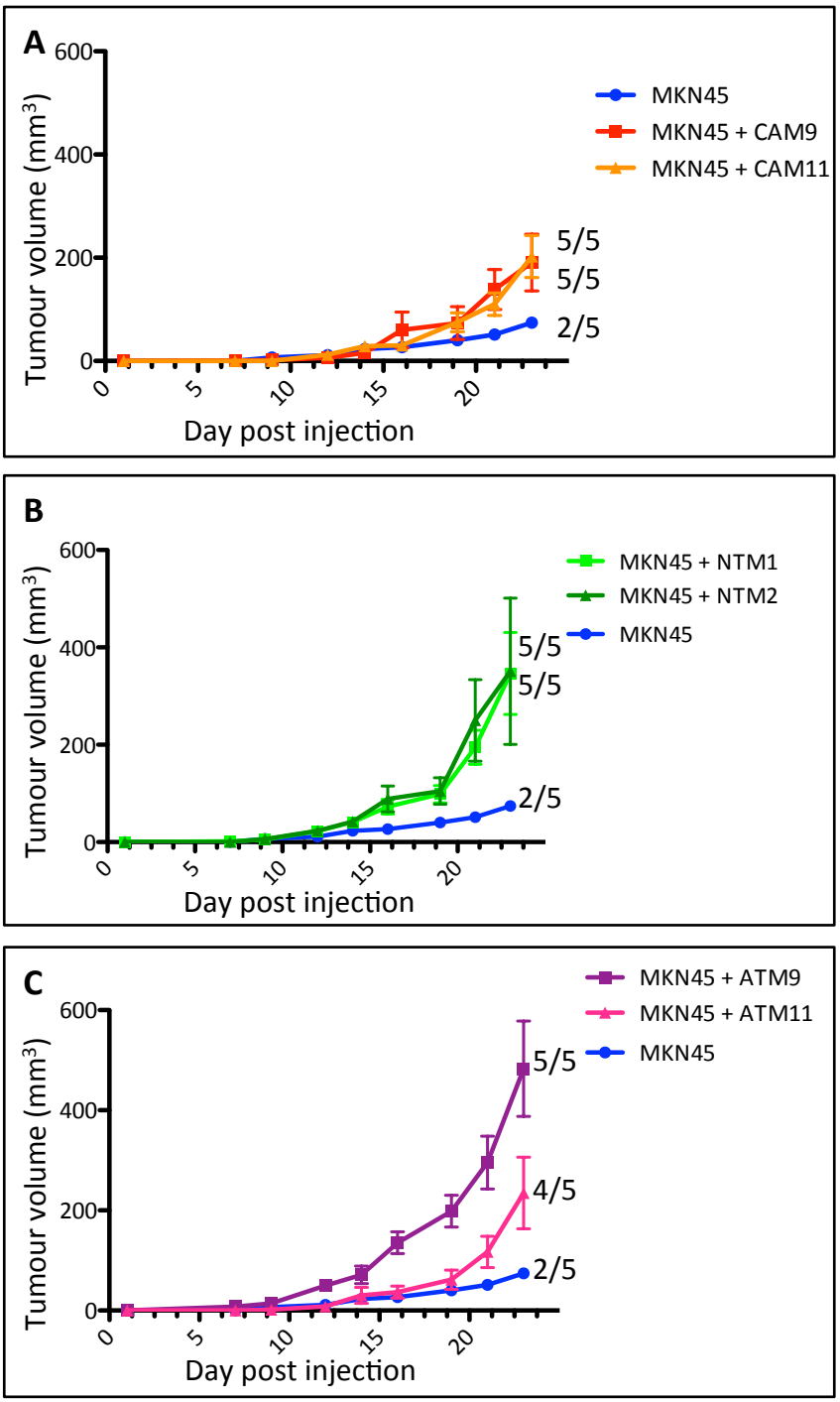

Figure 4.3. Myofibroblasts stimulate MKN45 xenograft growth. A, CAMs stimulate MKN45 xenograft growth. **B,** NTMs stimulate MKN45 xenograft growth. **C,** ATMs stimulate MKN45 xenograft growth. All experiments used 1 x 10^5 MKN45 cells with or without 5 x 10^4 myofibroblasts. Fractions denote the proportion of subcutaneous injections which eventually yielded a tumour. Mean results from 5 animals are shown.

4.3.3 Tumours with or without myofibroblasts exhibit similar features.

In situ the tumours appeared as subcutaneous masses, whose mean diameter approached 1.2cm at around the same time as developing ulceration at the skin surface. Macroscopically the tumours were firm lumps of tissue which were adherent to but easily removed from the underlying intercostal muscles. Where no ulceration had occurred, the overlying skin was normal and had not adhered to the tumour (Figure 4.4).

Histological examination revealed features of poorly differentiated gastric adenocarcinomas. Low power views show areas of cancer cells with patches of necrosis (Figure 4.5, images in left column). At higher power cancer cells with atypical nuclei and a high nuclear to cytoplasmic ratio are visible (Figure 4.5, images in right column). The areas of necrosis are bordered by cell debris. Ulceration of the tumour into the skin surface is seen (Figure 4.6**A-B**). Invasion into the muscle is also a feature of these tumours (Figure 4.6**C-D**). Development of blood vessels within the tumour parenchyma is evidence of angiogenesis (Figure 4.6**E**). Post-mortem the liver and lungs of the mice were removed and examined for macroscopic evidence of distant metastasis and none was found.

All of the features above were noted in xenografts composed of MKN45 cells alone and those containing myofibroblasts. An independent pathologist scored sections for necrosis, stromal content, invasion and presence of blood vessels and no difference between groups was identified.

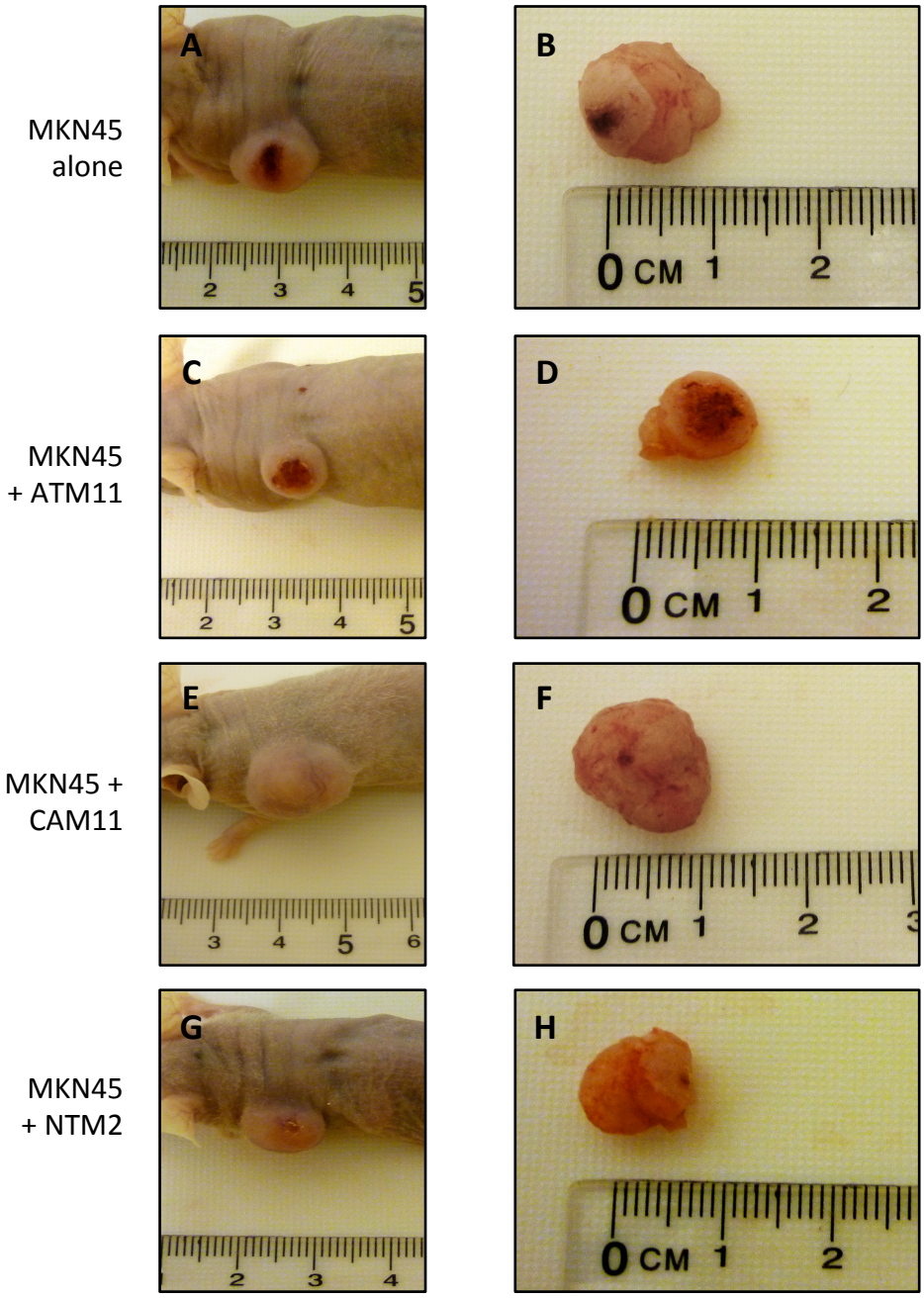

Figure 4.4. Similar macroscopic appearance of subcutaneous xenografts with or without myofibroblasts. **A, B** Representative images of subcutaneous MKN45 cell xenografts *in situ* and *ex vivo* demonstrating tumour size and superficial ulceration. **C, D** Representative images of MKN45 and ATM11 xenografts. **E, F** An example of MKN45 and CAM11 xenograft. Note the lack of skin ulceration in this example. **G, H** Images of MKN45 and NTM2 xenografts.

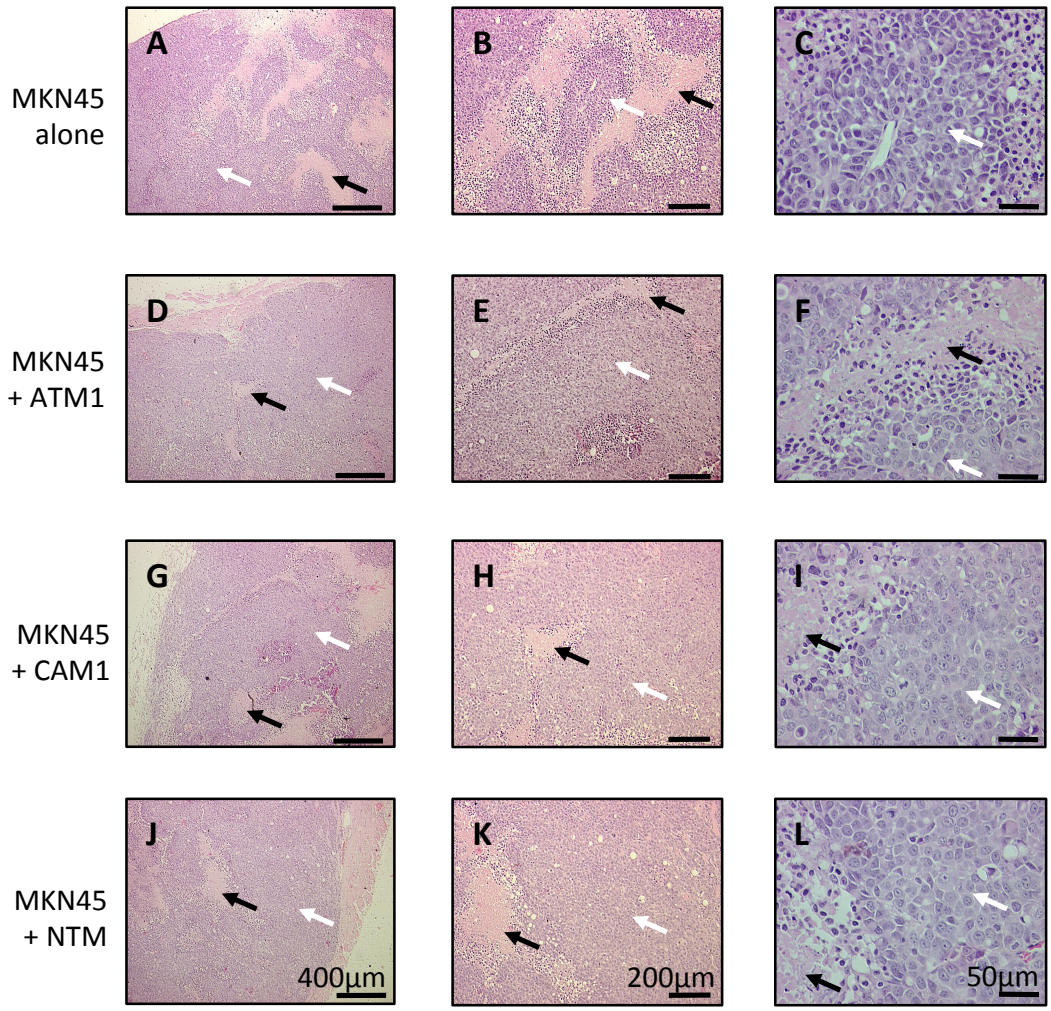

Figure 4.5. Tumours with or without myofibroblasts exhibit similar histological features. **A-C,** Representative images of sections from tumours composed of MKN45 alone. **D-F,** Sections from tumours containing MKN45 and ATM1 cells. **G-I,** Sections from tumours containing MKN45 and CAM1 cells. **J-L,** Sections from tumours containing MKN45 and NTM cells. In all cases H&E staining. Note epithelial cells (white arrows) and areas of necrosis (black arrows).

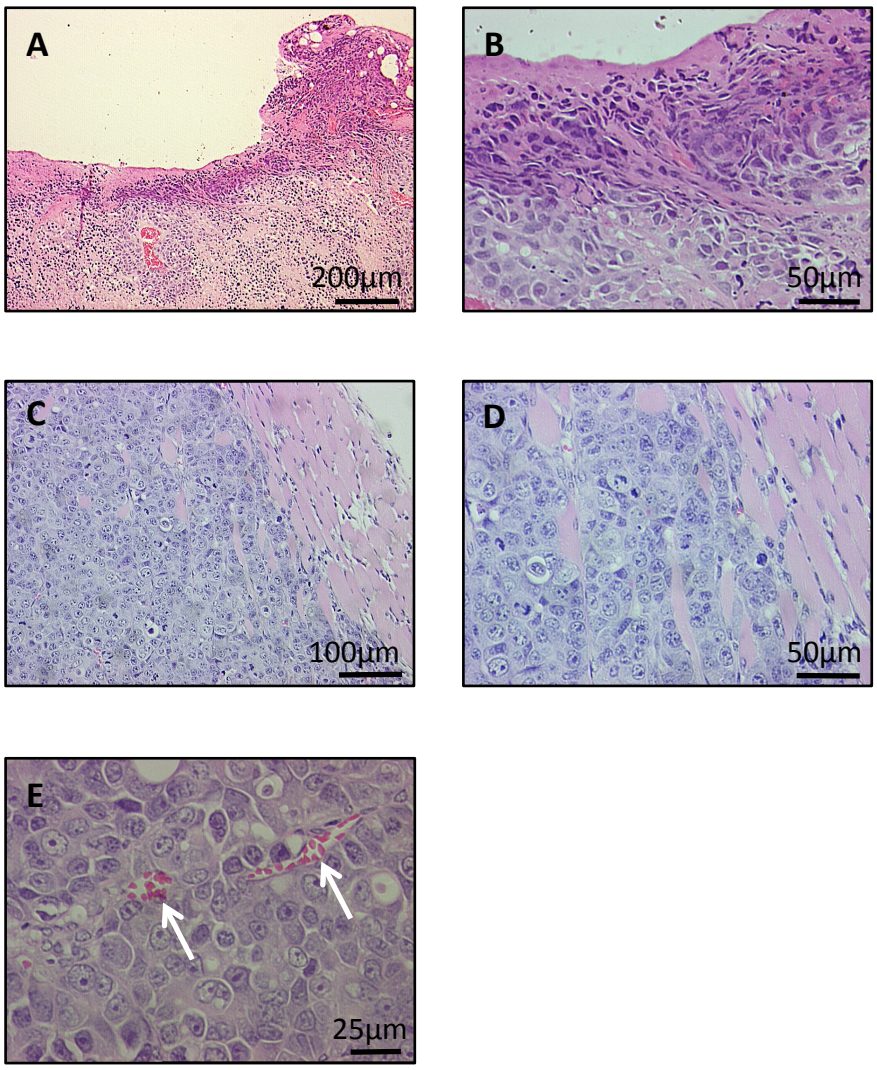

Figure 4.6. Subcutaneous MKN45 xenografts with or without myofibroblasts exhibit skin ulceration, muscle invasion and angiogenesis. A-B, Representative images of H&E stained tumour sections showing ulceration at the skin surface. **C-D,** Invasion into muscle. **E,** Formation of new vessels (arrow).

4.3.4 The presence of myofibroblasts in a xenograft suppresses the growth of a contralateral tumour composed of MKN45 cells alone.

A bilateral model of xenograft growth was developed in which the right flank of the mouse was injected with MKN45 cells and CAMs and the left with MKN45 cells alone (Figure 4.7**A-B**). It was noticed that when both sides were injected with MKN45 cells alone, the resulting tumours were of equal size. When the right side contained CAMs, however, the left-sided tumour was smaller or did not appear (Figure 4.7**C-D**).

In mice with bilateral MKN45 cell tumours, the appearance of the tumours occurred at the same time. In mice where the right side contained CAMs, the left-sided tumour's appearance was delayed or did not occur at all within the 42 days of the experiment (Figure 4.8).

This finding applied to most but not all CAMs. In the case of CAM7, neither the side containing CAMs nor the one injected with MKN45 cells alone developed a tumour. CAMs 2 and 12 failed to stimulate local xenograft growth but did not seem to affect the contralateral tumour. The experiment was repeated for these CAMs and the result found to be the same.

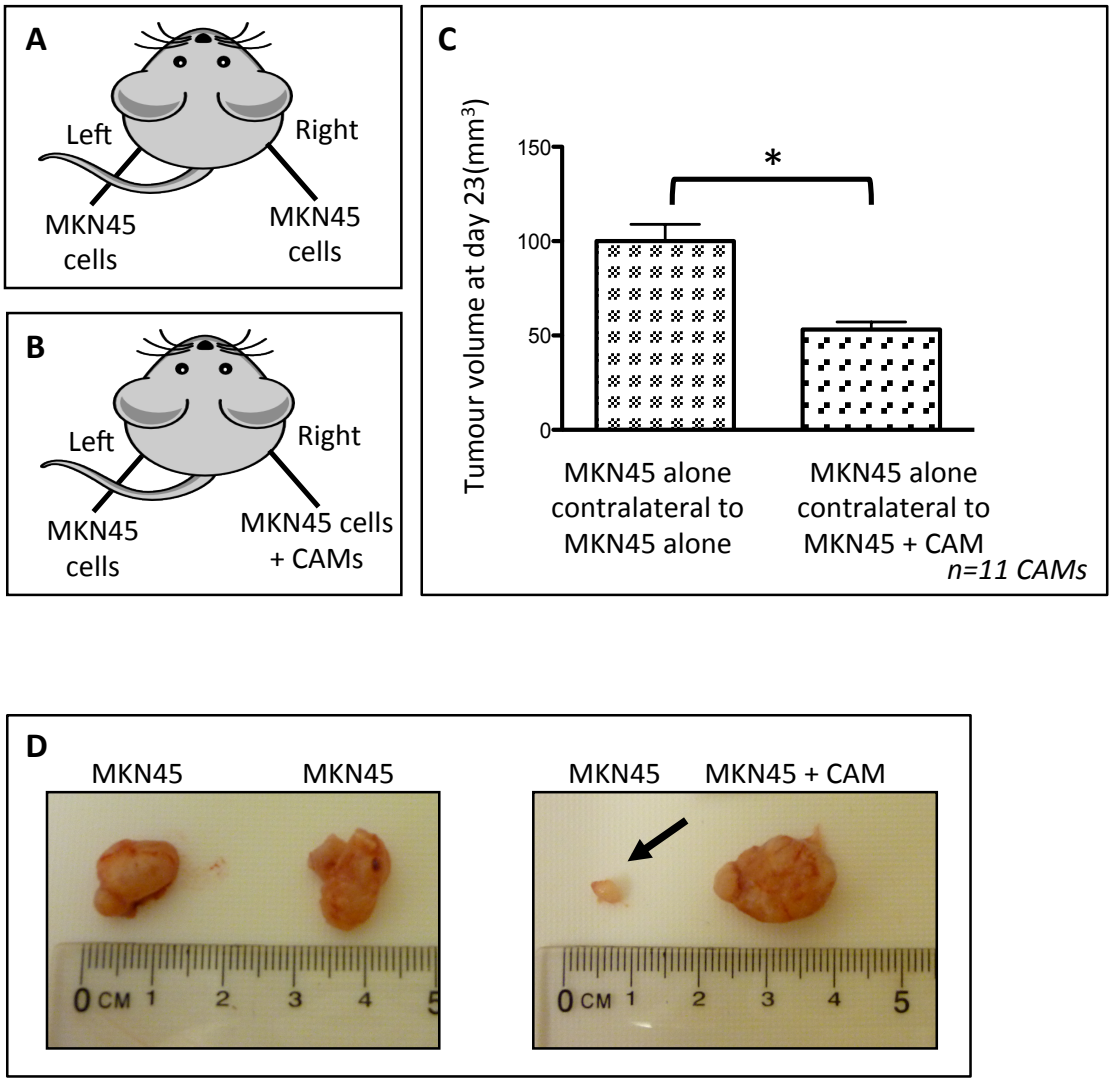

Figure 4.7. The presence of myofibroblasts in a xenograft suppresses the growth of a contralateral tumour composed of MKN45 cells alone. **A-B,** Experimental design. **C,** Larger volume of MKN45 tumour when contralateral to a tumour without myofibroblasts. Mean results from 11 CAMs are shown (the result for each CAM was the mean of the results from 3 mice per CAM). **D,** Representative photographs of MKN45 tumours demonstrating smaller MKN45 tumour grown opposite a tumour containing myofibroblasts (arrow).

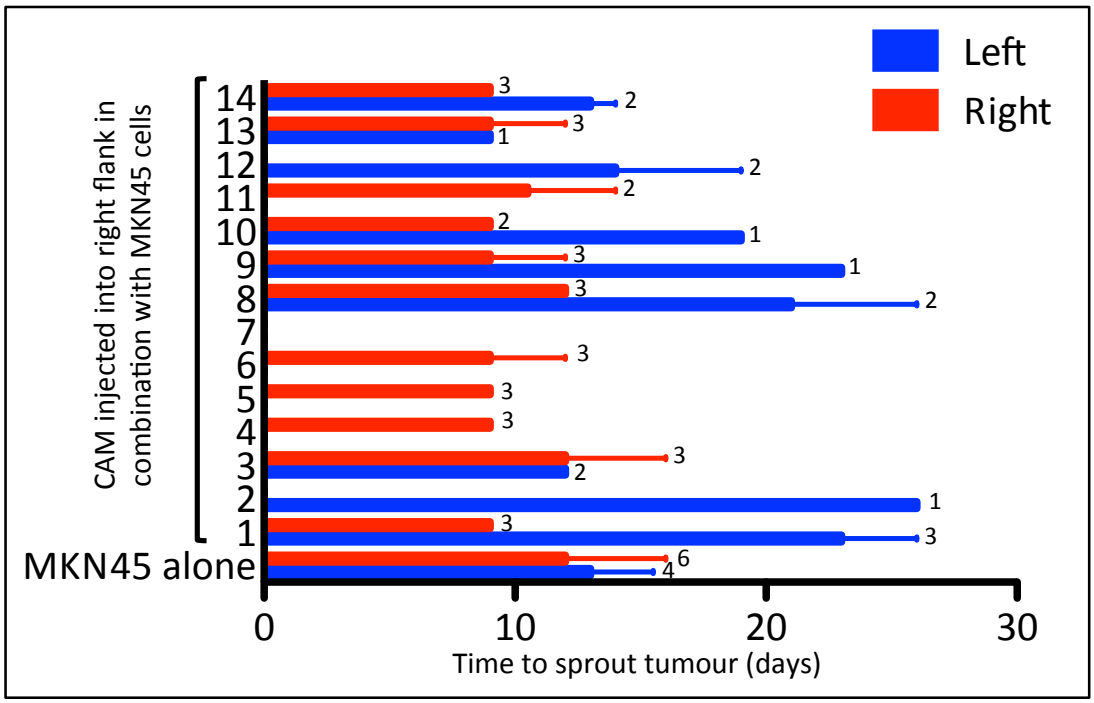

Figure 4.8. The time taken for a MKN45 tumour to sprout is longer when the contralateral tumour contains myofibroblasts. Median time to sprout (± interquartile range) for MKN45 cells on both sides is similar (bottom blue and red bars) whereas the time taken for a MKN45 tumour contralateral to a MKN45 + CAM tumour to sprout is longer (blue bars) than the MKN45 + CAM tumour (red bars). Results from 3 mice per CAM and 6 MKN45 alone mice are shown, IQ range shown when more than 2 tumours developed in that group. Numbers represent the number of tumours that developed from the subcutaneous injections.

4.3.5 Immunohistochemistry demonstrates no difference in cell proliferation, apoptosis or myofibroblast staining in tumours composed of MKN45 cells alone or with myofibroblasts.

Immunohistochemical staining for Ki-67, cleaved caspase-3 and α-SMA was then performed to further characterise MKN45 cell xenografts with or without CAM (Figure 4.9). Ki-67 staining demonstrated high proliferation rates in both MKN45 alone xenografts, and MKN45 plus myofibroblasts (all tumours scored 4), suggesting the altered tumour size is not due to changes in cell proliferation rates. Staining for cleaved caspase-3 revealed consistently low rates of apoptosis, with all sections scoring 1. Finally, the pattern of α-SMA staining showed that all tumours contained myofibroblasts (even if they had not been injected with myofibroblasts) suggesting that there is a mouse-derived source of myofibroblasts in these tumours. Immunohistochemical staining indicated cell proliferation, apoptosis and myofibroblast content per unit area were similar regardless of tumour size.

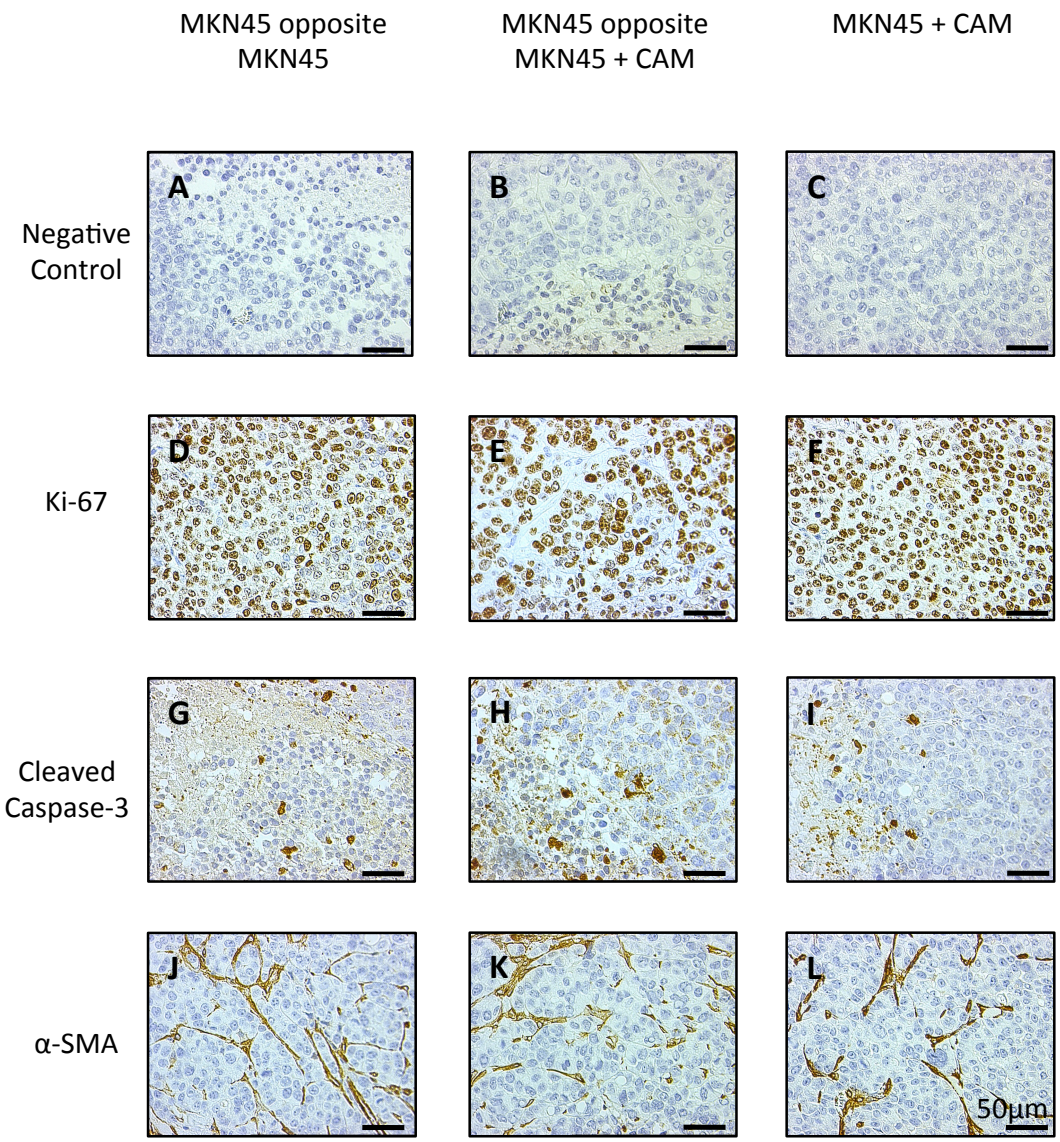

Figure 4.9. Immunohistochemistry for Ki67, α-SMA and cleaved caspase-3 demonstrates no difference in cell proliferation, apoptosis or myofibroblast content in tumours composed of MKN45 cells alone or in combination with myofibroblasts. A-C, Negative control (no primary antibody) **D-F,** Representative images of Ki-67 staining in areas of tumour containing cancer cells showing similar proportions of proliferating cells. **G-I,** Cleaved caspase-3 staining in areas of cancer cells showing no difference in apoptosis. **J-L,** α-SMA staining showing similar distribution and number of myofibroblasts. Fields containing cancer cells (rather than necrotic or ulcerated areas, or areas of inflammatory infiltrate) were selected and scored.

4.3.6. Tumours injected with human myofibroblasts stain positively for human vimentin.

To attempt to distinguish myofibroblasts of human origin from those of mouse origin, two primary antibodies for vimentin were used in immunofluorescence experiments. One was non-species specific and the other targeted the human vimentin V9 filament. Tumour sections were examined by confocal microscopy. The human vimentin-specific antibody only exhibited positive staining on sections from tumours injected with human myofibroblasts (Figure 4.10**A**). Sections from tumours composed of MKN45 cells alone were only positive for vimentin when the non species-specific antibody was used, suggesting that the stromal cells in these tumours were mouse-derived (Figure 4.10**B**).

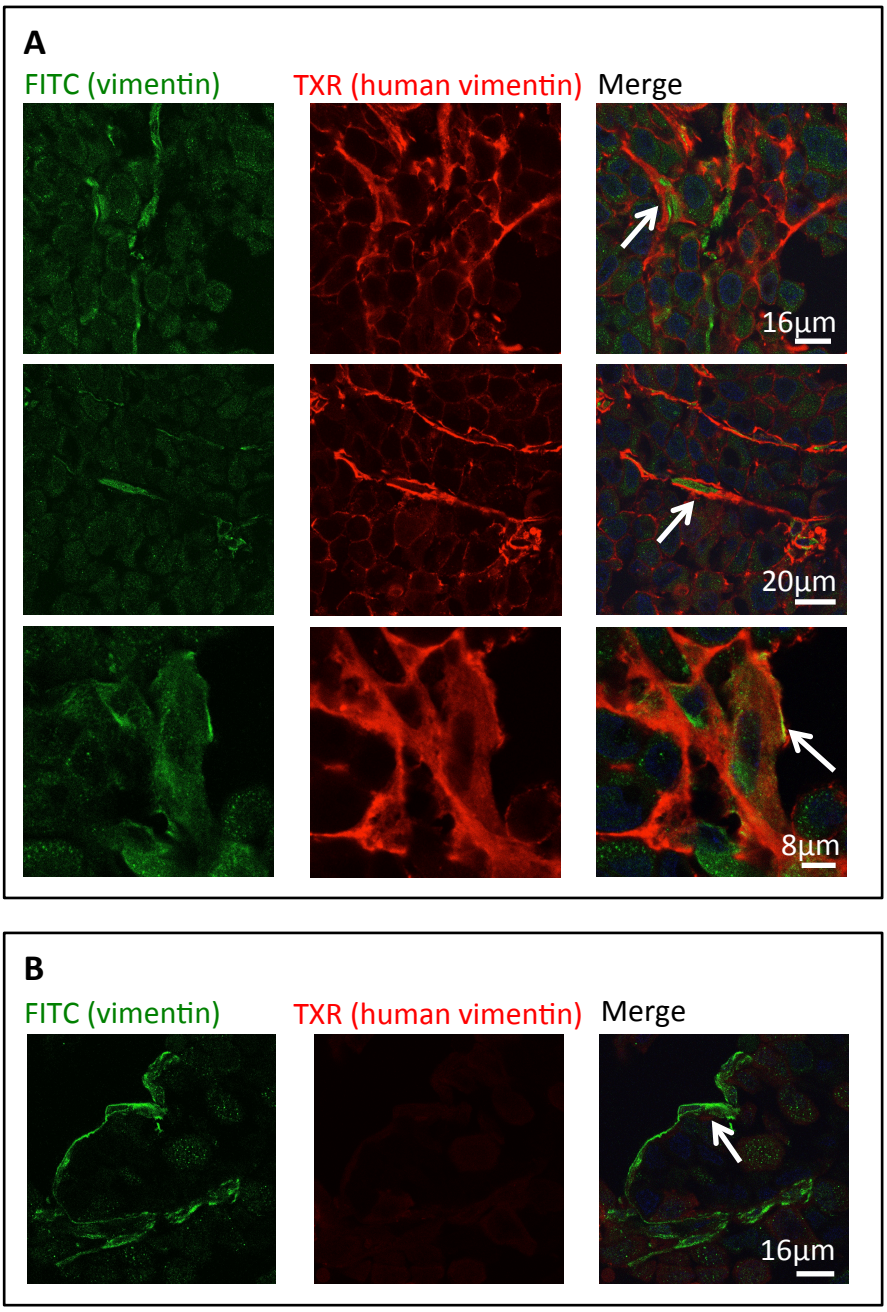

Figure 4.10. **Tumours injected with human myofibroblasts stain positively for human vimentin.** **A,** Representative images taken using confocal fluorescence microscopy showing vimentin (FITC) and human vimentin V9 filament (TXR) staining. This reveals myofibroblasts stained with both antibodies in tumours composed of MKN45 + CAM3 (arrows). **B,** In MKN45 tumours there is no positive staining for human vimentin but myofibroblasts do stain for vimentin (arrow). From left to right: localisation of non species-specific vimentin conjugated to FITC secondary antibody, human vimentin V9 filament localisation using TXR-labelled secondary antibody, merged images.

4.3.7 MKN45E2-C cells are not identified in the tumours containing CAMs, suggesting cell migration towards tumours containing CAMs is not responsible for the smaller contralateral tumour size.

In 4.3.4 we showed that MKN45 cell xenografts contralateral to a MKN45 + CAM xenograft appeared later and achieved a smaller volume than those contralateral to MKN45 cells alone. In order to investigate whether the migration of cells from one side towards the side containing CAMs was responsible for this effect, MKN45 E2-C cells were injected opposite tumours composed of MKN45 cells + CAMs (Figure 4.11**A**).

Examination of frozen sections under a TXR filter did not reveal any red cells in the contralateral tumour, although the E2-C cells were seen in the tumours which appeared at the site of their injection (Figure 4.11**B**). Results from EdU staining confirmed the findings (Figure 4.9**D-F**) that xenografts contain areas of cancer cells exhibiting high proliferation (figure 4.12**A**). This suggested that the cells injected at one site did not make their way to the CAM-containing tumour.

4.3.8 Myofibroblasts do not colocalise with E2-C positive cells, suggesting the myofibroblasts are not derived from MKN45 cells.

In order to investigate the origin of myofibroblasts within MKN45 cell xenografts, sections from MKN45 E2-C tumours were examined for co-localisation of E2-C and vimentin. This would show whether the epithelial MKN45 cells had acquired mesenchymal markers, which would be evidence for epithelial-mesenchymal transition (EMT). No cells were found which were both E2-C and vimentin positive

(Figure 4.12**A**), indicating that the myofibroblasts were not a product of EMT of the MKN45 cells.

4.3.9 Tumours contains areas of cells with a high proliferative rate; these colocalise with E2-C positive cells

Use of fluorescent MKN45 cells demonstrated that EdU positive cells colocalise with E2-C positive cells (figure 4.12**B**) showing that the source of the proliferating cells is indeed the MKN45 E2-C cells injected at the start of the experiment.

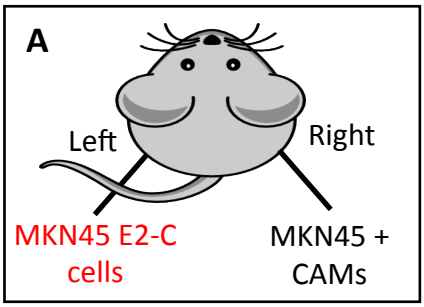

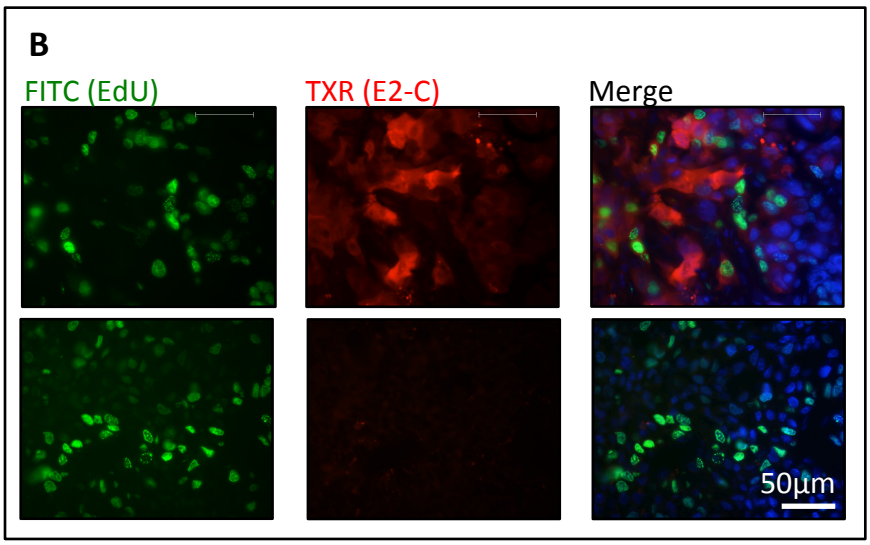

Figure 4.11. MKN45 E2-C cells are not identified in the tumours containing CAMs. **A,** Experimental design showing MKN45 E2-C xenografts contralateral to ones composed of MKN45 cells + CAMs. **B,** Representative fluorescence microscopy images demonstrating no evidence of E2-C positive cells (TXR filter) in the MKN45 + CAM tumours (bottom row) compared to the MKN45 E2-C tumours (top row). Areas of proliferating cells are identified by EdU positivity. From left to right: EdU localisation using FITC-labelled secondary antibody, E2-C visualisation under TXR filter, merged images.

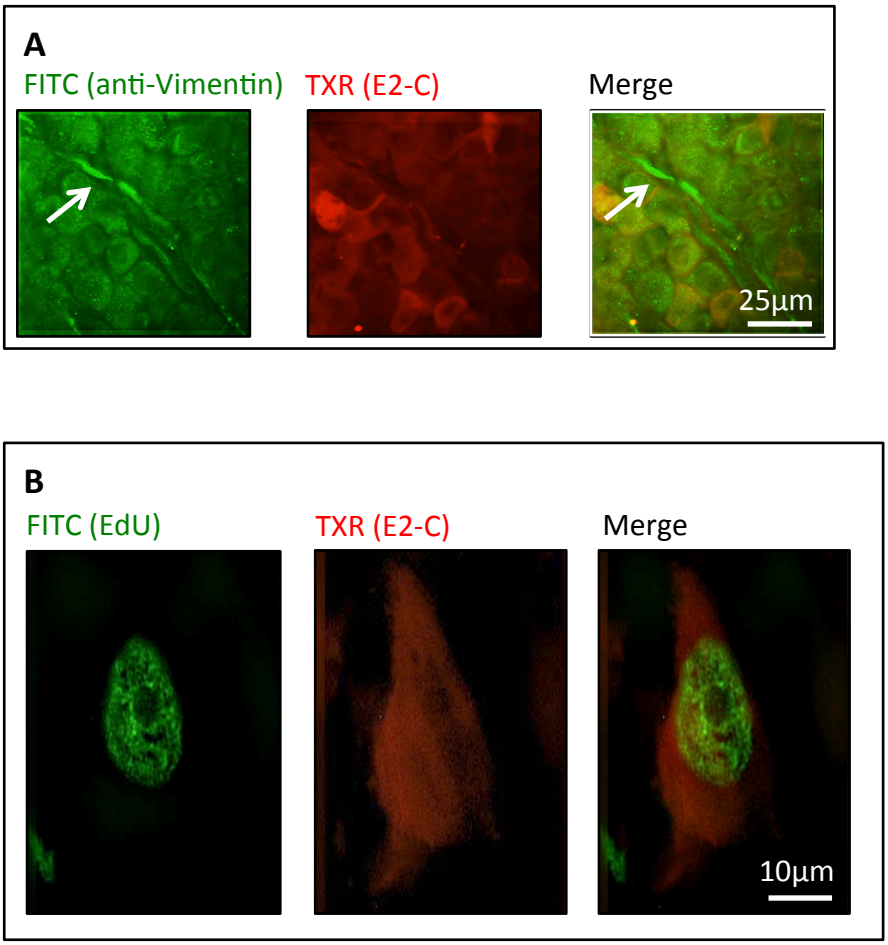

Figure 4.12. E2-C cells do not colocalise with myofibroblasts but proliferate *in vivo.* **A,** Myofibroblast (arrow) does not colocalise with E2-C +ve cells, suggesting EMT does not occur. From left to right: vimentin localisation using FITC-labelled secondary antibody, E2-C visualisation under TXR filter, merged images. **B,** E2-C positive cells colocalise with EdU positive cells, suggesting that the proliferating cells within a tumour are MKN45 E2-C cells. Left panel shows EdU localisation using FITC-labelled secondary antibody, centre panel shows E2-C localisation under TXR filter and right panel shows merged images.

4.4 Discussion

The present study has characterised a model for gastric tumour xenografts using MKN45 cells. Tumour growth is accelerated by the addition of gastric myofibroblasts, and CAMs, ATMs and NTMs are equally effective in this regard. Tumours generated without or with myofibroblasts are macroscopically similar and demonstrate histological features of a poorly differentiated carcinoma with areas of necrosis. Interestingly, MKN45 cell xenografts injected contralateral to MKN45 plus CAM xenografts are smaller and develop later than those opposite xenografts without CAMs.

The present subcutaneous xenograft model reconstitutes *in vivo* a tumour microenvironment based on interactions between myofibroblasts and cancer cells. It is important to recognise that the growth of xenografts is also influenced by mouse-derived responses to these tumours, including the influx of endothelial cells, mouse myofibroblasts, immune cells and MSCs. Inevitably, the use of immunosuppressed mice influences the immune component of the host response to a tumour. Thus while subcutaneous xenografts in immunosuppressed mice do not fully reproduce the cancer microenvironment they nevertheless provide a basis for studying the interactions between cancer cells and key stromal cell types.

In order to circumvent the use of immunosuppressed animals, mouse models of gastric cancer have been developed. Chronic *H. felis* infection in C57BL/6 mice

mimics the effect of *H. Pylori* in humans, a potent gastric carcinogen which eventually leads to the development of gastric dysplasia, metaplasia and neoplasia closely mirroring the sequence of lesions seen in the development of human gastric cancer (185). This process can be accelerated by combining *H. felis* infection with the use of insulin-gastrin (INS-GAS) mice, a genetically-engineered mouse model of hypergastrinaemia (187). These models have been limited by modest gastric pathology and slow time course, and are affected by environmental conditions such as housing, temperature and humidity.

The histological and immunohistochemical analysis of the tumours did not reveal significant differences between xenografts with or without myofibroblasts with respect to tumour composition or architecture in spite of differences in tumour growth. It may be that myofibroblasts act at the time of cell injection to promote MKN45 cell survival, increasing the proportion of injected MKN45 cells which grow to form a tumour. This would explain why, at the time of harvesting, there are no differences in cell proliferation or apoptosis. Although these processes contribute to the growth of tumours, it may be that the difference we observed is attributable to other processes, such as angiogenesis, hypoxia and ability to invade. Clearly further work is required to characterise the mechanism of myofibroblasts.

The use of α-SMA and vimentin staining to identify myofibroblasts is established. It is important to remember, however, that neither of these markers is restricted entirely to expression in myofibroblasts. Endothelial cells are able to express vimentin (240) and α-SMA is expressed by pericytes (241). Staining with markers for

these cells (which are also found in the tumour stroma) would have aided in the definitive identification of myofibroblasts. The use of human-specific fluorescence *in situ* hybridisation in combination with immunohistochemistry may accurately identify myofibroblasts of human origin.

The finding that MKN45 cells formed tumours more readily than AGS cells is in agreement with published literature, where examples of MKN45 cell xenografts (242,243,244) and xenografts using other gastric cancer cell lines, such as MGC-803 and SGC-7901 cells (245) abound compared with AGS cell xenografts. Although examples of AGS xenografts do exist, they use higher cell numbers than we attempted (246). The lack of subcutaneous masses even in the presence of myofibroblasts precluded the use of AGS cells in further experiments.

Our finding that CAMs stimulated xenograft growth is in agreement with previous data, where the growth of MKN45 cells injected subcutaneously in SCID mice was potentiated by gastric CAMs (43). Similar findings have been obtained in a subcutaneous xenograft study in breast cancer using α-SMA positive cancer-associated myofibroblasts (48) and in a prostate cancer study, where fibroblasts from prostate cancers stimulated the growth of tissue recombinants implanted beneath the renal capsule of athymic mice (47). Both of these studies also examined the effect of fibroblasts taken from normal tissue and found that they did not stimulate tumour growth. This would initially seem to be in contrast to our finding that NTMs stimulated xenograft growth as effectively as CAMs. However, the populations of fibroblasts from normal prostate and breast tissue in these

studies were not α-SMA-expressing, a feature which denotes an 'activated,' myofibroblast phenotype (247). The NTMs in our study express α-SMA, which may be a reflection of the constant cycle of damage and repair in the normal gastric epithelium, resulting in a larger population of activated myofibroblasts. Indeed, myofibroblasts are found at the sites of gastric ulcers (248). Perhaps the ability of a mesenchymal cell to stimulate xenograft growth is dependent on its possession of an activated phenotype.

The addition of ATMs to MKN45 cells also enhanced tumour growth. In the case of patient 9, use of the ATM potentiated tumour growth significantly more than the CAM. There are *in vitro* data to suggest that ATMs are more capable of modulating the behaviour of cancer cells than NTMs or CAMs (46). However, this was not confirmed by the data from patient 11, where CAMs and ATMs stimulated tumour growth to a similar degree.

Histology of these tumours revealed invasion into the skin and muscle, angiogenesis and areas of necrosis. Staining for α-SMA did not show any differences in myofibroblast content, regardless of whether tumours had been co-injected. In tumours injected with MKN45 cells alone the positive α-SMA staining is likely to have arisen from mouse-derived stromal cells. In tumours where human myofibroblasts were co-injected, these could not be distinguished from the mouse-derived stroma using α-SMA staining. However, the positive staining of cells in MKN45 with CAM xenografts using human-specific and the non species-specific vimentin antibodies

demonstrated that it is likely that the injected CAMs persist in the tumour weeks after injection.

Most xenograft studies involving the co-injection of cancer cells and myofibroblasts do not distinguish between mouse and human-derived myofibroblasts, choosing to use α-SMA staining as a non species-specific marker of myofibroblast content (249,250). Attempts to identify the origin of the stroma in subcutaneous xenografts have shown mixed results. One study identified mouse-derived myofibroblasts in subcutaneous xenografts established from a breast cancer cell line by demonstrating positive α-SMA staining and an absence of human cytokeratin (251). Another study also suggested that the stroma is host-derived by showing that stromal cells implanted together with cancer cells into mice are replaced by host-derived stoma over a period of weeks (252). Studies using mice expressing GFP have shown that subcutaneous tumours in mice acquire host stroma. One group created tumours with GFP-labelled stroma by subcutaneously implanting cancer cells into GFP-expressing mice. These tumours, when implanted into other mice, retained their GFP-positive stroma after 4 weeks but the persisting cells were thought to mainly represent endothelial cells rather than myofibroblasts (250). Another group established subcutaneous pancreatic xenografts and sequentially passaged them in red fluorescent protein (RFP), GFP and cyan fluorescent protein-expressing mice, showing the progressive acquisition of red, green and cyan-fluorescent stroma from the host mouse but also persistence of the RFP expressing stroma throughout the *in vivo* passages (253). These studies have not identified which cells in the host give

rise to the stroma but there is emerging evidence that some of the CAMs are derived from bone marrow-derived MSCs (254).

The finding that E2-C positive cells do not colocalise with vimentin-stained cells reinforces the notion that the MKN45 cells within the tumour do not acquire mesenchymal markers, suggesting EMT does not occur. The origin of myofibroblasts within tumours continues to be debated, and EMT of cancer cells has been shown to be a source of some myofibroblasts in some tumours (255). However, *in vitro* evidence suggests myofibroblasts can arise from normal fibroblasts, present in normal tissues (256), or may be from bone marrow-derived mesenchymal stromal cells (62).

The finding that when a tumour contains CAMs, the growth of a contralateral tumour containing MKN45 cells alone was suppressed was unexpected. It seems that in addition to the short-range stromal-epithelial signals co-ordinating increased local tumour growth, a long-range factor influenced distant tumour growth. As immunohistochemical staining did not show any difference in proliferation or apoptosis once the tumour had developed, it may be that the effect was due to a delay in the initiation of tumour growth rather than the rate of proliferation within the tumour. There is now evidence to suggest that tumours release systemic factors capable of affecting the growth of a distant tumour (257), which supports the notion that a factor released from the CAM-bearing tumour could mediate growth suppression. Holmberg *et al*. showed that TGFβIgh3 is released from stromal cells and its systemic administration suppresses the growth of subcutaneous xenografts

containing CAMs (43). It has also been shown that cells from tumours are released into the circulation and can lodge in a distant tumour (258); it may be that the signal released from the CAM-bearing tumour encouraged cells to migrate towards it.

Chapter 3 demonstrated that FMT is a good method for detecting E2-C-labelled tumours, having shown that tumours containing these cells are much more fluorescent than tumours composed of untransfected cells. The sensitivity of FMT for small numbers of fluorescent cells within a tumour mass remains undetermined, so to establish whether E2-C positive cells were present in a tumours contralateral to one containing MKN45 E2-C cells frozen sections from these tumours were examined, an approach which ought to be sensitive even for individual cells. By examining tumour sections for evidence of E2-C positive cells we did not identify any evidence of cell migration between 2 tumours. This conflicts with the evidence that cell migration contributes to the seeding of distant tumours (256).

Macroscopically and histologically tumours with or without myofibroblasts were indistinguishable, emphasising the ability of MKN45 cells to recruit stroma from the host mouse. Identification of mouse *vs.* human derived myofibroblasts will enable further characterisation of the stroma within these xenografts. Discovering how tumours containing myofibroblasts exhibit differing growth rates will rely on the investigation of factors such as extracellular protease activity and the contribution of mesenchymal stromal cells. Tumours containing myofibroblasts exert a systemic effect, capable of suppressing the growth of a distant tumour. In order to study the

role of cell migration in this process, labelling tumour cells will allow their visualisation within another tumour.

4.5 Conclusions

1. Subcutaneous MKN45 cell xenografts grow adequately in BALB/c nu/nu mice.
2. Xenograft growth is potentiated by the addition of myofibroblasts; this is not accounted for by differences in cell proliferation rate, apoptosis or final stromal content.
3. A xenograft containing CAMs suppresses the growth of a contralateral xenograft without CAMs, demonstrating that a long-range signal can be generated as a result of stromal-epithelial interactions (Figure 4.13).

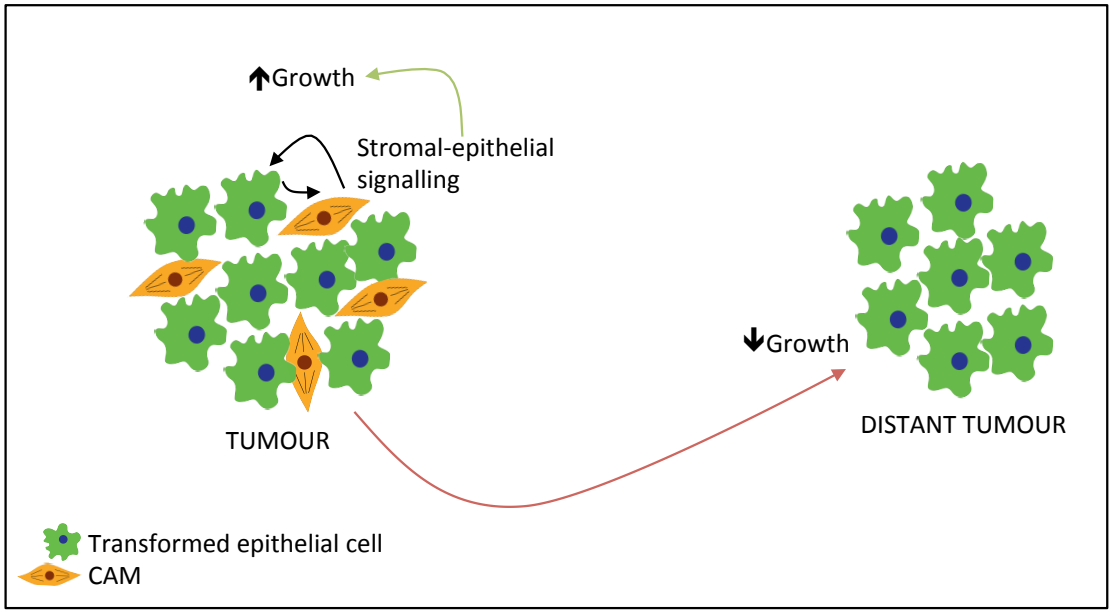

Figure 4.13. Myofibroblasts enhance xenograft growth and their co-injection into one xenograft can affect the growth of another, distant tumour. Myofibroblasts potentiate the growth of a xenograft. The interaction between myofibroblasts and tumour cells results in the suppression of the growth of a distant xenograft.

CHAPTER 5: THE ROLE OF MMPS IN TUMOUR GROWTH AND INVASION

5.1 Introduction

MMPs are a diverse group of proteases that are released into the extracellular milieu where they exert a variety of effects not limited to the degradation of components of the ECM (259). The contribution of myofibroblasts to the proteolytic extracellular environment has been assessed using proteomic analysis of the myofibroblast secretome (212). This identified a differential abundance of neo-N-termini (*ie* cleavage products) in the secretomes of gastric cancer-associated myofibroblasts (CAMs) compared with controls, consistent with cleavage of matrix metalloproteinases (MMP)-1, -2 and -3 and cathepsin B (Table 5.1).

MMPs -1, -2 and -3 share similarities in structure (Table 5.2). Cathepsin B is a lysosomal protease but aberrant expression of this protein has been demonstrated in cancer (260). This work extended the assessment of protease activity to the *in vivo* subcutaneous model of myofibroblast-stimulated xenograft growth.

Organotypic cultures provide a three-dimensional model of myofibroblast-stimulated invasion (261). They replicate the pattern of invasion seen in human cancers more accurately and allow the study of different stromal cell types and individual MMPs. Using specific MMP inhibitors the contribution of each MMP to cancer cell invasion has been assessed.

Description	Functional Classification	Cleavage site
Cathepsin B	protease	Cathepsin B heavy chain
CD99 antigen	binding protein	Extracellular domain
Collagen alpha-2(VI) chain	ECM	Nonhelical region
HLA class I histocompatibility antigen, A-1 alpha chain	receptor	Alpha-1 region
HLA class I histocompatibility antigen, B-7 alpha chain	receptor	Alpha-1 region
HLA class I histocompatibility antigen, Cw-7 alpha chain	receptor	Alpha-1 region
Interstitial collagenase (MMP-1)	protease	Propeptide
Latent-transforming growth factor beta-binding protein, isoform 1S	binding protein	Main chain
Lysyl oxidase homolog 2	enzyme	SRCR1 domain
Major prion protein	unknown	Main chain
Pro-neuregulin-1, membrane-bound isoform	ligand	Main chain
Stromelysin-1 (MMP-3)	protease	Propeptide
Tumor necrosis factor receptor superfamily member 10D	receptor	TBFR-Cys 1 repeat

Table 5.1 Analysis of myofibroblast secretomes revealed 13 proteins exhibiting the formation of unique neo-N-termini in CAMs relative to their ATM counterparts, excluding those representing removal of a signal sequence. Functional classification and cleavage sites were manually annotated using the Uniprot database. This analysis identified cleavages in the pro-peptide domains of MMP-1 and MMP-3 and in the cathepsin B heavy chain (Adapted from (2)).

Name	Aliases	Class	How the protein structure differs from Figure 1.5
MMP-1	Intersitial collagenase Fibroblast collagenase Collagenase-1	Collagenase	Tyrosine, aspartic acid and glycine amino acids are all present in the catalytic domain
MMP-2	72kDa Type IV Collagenase Gelatinase A 72 kDa Gelatinase	Gelatinase	Fibronectin type II modules in the catalytic domain
MMP-3	Stromelysin-1	Stromelysin	No difference

Table 5.2 Nomenclature and classification of MMPs -1, -2 and -3 based on class and deviation from the generic MMP structure shown in Figure 1.5.

5.1.1 Aims

1. To examine the effect of myofibroblast-derived proteases in an *in vivo* model of myofibroblast-stimulated tumour growth.
2. To determine the effect of myofibroblasts on cell invasion in a 3D organotypic cell culture model.
3. To examine the contribution of individual MMPs to cell invasion.

5.2 Methods

5.2.1 Cell culture

Primary gastric myofibroblasts and MKN45 cells were cultured as detailed in 2.2.1-2.

5.2.2 Subcutaneous xenografts

Cells for injection were trypsinised, counted and aliquots containing appropriate numbers of cells prepared as described in 2.2.3. MKN45 cell doses (5×10^5 when injected alone or 1×10^5 when injected with 5×10^4 CAM4 cells) were calculated so that tumours attained approximately equal volumes at a similar time, as described in 2.2.4.

5.2.3 FMT imaging

MMPSense 750 FAST™, ProSense 750 FAST™ and Cat B 750 FAST™ (100µl) were administered by IV tail vein injection under GA and FMT imaging performed before injection and 6 and 24 h post injection, as detailed in 2.2.5a. The fluorescent signal at 750nm in the region of the tumour was quantified using TrueQuant software. Where animals were imaged using more than one reagent, an interval of 96 h was left between injections. If this was not possible, the baseline signal prior to injection was subtracted from the final signal.

5.2.4 Organotypic cultures

Organotypic cultures were established as described in 2.2.16, with 5 x 10^5 CAM4 cells seeded on day 1 and 2 x 10^6 MKN45 cells added to the top on day 2. Where treatments with MMP inhibitors were used, the MMP inhibitor was added to the gels on day 1 and also to the FM used to replenish the cultures every 48 h. MMP-2 inhibitor I was used at 6µM and MMP-3 Inhibitor IV was used at 30µM.

Gels were paraffin-embedded, cut and stained with H&E or for Ki-67, cleaved caspase-3 and α-SMA by the Department of Cellular Pathology, Royal Liverpool University Hospital. Quantification of invasion was carried out using ImageJ software. Quantification of immunohistochemical staining was performed by counting positive cells within a 150µm x 120µm field in the MKN45 cell layer. Experiments were carried out in triplicate and the mean result reported.

5.3 Results

5.3.1 ProSense 750 FAST™ activity is not significantly altered in xenografts containing CAMs.

In order to examine protease activity *in vivo*, xenografts were generated and imaged 6 h post IV injection of ProSense 750 FAST™, a reagent which fluoresces when cleaved by cathepsins B, L, S or plasmin. There was no significant difference in ProSense 750 FAST™ activity between tumours composed of MKN45 cells alone and those composed of MKN45 cells and CAMs (Figures 5.1-2). In order to achieve similar-sized subcutaneous tumours at the time of imaging, xenografts were generated using 5 times more MKN45 cells when they were injected without CAMs. The tumour volume in both groups at the time of imaging was found to be similar, thereby eliminating differences in protease activity due to tumour volume (Figure 5.2**B**).

5.3.2 Cathepsin B activity is not significantly altered in xenografts containing CAMs.

In order to examine the contribution of cathepsin B to the protease activity in xenografts, tumours were generated as above and imaged 24 h post IV injection of Cat B 750 FAST™, a reagent which fluoresces when cleaved by cathepsin B. There was no significant difference in cathepsin B activity between tumours composed of MKN45 cells alone and those composed of MKN45 cells and CAMs (Figure 5.3). The

tumour volume at the time of imaging was similar between groups, as described above.

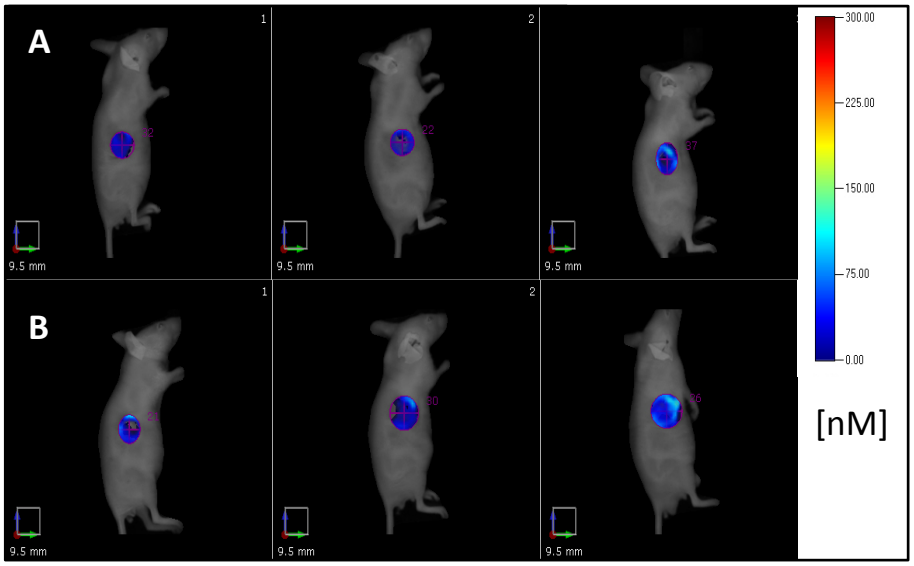

Figure 5.1. ProSense 750 FAST™ activity is not significantly altered in xenografts containing CAMs. **A,** Representative FMT images illustrating signal at 750nm from mice bearing xenografts composed of MKN45 cells alone. **B,** FMT images illustrating signal at 750nm from mice bearing xenografts composed of MKN45 cells and CAM4.

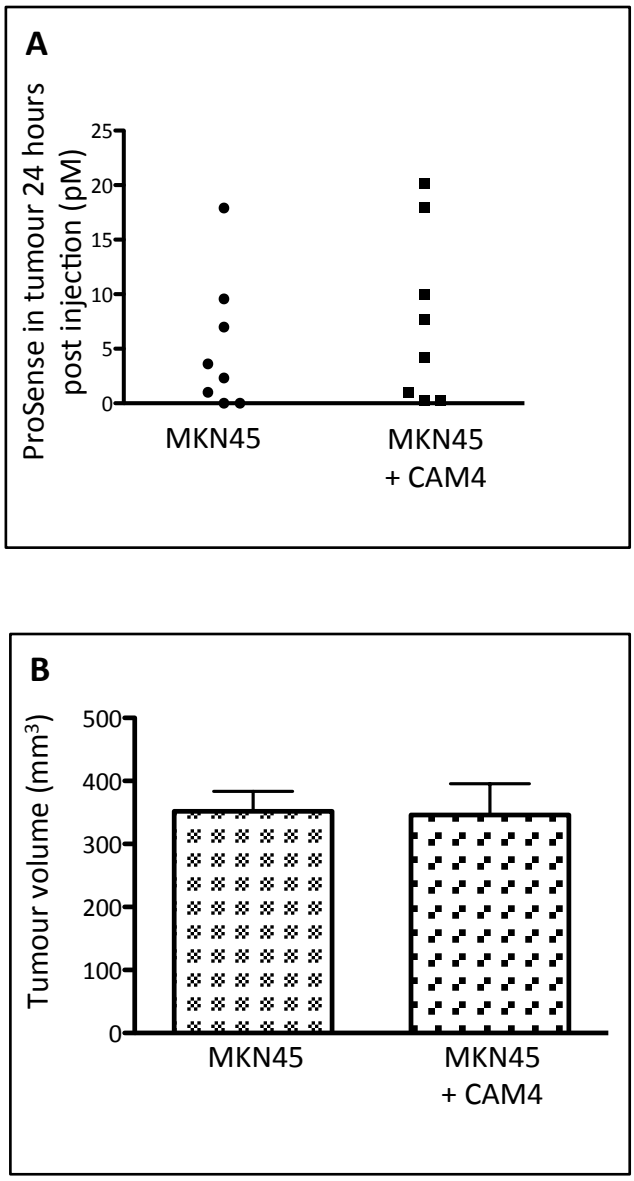

Figure 5.2. ProSense 750 FAST^{TM} activity is not significantly altered in xenografts containing CAMs. **A,** FMT assessment of protease (cathepsins and plasmin) activity *in vivo* using ProSense 750 FAST^{TM} indicated no difference between xenografts containing CAM4 cells compared with xenografts containing MKN45 cells alone. **B,** Tumour volume at the time of imaging was similar in the two groups. Mean results from 8 animals are shown.

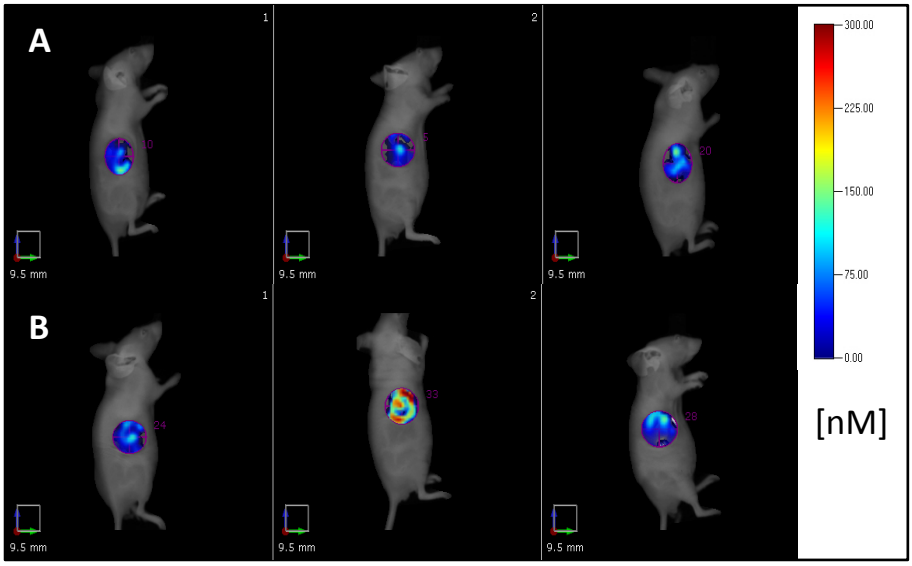

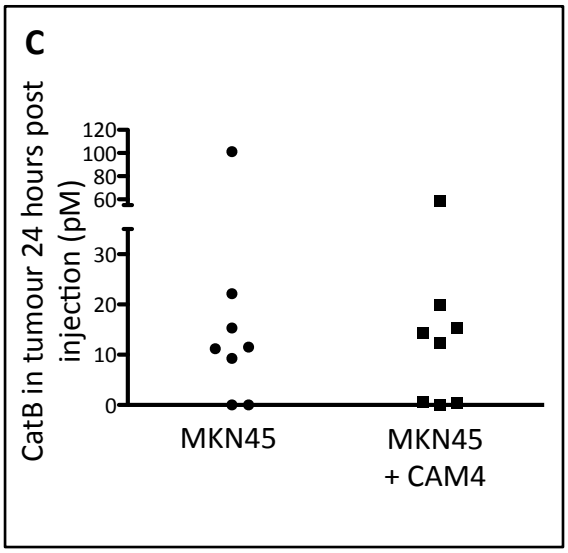

Figure 5.3. **Cathepsin B activity is not significantly altered in xenografts containing CAMs**. **A,** Representative FMT images illustrating signal at 750nm from mice bearing xenografts composed of MKN45 cells alone. **B,** Representative FMT images illustrating signal at 750nm from mice bearing xenografts composed of MKN45 cells + CAM4. **B,** Quantification of FMT assessment of cathepsin B activity *in vivo* using CatB 750 FAST™ indicated no difference between MKN45 cell xenografts containing CAM4 compared with those composed of MKN45 cells alone. Mean results from 5 animals are shown. Equivalent tumour volumes within 4 days of imaging are illustrated in figure 5.2**B**.

5.3.3 MMP activity is increased in xenografts containing CAMs.

To measure MMP activity in subcutaneous tumours *in vivo*, mice were injected with MMPSense 750 FAST™, a reagent which emits a fluorescence signal on cleavage by a broad range of MMPs (e.g. 2, 3, 7, 9, 12 and 13); the fluorescence in the tumour measured 24 h later. MMP activity was significantly increased in xenografts composed of MKN45 with CAMs compared to MKN45 cells alone or even MKN45 cells and NTMs (Figures 5.4-5). To eliminate differences in MMP activity arising from differences in tumour size, the tumour volume at imaging was measured and found to be similar in all groups (Figure 5.5**B**).

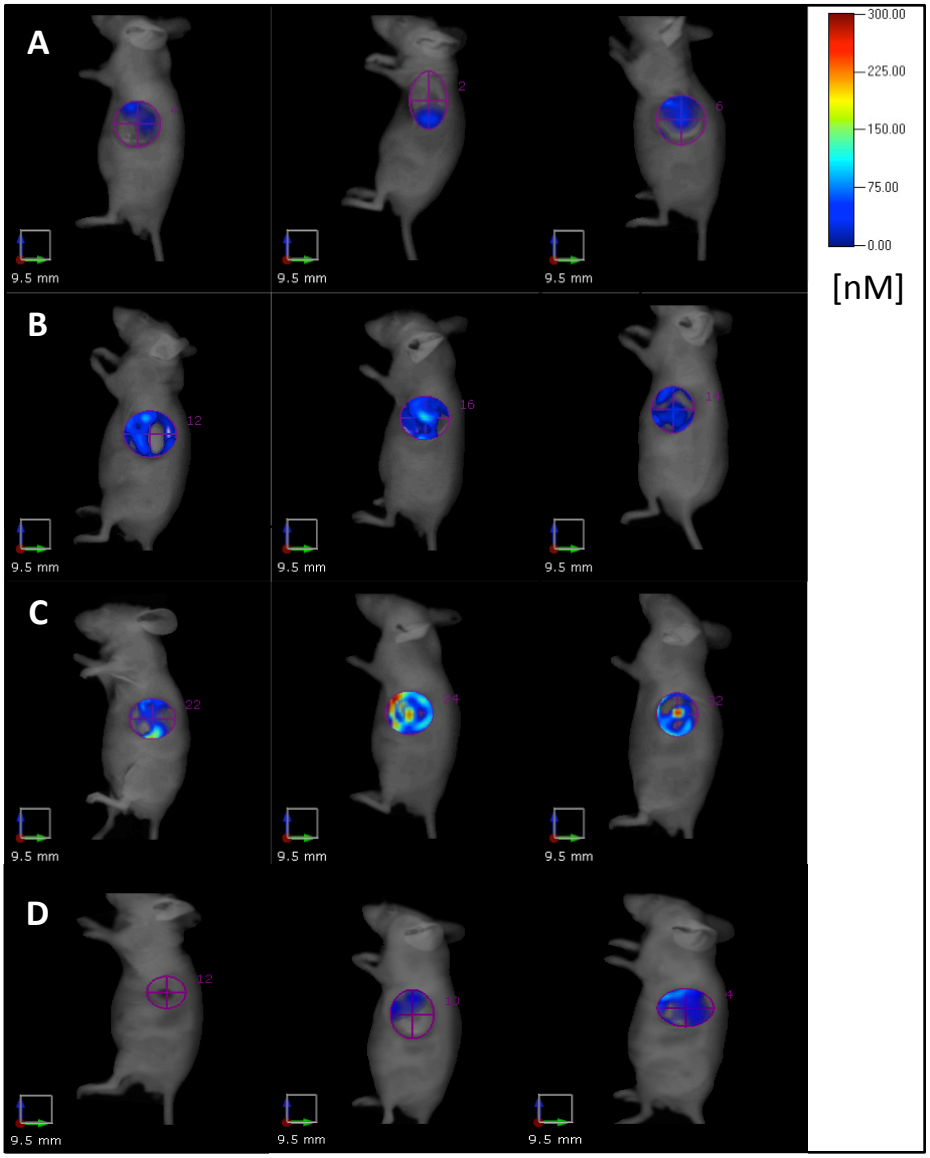

Figure 5.4. MMP activity is increased in xenografts containing CAMs. **A,** Representative FMT images show low MMP activity measured with MMPSense 750 FAST™ in tumours composed of MKN45 cells alone. **B,** Representative FMT images show elevated *in vivo* MMP activity in the presence of CAM8. **C,** Representative FMT images show elevated *in vivo* MMP activity in the presence of CAM4. **D,** FMT images showing low MMP activity in tumours with MKN45 and NTMs.

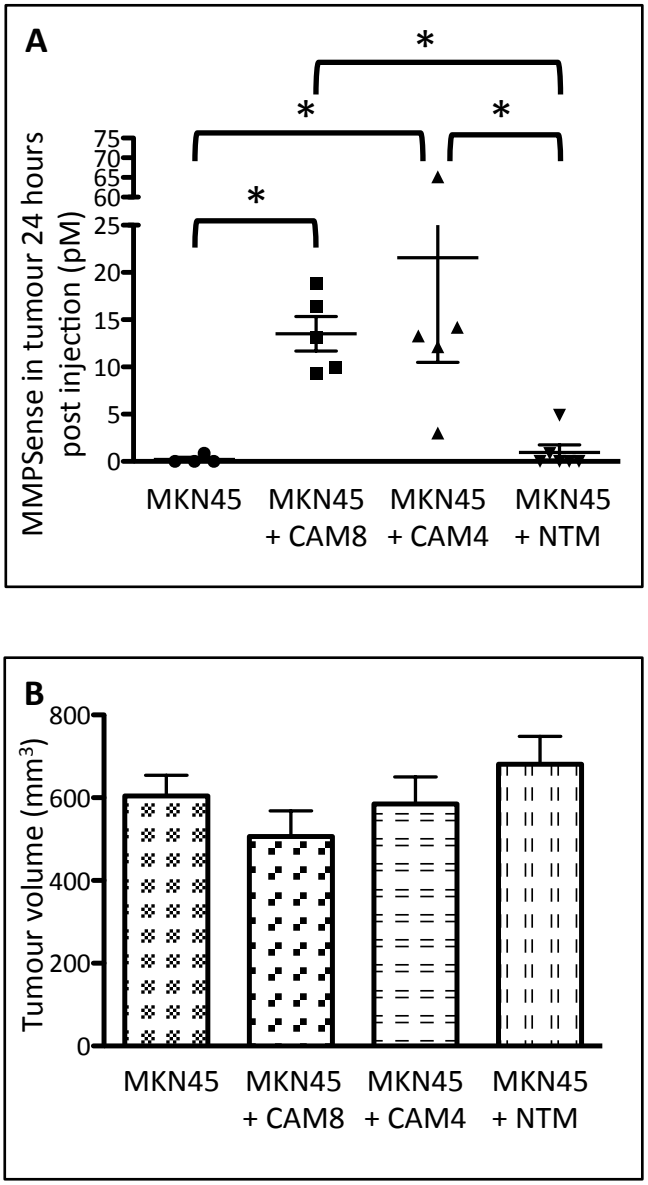

Figure 5.5. MMP activity is increased in xenografts containing CAMs. A, FMT assessment of MMP activity *in vivo* using MMPSense 750 FAST^{TM} indicated an increase in the presence of CAMs (mean ± SEM, 0.22±0.21 *vs* 13.52±1.83 pM for CAM8 and 21.56±11.09 for CAM4) when compared with MKN45 cells alone. **B,** Tumour volume at the time of imaging was similar in all groups. Mean results from 4-5 animals are shown; horizontal bars represent statistical significance by Kruskal-Wallis test with Dunn's post-hoc comparison.

5.3.4 Myofibroblasts enhance MKN45 cell invasion in an organotypic model of cell invasion.

In an attempt to dissect the contribution of myofibroblasts to MMP-driven tumorigenic processes, an organotypic co-culture model of cell invasion was developed. Myofibroblasts were seeded into a collagen/Matrigel^{TM} gel and a layer of MKN45 cells was plated on top. After 2 weeks, the gels were examined and the invasion of MKN45 cells into the gel was examined. The projection of the MKN45 cell layer into the gel layer was quantified as detailed in figure 3.10**A** such that higher numbers of MKN45 cells intruding into the gel resulted in a higher X/Y ratio. Gels not seeded with myofibroblasts did not cause MKN45 cell intrusion into the gel, whereas those with myofibroblasts caused the MKN45 cell layer to project into the gels (Figure 5.6**A-F**). It was also noted that in gels seeded with myofibroblasts, the MKN45 cell layer appeared to be thicker. Staining of the gels with the marker of cell proliferation Ki-67 did not reveal any difference in the proliferation rate of MKN45 cells (Figure 5.7), suggesting that the difference observed is not due to increased proliferation 2 weeks after the cells were seeded.

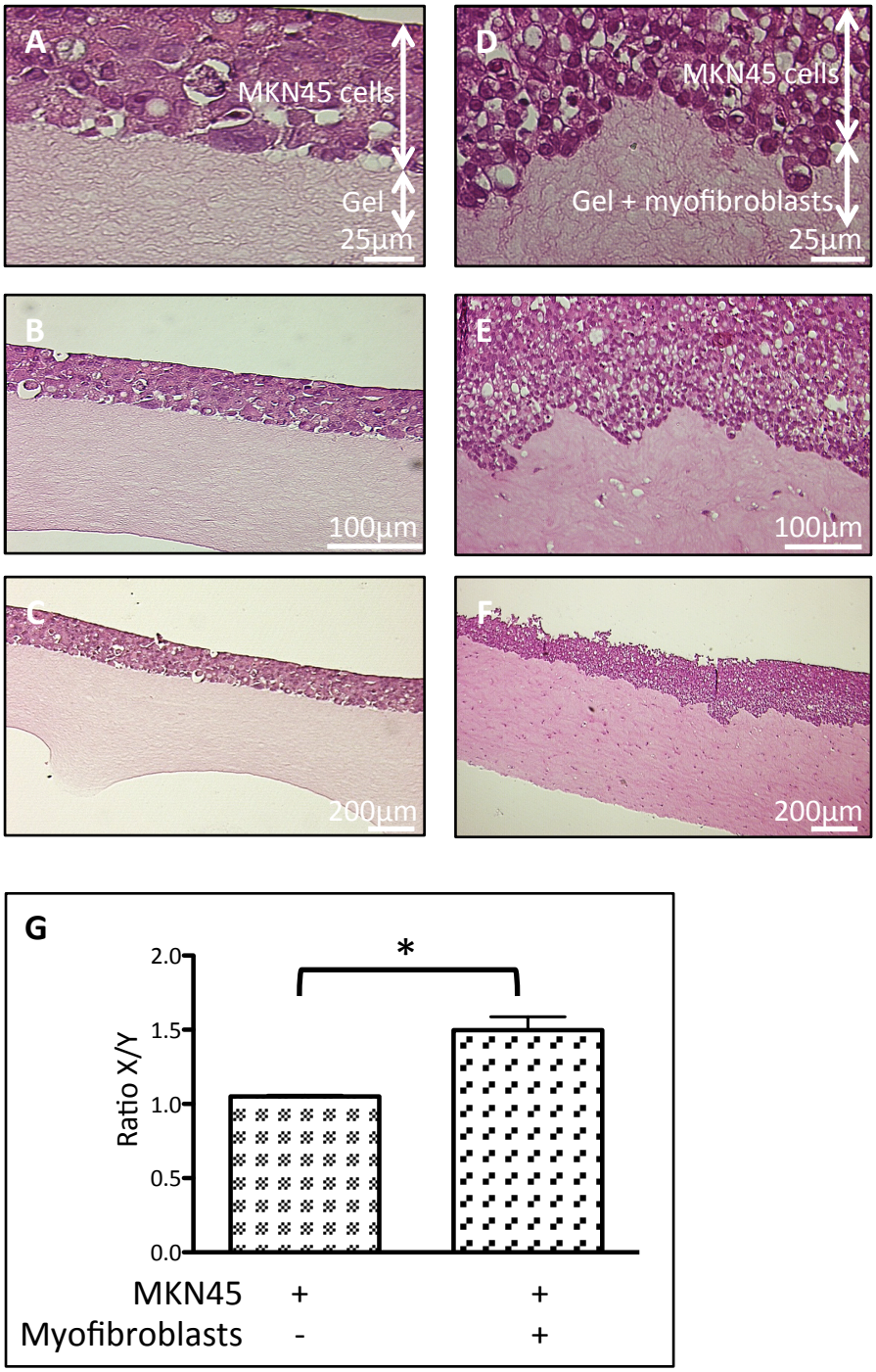

Figure 5.6. Myofibroblasts enhance MKN45 cell invasion in organotypic cultures. A-C, Representative images of organotypic cultures where the gel contains no myofibroblasts. **D-F,** Representative images of organotypic cultures with myofibroblasts seeded in the Matrigel/collagen gel. **G,** Seeding of myofibroblasts into the gel enhances MKN45 cell invasion compared with a gel without myofibroblasts, as shown by the higher X:Y ratio.

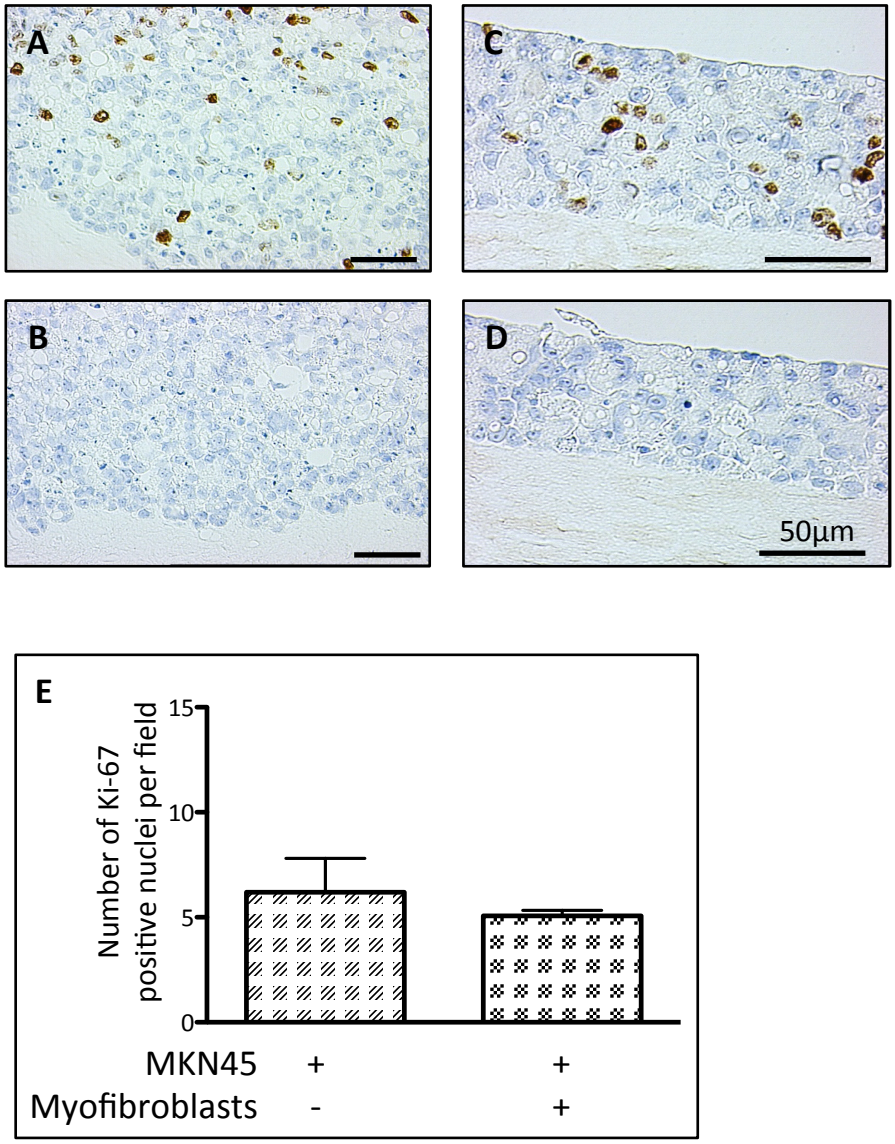

Figure 5.7. Proliferation in MKN45 cells is unaffected by the presence of myofibroblasts in the gel. A-B, Representative images of organotypic cultures with myofibroblasts stained for Ki-67 (**A**) and negative control (no primary antibody) (**B**). **C-D,** Representative images of organotypic cultures without myofibroblasts stained for Ki-67 (**C**) and corresponding negative control (**D**). **E,** Quantification of Ki-67 positive nuclei in the MKN45 cell layer revealed no change in MKN45 cell proliferation in response to the myofibroblasts in the gel.

5.3.5 MMP-2 inhibition decreased cell invasion.

Addition of an MMP-2 inhibitor to the gels decreased MKN45 cell invasion (Figure 5.8). This is in agreement with earlier data from our group showing that MMP-2 activity is increased in the media of CAMs and its inhibition decreases AGS cell migration in Boyden chamber assays (212) The effect of MMP-2 inhibition on cell proliferation was again investigated using Ki-67 staining and no difference in MKN45 cell proliferation was noted (Figure 5.9). Although in Boyden chamber assays MMP-3 inhibition suppressed AGS cell migration, these findings were not replicated in the organotypic model of MKN45 cell invasion (Figure 5.8**H**).

5.3.6 The presence of myofibroblasts in the gel does not affect the apoptotic rate of MKN45 cells.

Gels were stained for cleaved caspase-3, a marker of apoptotic cells. This revealed no evidence of apoptosis in the myofibroblasts seeded within the gel (data not shown). The proportion of apoptotic MKN45 cells in the gels was quantified using the same fields as for Ki-67 quantification and no difference in apoptosis was found between MKN45 cells grown on a gel seeded with myofibroblasts, compared to one without (Figure 5.10**D-E**). No difference in apoptosis was found in the presence of the MMP-2 inhibitor (Figure 5.10**E-F**). In the gels seeded with myofibroblasts, these could be identified using α-SMA staining (Figure 5.10**K-L**, arrows). There was no difference in their number or distribution in gels replenished with medium containing MMP-2 inhibitor compared to those replenished with FM alone. In all gels the MKN45 layer did not exhibit any positive α-SMA staining (Figure 5.10**G-I**).

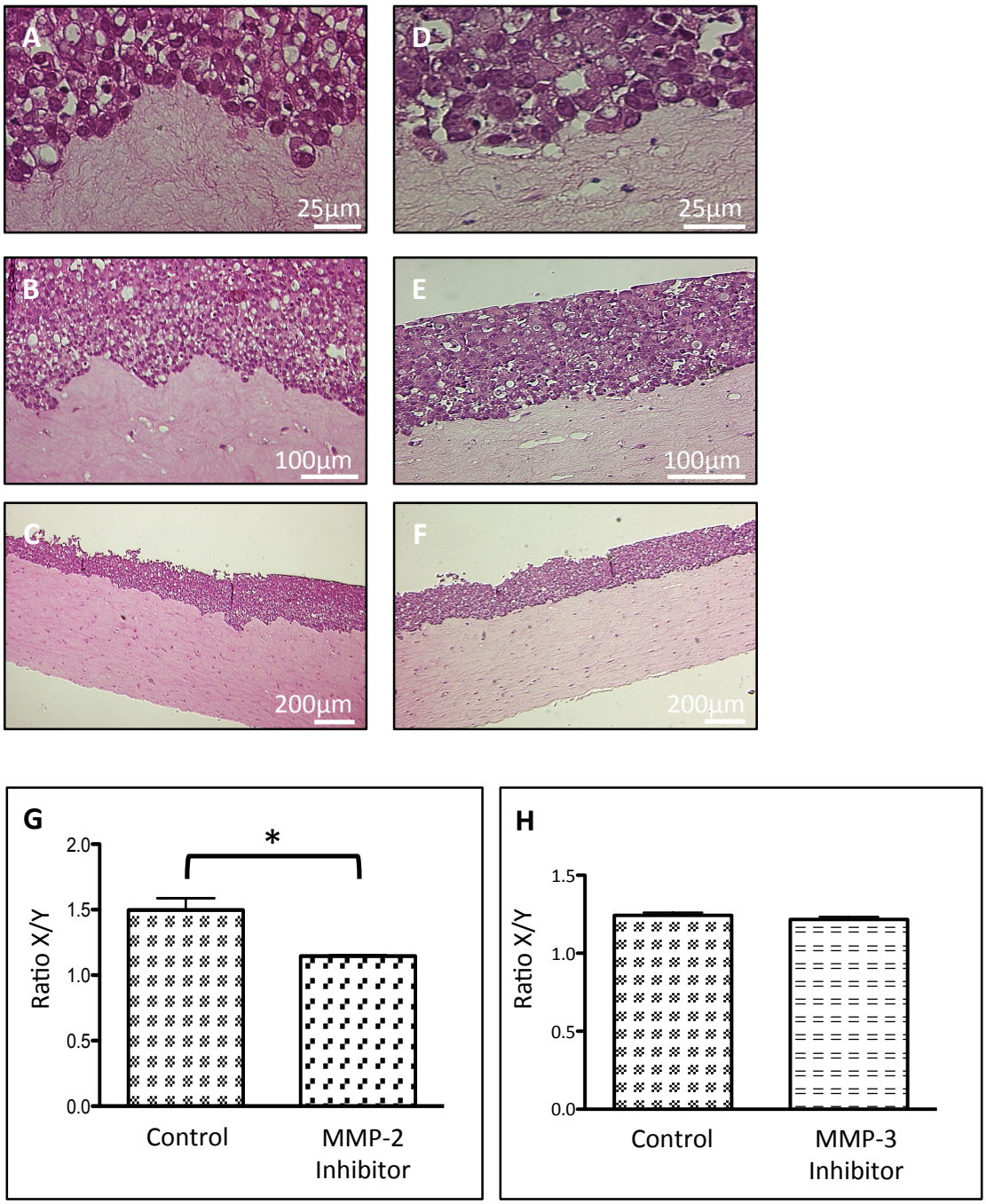

Figure 5.8. Addition of an MMP-2 inhibitor suppressed MKN45 cell invasion in organotypic cultures. A-C, Representative images of organotypic cultures without MMP-2 inhibitor. **D-F,** Representative images of organotypic cultures when MMP-2 inhibitor has been added. **G,** The addition of an MMP-2 inhibitor to the gel and the media suppresses MKN45 cell invasion. **H,** The addition of an MMP-3 inhibitor did not suppress MKN45 cell invasion.

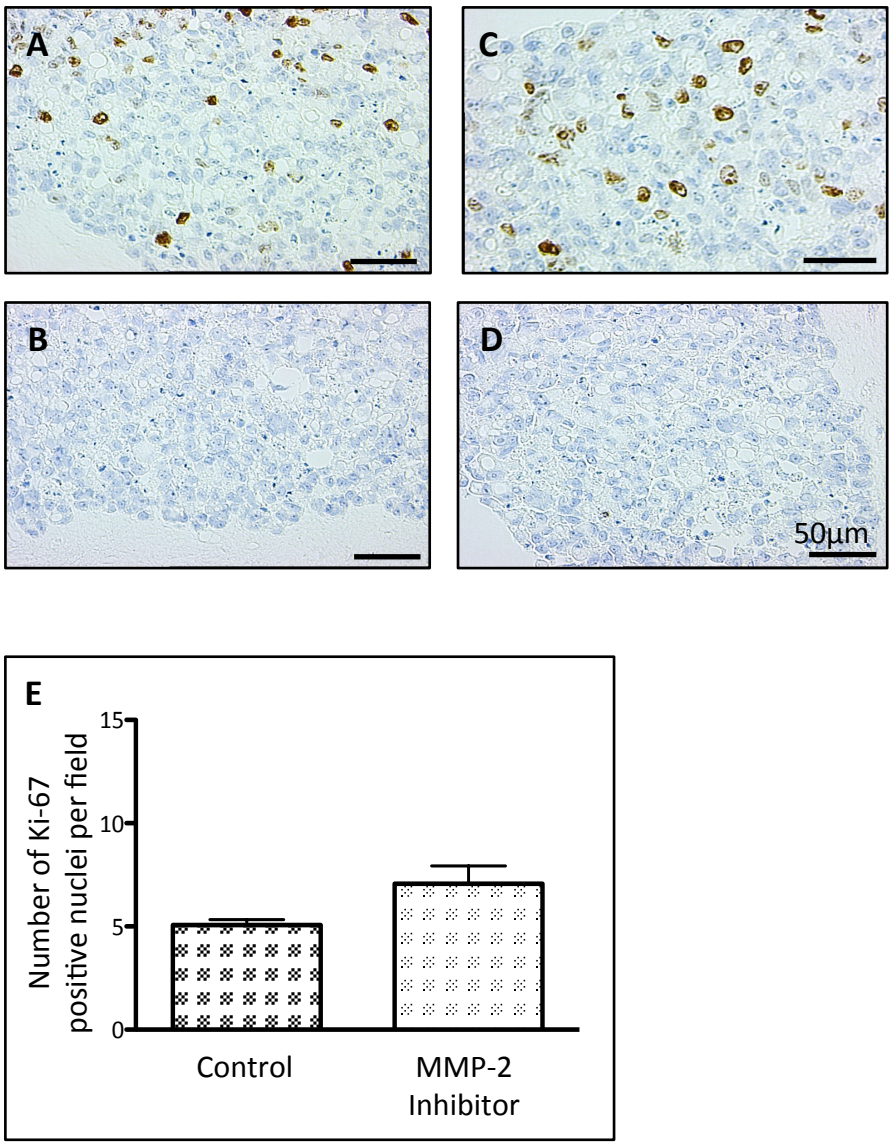

Figure 5.9. Proliferation in MKN45 cells is unaffected by the presence of MMP-2 Inhibitor. A-B, Representative images of organotypic cultures without MMP-2 inhibitor stained for Ki-67 (**A**) and negative control (no primary antibody) (**B**). **C-D,** Representative images of organotypic cultures with MMP-2 inhibitor stained for Ki-67 (**C**) and corresponding negative control (**D**). **E,** Quantification of Ki-67 positive nuclei in the MKN45 cell layer revealed no change in MKN45 cell proliferation in response to MMP-2 inhibitor.

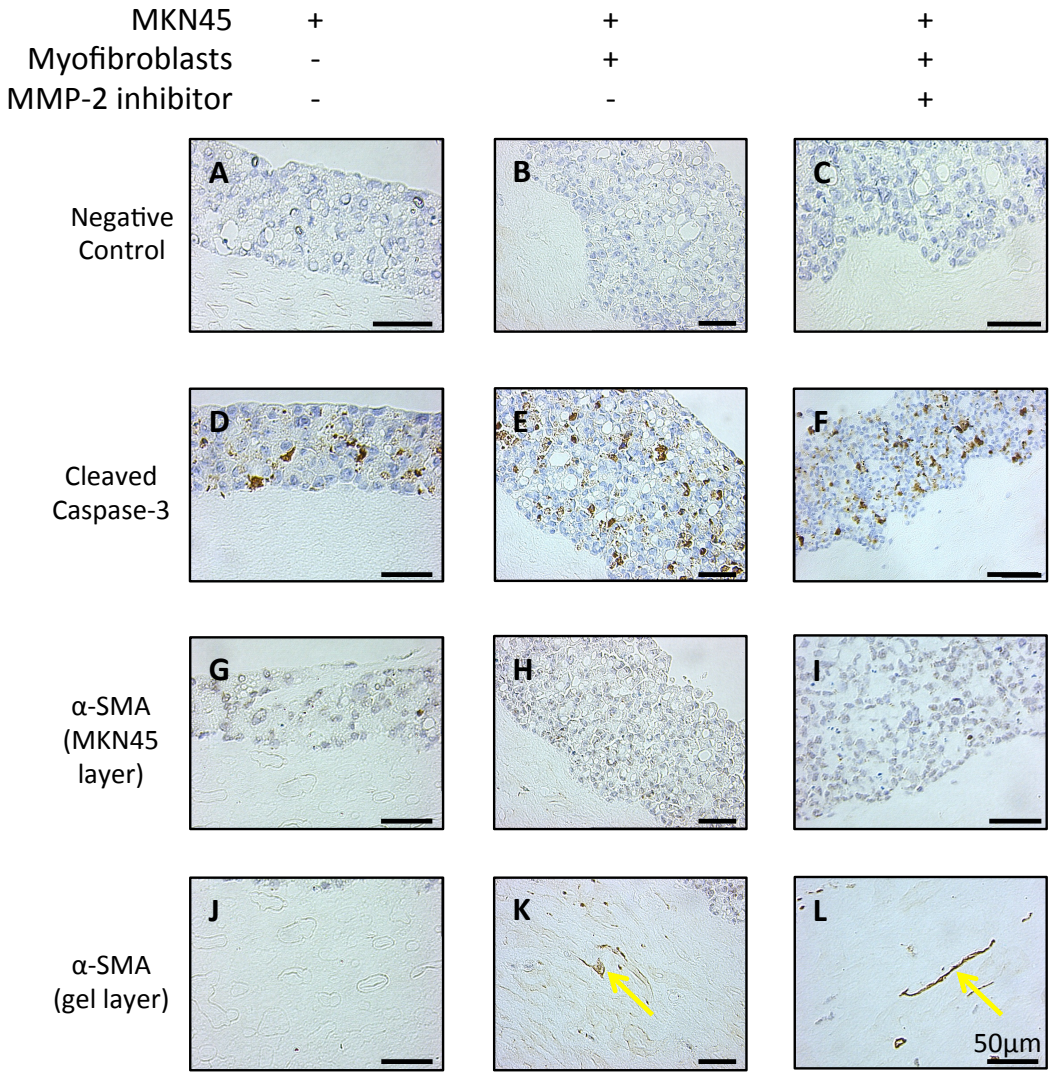

Figure 5.10. Immunohistochemistry for α-SMA and cleaved caspase-3 demonstrates no difference in apoptosis and confirms myofibroblasts within the gels A-C, Negative control (no primary antibody) **D-F,** Representative images of cleaved caspase-3 staining showing no difference in apoptotic cells. **G-I,** α-SMA staining in the MKN45 layer is negative. **J-L,** α-SMA staining of the myofibroblasts within the gels (arrows) seeded with these cells (**K,L**)

5.4 Discussion

This study has shown that the *in vitro* observations of increased MMP activity in CAMs are also reflected *in vivo*. Quantification of *in vivo* MMP activity in MKN45 cell xenografts revealed an increase in the presence of CAMs. In contrast, similar experiments to determine the *in vivo* activity of other proteases, including cathepsins and plasmin did not demonstrate any increase in the presence of CAMs. Inhibition of MMP-2 activity led to a decrease in myofibroblast-mediated cell invasion assessed using an organotypic model. These data demonstrate that the increased activation of stroma-derived MMPs found *in vitro* results in increased xenograft growth and increased cancer cell invasion.

Imaging proteolytic processes *in vivo* is a fast-growing field where the development of newer imaging modalities and probes constantly widens the options for research. Positron-emission tomography (PET) is already in clinical use but attempts at imaging MMPs using this technique have been restricted by unsuccessful attempts at developing appropriate radiolabelled tracer molecules (262). The generation of suitable contrast agents for MRI has shown more promise (263). Bioluminescent techniques have the advantage of low background and a large signal window but imaging MMP activity using this technique has proven difficult due to problems in designing the recognition site of a bioluminescent substrate (264).

Our assessment of *in vivo* MMP activity relied on the use of FMT, a technique which utilizes the ability of far-red light to propagate a few cm within animal tissue and combines it with improvements in the mathematical modelling of photon scattering behaviour. FMT is appealing because of the variety of fluorescent probes available to measure different cellular processes. We have used MMPSense 750 FASTTM, a reagent which produces fluorescence on cleavage by a broad range of MMPs. Specific probes capable of assessing the activity of individual MMPs are not available for *in vivo* work, and based on the present findings are now urgently needed. Assessment of other protease systems was possible, however, and we utilised this approach to examine the contributions of cathepsins and plasmin to *in vivo* protease activity.

The development of the organotypic co-culture system allowed us to examine the specific contribution of myofibroblast-derived MMPs to cell invasion, as an *in vivo* model incorporates contributions from other, mouse-derived, stromal cell types such as inflammatory cells, endothelial cells, MSCs and myofibroblasts. The use of specific MMP inhibitors in this myofibroblast-stimulated model of cell invasion also allowed us to examine the contribution of individual MMPs. The patterns of invasion observed in organotypic cultures mimic invasion in human cancers and allow the incorporation of stromal cell types (258).

Our previous study showed that myofibroblasts secrete MMPs (212) and this is in agreement with existing evidence of high MMP expression by stromal cells (265). In a xenograft model of cutaneous melanoma MMP-13 deficiency in the host mice led

to decreased tumour growth and angiogenesis, showing that stromal-derived MMPs are important in these processes (266). Our findings show that CAMs contribute to increased MMP activity *in vivo*. It is known that gastric epithelial cells express MMP-7 (147) and it is likely that *in vivo* high protease activity in the extracellular milieu arises as a result of reciprocal activation of stromal and epithelial-derived MMPs. The contributions to MMP activity by host-derived stroma and gastric cancer cells explain our finding that there is some MMP activity in xenografts injected with MKN45 cells alone. NTMs did not mediate an increase in MMP activity, suggesting that MMP activation is part of an altered CAM phenotype. Our previous study did not examine MMP activity in NTMs, but did show decreased activity in ATMs relative to CAMs (212).

Previous work has used a fluorescent probe activated by a variety of proteases to track the development of orthotopic mesothelioma xenografts using FMT (267). Another study used the activity of cathepsin, MMP and integrin activatable reagents as a surrogate measure of tumour volume and applied this system to monitor the response to therapy. Interestingly this group found that MMP activity in the tumour was not an accurate predictor of tumour volume, suggesting that MMP activity within the tumour was dependent on other factors (268). Our experiment was designed such that the tumour volume was equivalent across groups at the time of imaging, although this necessitated the injection of different amounts of MKN45 cells at the start.

Our finding that the total activity of cathepsins and plasmin were unchanged in xenografts containing CAMs may illustrate that MMPs represent particularly important stroma-derived proteases. Increased cleavage of cathepsin B in the medium of CAMs compared to ATMs was noted in the proteomic investigation of the myofibroblast secretome (212) but it is uncertain whether the cleavage identified led to activation of the protease. Cathepsin B expression is known to be associated with tumour invasion and metastasis in a variety of tumours (269). *In vitro* data from breast cancer cells suggests that cathepsin B inhibition decreases cell invasion (270). Cancers from different cells of origin may not share some characteristics; caution is therefore required in extrapolating between cancer cell types.

Although in our system, high MMP activity is associated with the presence of stromal cells and increased tumour growth, there is increasing evidence that the role of MMPs in cancer is more complex. Mice overexpressing MMP-9 developed a smaller primary tumour but an increased rate of metastasis (271,272). It is well recognised that MMPs are expressed in a variety of stromal cell types and that the interactions between these in the extracellular environment determine overall activity (262). The use of *in vivo* xenografts allowed us to identify increased MMP activity as a result of the addition of myofibroblasts but the presence of other cell types in this model does not permit us to examine whether MMPs from myofibroblasts directly contribute to overall MMP activity, or whether they trigger the activation of MMPs derived from other cells.

In the organotypic co-culture model, the interaction between cancer cells and myofibroblasts is examined in a way that replicates the patterns of invasion seen *in vivo*, without the influence of other cell types. The collagen/Matrigel^{TM} gel simulates extracellular matrix and the myofibroblasts seeded within secrete a range of factors which promote the invasion of cancer cells. Our finding that fibroblasts enhance cancer cell invasion is in agreement with previous data from 3D co-cultures in breast cancer (273). This study also found that only cancer-derived fibroblasts enhanced invasion, whereas those from normal breast tissue did not. Another study in breast cancer showed that increased invasion was associated with MMP-2 expression (274). Our finding that MMP inhibition decreases invasion in an organotypic co-culture system is consistent with similar studies using organotypic cultures of skin fibroblasts and skin cancer cells (275). Together the data indicate that myofibroblast-derived MMPs contribute to extracellular protease activity and this facilitates local invasion by the cancer cells.

Similar rates of proliferation and apoptosis were seen in organotypic cultures with or without myofibroblasts, suggesting that at the end of the experiment the rate of MKN45 cell turnover is similar. It remains possible that differences in cell survival and proliferation exist early in the experiment but are no longer evident at the end. This might explain why the MKN45 layer appeared thicker in gels seeded with myofibroblasts, although the contractile properties of myofibroblasts cause gel contraction, which may give the impression of a thicker gel. The addition of MMP-2 inhibitor to the gel and the medium did not affect MKN45 layer thickness,

proliferation or apoptosis, suggesting that the decrease in invasion seen in the presence of the MMP-2 inhibitor was not due to changes in cell turnover.

We have examined the role of MMP activity and demonstrated that myofibroblast-stimulated xenografts show increased MMP activity *in vivo* and that MMP-2 contributes to MKN45 cell invasion *in vitro*. Our findings provide further evidence for the important contribution of stroma-derived MMPs in the promotion of tumour growth and invasion.

5.5 Conclusions

1. *In vivo*, MMP activity is increased in xenografts injected with CAMs, compared to those injected with NTMs or with MKN45 cell alone (Figure 5.11).
2. Myofibroblasts enhance cancer cell invasion in an organotypic co-culture model.
3. MMP-2 inhibition decreases myofibroblast-stimulated cancer cell invasion in organotypic cultures.

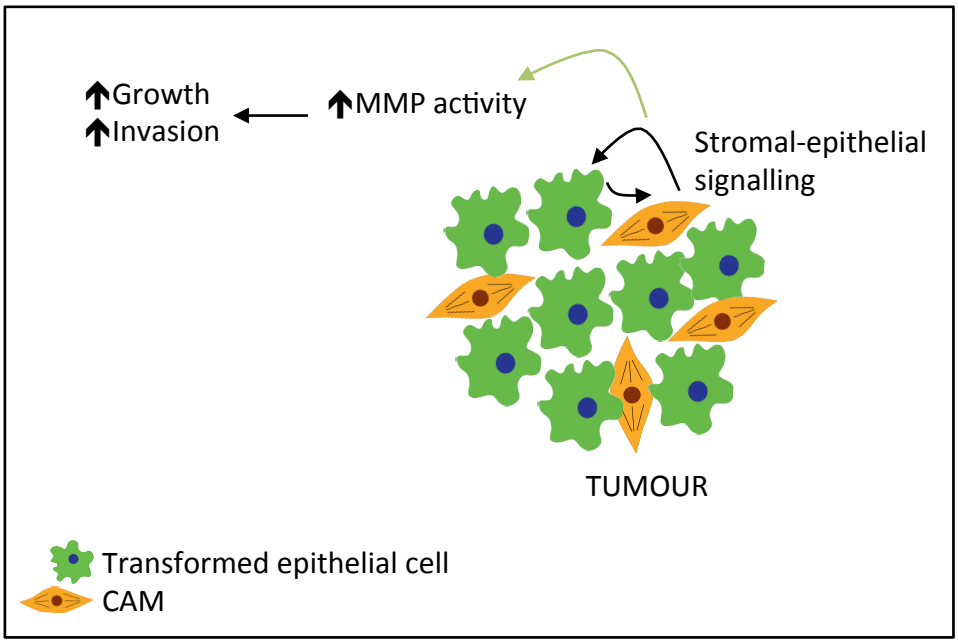

Figure 5.11. The contribution of MMPs to tumour growth and invasion. MMP activity is increased in tumours co-injected with CAMs. MMPs also contribute to the process of stroma-stimulated invasion.

CHAPTER 6: THE ROLE OF CHEMERIN SIGNALLING IN THE RECRUITMENT OF MSCS TO OESOPHAGEAL TUMOURS

6.1 Introduction

Oesophageal, like gastric, cancer presents at an advanced stage and has a poor prognosis (276). Also like gastric cancer, oesophageal tumours rich in stroma have a poor prognosis (277) and myofibroblasts form an important part of the oesophageal cancer stroma (278). Oesophageal myofibroblasts are known to stimulate cancer cell migration and invasion (J. D. Kumar, personal communication) and this work investigates their role in subcutaneous xenografts.

The recruitment of cells to tumours from the bone marrow has already been demonstrated and it has been postulated that bone marrow-derived cells may become myofibroblasts or CAFs (41). The interaction between myofibroblasts already in the tumour and bone marrow cells has not previously been studied.

Work from this group has demonstrated that oesophageal myofibroblasts release chemerin, which acts as a chemoattractant to MSCs, which express the ChemR23 receptor (J. D. Kumar, personal communication). Using labelled MSCs, this work aims to extend the previous observation to an *in vivo* model of myofibroblast-stimulated oesophageal xenograft growth and to determine whether chemerin-chemR23 signalling plays a role in the recruitment of MSCs to oesophageal tumours.

CCX832 is a chemR23 antagonist developed by ChemoCentryx trialled in the treatment of psoriasis but now withdrawn from progression (279).

6.1.1 Aims

1. To expand the *in vivo* model of stroma-stimulated xenograft growth from gastric cancer cells to oesophageal cells.
2. To model MSC homing to xenografts composed of MKN45 cells and OE21 cells.
3. To ascertain the effect of antagonism of the ChemR23 receptor on MSC homing.

6.2 Methods

6.2.1 Cell culture

MKN45 cells were cultured as detailed in 2.2.1-2. J. Dinesh Kumar cultured OE21 cells, oesophageal CAMs and human MSC lines.

6.2.2 Subcutaneous xenografts

Cells were prepared as described in 2.2.3. Where myofibroblasts and cancer cells were co-injected, they were mixed and re-suspended in PBS such that one injection corresponded to 100µl. For the MKN45 cell xenograft pilot experiment, 1 x 10^5 MKN45 cells were injected with or without 5 x 10^4 oesophageal CAMs. For the oesophageal xenografts, 1 x 10^6 OE21 cells were injected with or without 5 x 10^5 CAMs.

6.2.3 IV injection of MSCs

MSCs for IV injection were prepared by J. Dinesh Kumar. First, they were labelled using the cell membrane labels CellVue® Claret and PKH67. Labelling was evaluated by flow cytometry (CellVue® Claret) or fluorescence microscopy (PKH67). For the MKN45 cell pilot experiment, 1 x 10^6 labelled MSCs (CellVue® Claret or PKH67) were injected (IV tail vein) under GA 24 h prior to sacrifice. For the OE21 xenografts, 7.5 x 10^5 CellVue® Claret and 7.5 x 10^5 PKH67 labelled cells were combined, suspended in 100µl PBS and injected (IV tail vein) under GA 24 h prior to sacrifice (Figure 6.1).

6.2.4 CCX832

Animals received 2 subcutaneous doses of 125µl of 2mg/ml CCX832 a ChemR23 antagonist (equivalent to 10mg/kg dose) or 125µl vehicle (corn oil), 24 h prior to MSC injection and at the time of MSC injection (Figure 6.1).

6.2.5 FMT imaging

FMT imaging was performed under GA as described in 2.2.5b. Imaging for CellVue® Claret labelled MSCs was performed at baseline and 6 and 24 h post MSC injection in the 680nm channel and quantification was performed using TrueQuant software.

6.2.6 Microscopy for PKH67 labelled cells

Tumours were processed as described in 2.2.4. Six sections per tumour were stained with DAPI and PKH67 positive cells counted in 6 fields by an independent observer.

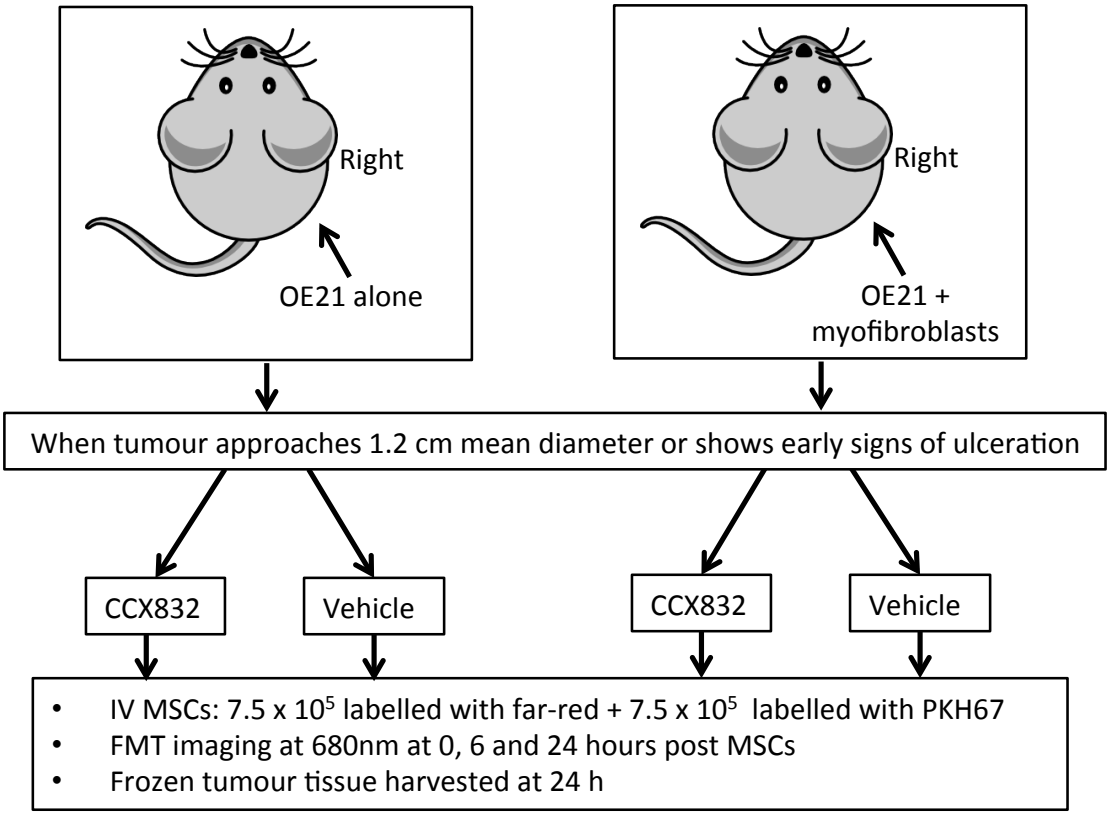

Figure 6.1. Experimental design to investigate the effect of ChemR23 inhibition on *in vivo* MSC homing. Subcutaneous xenografts composed for OE21 cells with or without CAMs were established in BALB/c nu/nu mice. Prior to the mean tumour diameter exceeding 1.2 cm the mice were given a dose of CCX832 or vehicle. After 24 h this dose was repeated, and MSCs were injected IV. FMT imaging was performed 6 and 24 h post MSC injection. Frozen sections were examined for evidence of labelled cells.

6.3 Results

6.3.1 The addition of CAMs to OE21 xenografts stimulates tumour formation

In order to create an *in vivo* model of MSC tumour homing, OE21 subcutaneous xenografts were established. Co-injection with oesophageal CAMs improved the tumour yield from 25% of animals (3/12) to 58% (7/12). Where tumours appeared, the rate of tumour growth was similar regardless of whether CAMs had been injected (Figure 6.2**G**). The histology of these tumours also appeared similar (Figure 6.2**A-F**). OE21 xenografts exhibited fewer areas of necrosis and no ulceration at the skin surface compared with MKN45 cell xenografts. The morphology of the cells reflected the squamous origin of the OE21 cells, with abundant mitotic cells.

6.3.2 MSCs labelled with CellVue® Claret membrane dye fluoresce at 680nm

To validate the detection system for CellVue®-labelled cells, initially droplets containing varying concentrations of labelled MSCs were visualised using FMT at 680nm. The intensity of fluorescence was proportional to the cell number (Figure 6.3). Droplets containing PBS only did not exhibit fluorescence.

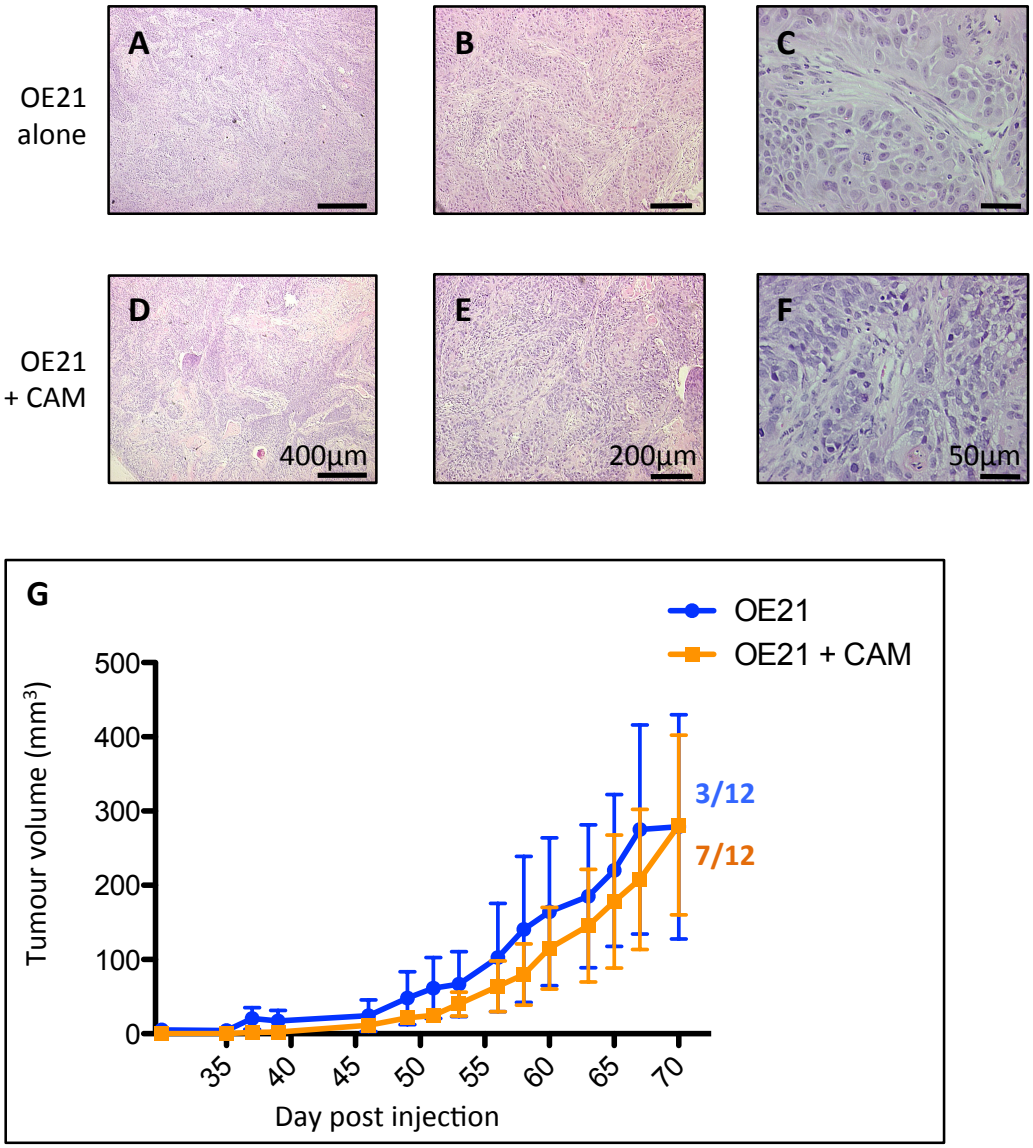

Figure 6.2. Histology and growth of OE21 xenografts. A-C, Representative images of H&E stained sections of tumours composed of OE21 alone. **D-F,** H&E stained sections of tumours containing OE21 + CAM cells. **G**, OE21 xenografts exhibit increased tumour yield when CAMs are co-injected compared to OE21 alone. Fractions denote the proportion of injections which yielded a tumour. Mean results from 3 OE21 animals and 7 OE21 + CAM animals are shown.

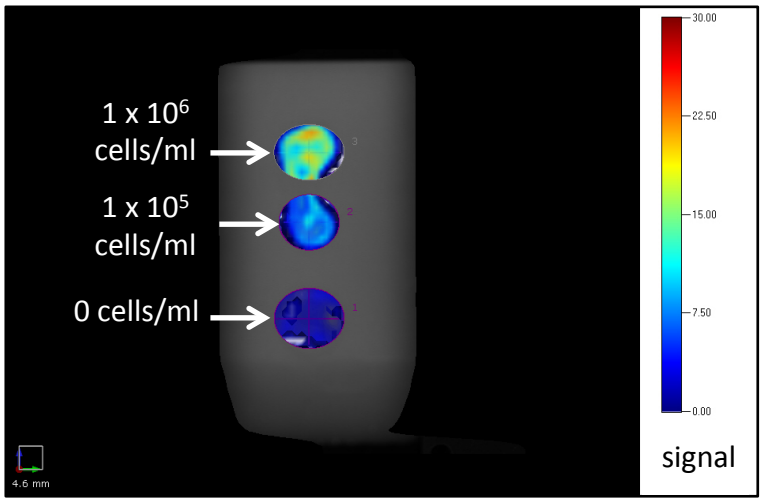

Figure 6.3. MSCs labelled with CellVue® Claret can be visualised using FMT. Representative images of droplets of MSCs suspended in PBS visualised using FMT at 680nm show increased fluorescence in droplets containing higher concentrations of labelled MSCs.

6.3.3 Increased fluorescence in the tumour following MSC injection

A pilot experiment to examine the feasibility of imaging MSCs recruited to tumours was conducted. This examined the fluorescence in xenografts 0, 6 and 24 h following IV MSC injection in xenografts composed of MKN45 cells and oesophageal CAMs. The fluorescence in the region of the tumour increased during the 24 h period (Figure 6.4**A**).

Imaging of these mice also revealed increased fluorescence in the region of the spleen following MSC injection (Figure 6.4**B**). Although these mice are immunosuppressed it is likely that the human MSCs are recognised as foreign material by the mouse immune system and most are processed and broken down in the spleen. The position of the mouse spleen beneath the left flank of the mouse had the potential to confound future fluorescence readings taken from tumours located immediately superficial to the spleen, so all further experiments injected the subcutaneous xenografts on the right side in an attempt to remove this problem.

Accumulation of fluorescently-labelled cell debris in the spleen was confirmed in mice injected with PKH67-labelled MSCs, where microscopic examination of frozen tumour sections revealed intense green staining in the spleen compare to mice injected with CellVue® Claret labelled MSCs only (Figure 6.5).

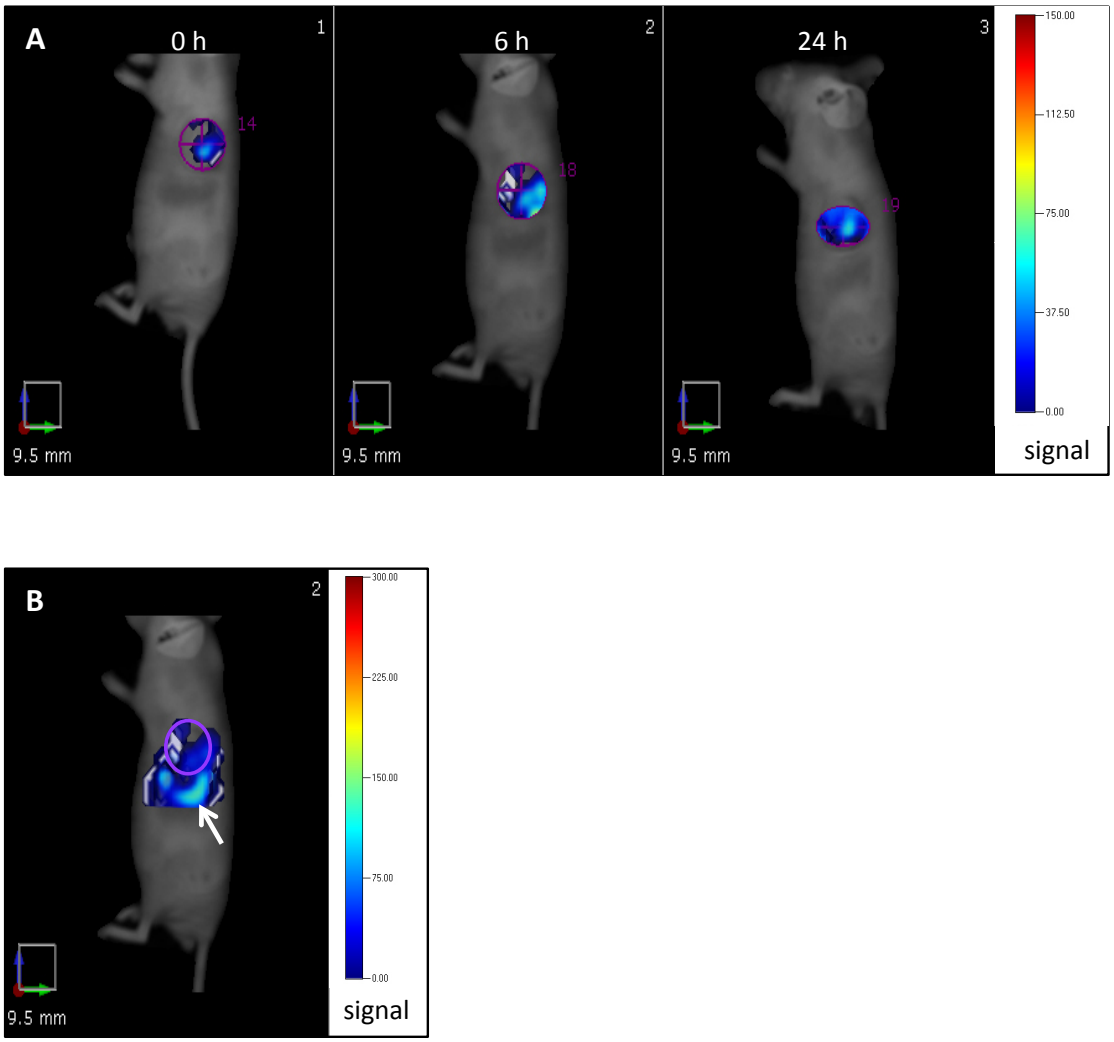

Figure 6.4. Increased fluorescence in the tumour following injection of labelled MSCs. **A,** Representative FMT images illustrating signal at 680nm from a mouse bearing a tumour composed of MKN45 cells + oesophageal CAMs showing increased fluorescence in the tumour 6 and 24 h post IV injection of CellVue® Claret labelled MSCs. **B,** FMT image of fluorescence outside the tumour boundary (purple outline) located in the region of the mouse spleen (arrow) 6 h post MSC injection.

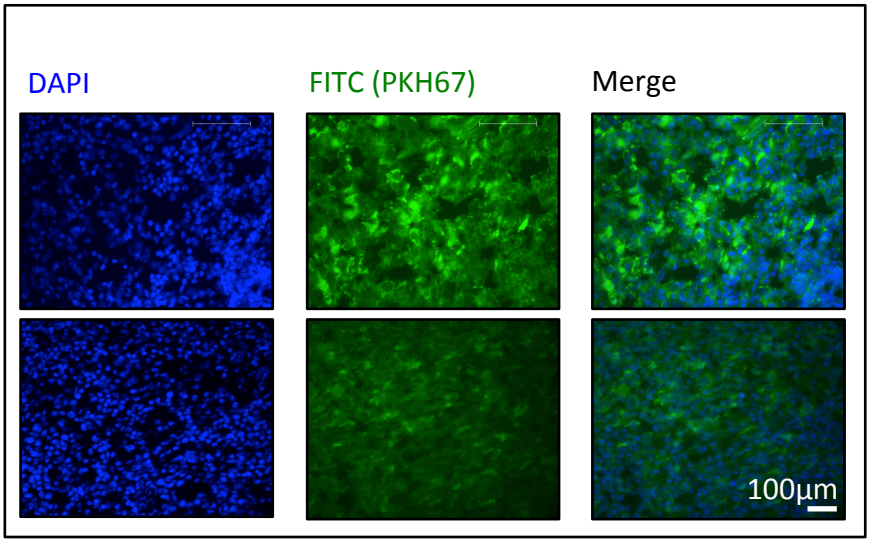

Figure 6.5 Accumulation of PKH67-labelled cell debris in mouse spleen. Representative fluorescence microscopy images demonstrating fluorescent cell debris (FITC filter) in the spleens of animals 24 h post injection of PKH67-labelled MSCs (top row). In mice injected with CellVue® Claret labelled MSCs (bottom row) no green fluorescence accumulates in the spleen. From left to right: nuclear localisation using DAPI, PKH67 visualisation under FITC filter, merged images.

6.3.4 Xenografts containing myofibroblasts demonstrate increased fluorescence following injection of labelled MSCs

In all cases the imaging performed immediately prior to MSC injection did not reveal any fluorescence in the region of the tumour. When the tumour was composed of OE21 cells and CAMs, increased fluorescence 24 h post MSC injection was noted, although this did not reach statistical significance (Figure 6.6**A**). Treatment of mice bearing OE21 and CAM tumours with CCX832 appeared to decrease the fluorescence from tumours but this did not reach statistical significance (Figure 6.6**B**).

The same tumours were examined microscopically for evidence of PKH67-labelled MSCs and areas of fluorescent cells were identified (Figure 6.7**A**). Quantification of the number of green cells per section showed decreased green cells in mice injected with CCX832 compared to those injected with vehicle, demonstrating inhibition of MSC homing by antagonism of ChemR23 (Figure 6.7**B**).

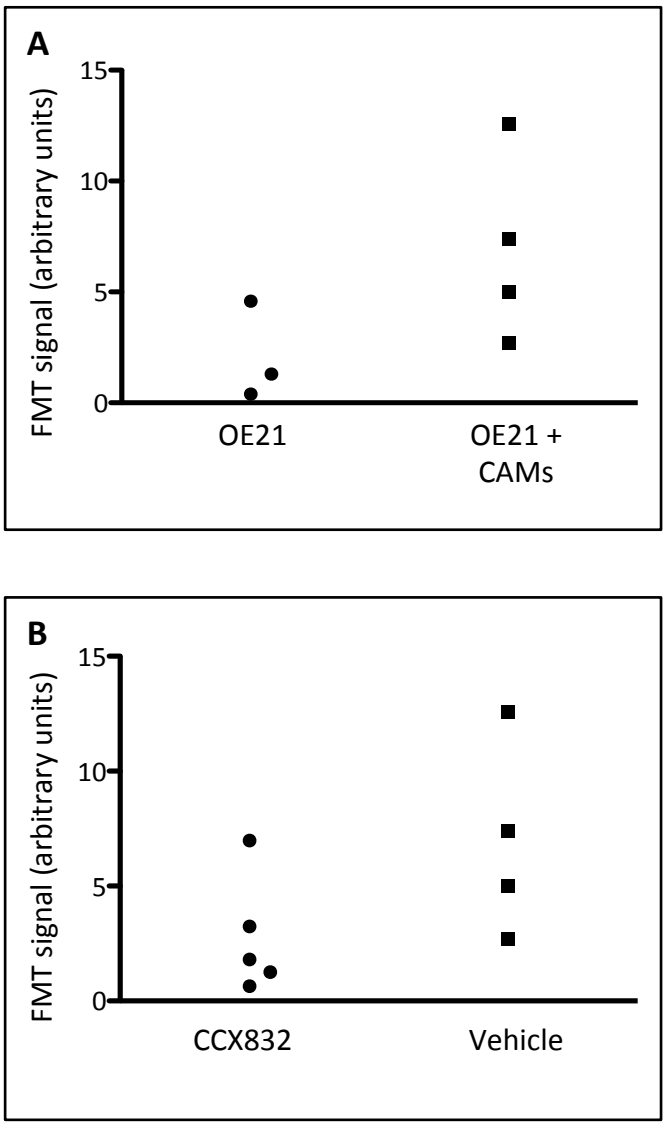

Figure 6.6. Effect of the addition of CAMs on MSC recruitment and its inhibition by CCX832. A, FMT signal at 680nm 24 h post injection of 7.5 x 10^5 CellVue® Claret-labelled MSCs is not significantly different in OE21 + CAM xenografts compared to OE21 alone. **B,** FMT signal at 680nm 24 h post injection of 7.5 x 10^5 CellVue® Claret-labelled MSCs in OE21 + CAM xenografts is not significantly different when the animals received 2 doses of CCX832 prior to MSC injection compared to injections of vehicle. Results from 3-5 animals per group are shown.

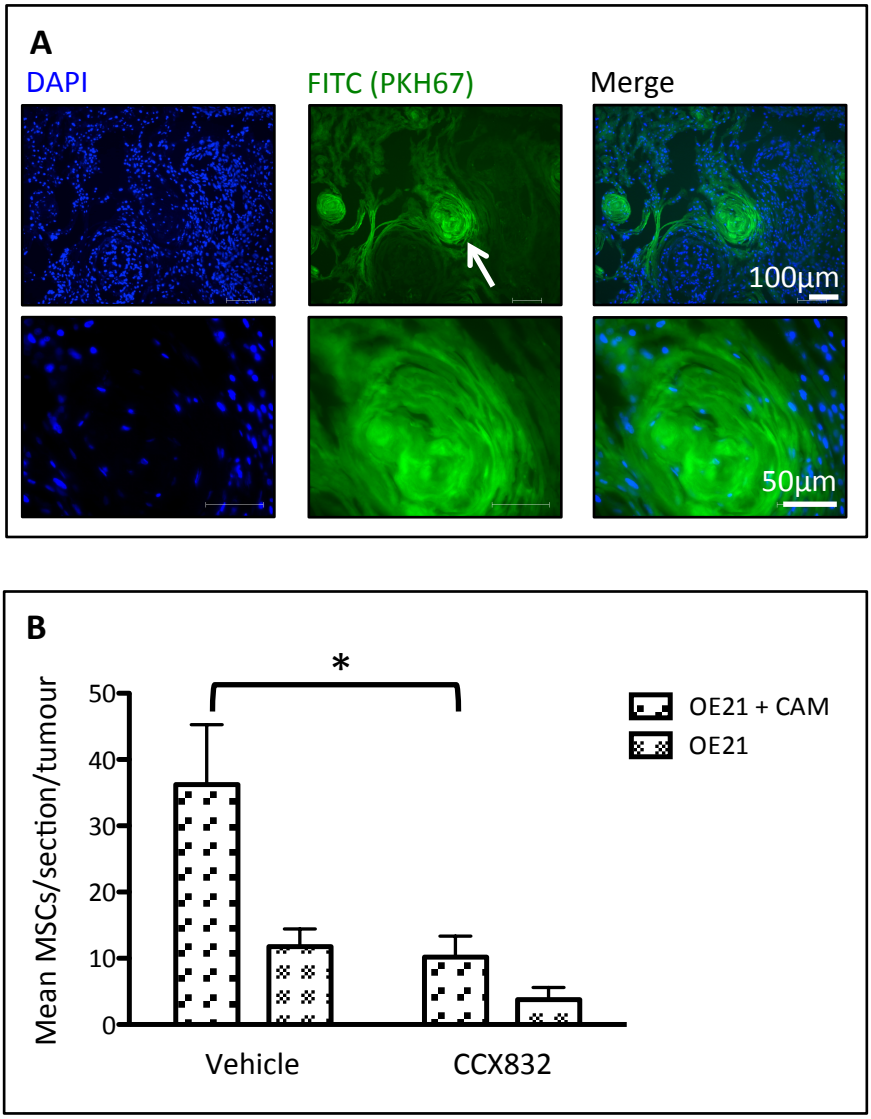

Figure 6.7. CCX832 administration suppresses MSC homing to OE21 + CAM tumours. A, Representative fluorescence microscopy images demonstrating areas of fluorescent cells (FITC filter) in the OE21 + CAM tumours (arrow). Top row: low power view, bottom row: high power view. **B,** Tumours without CAMs have lower overall MSC homing than those containing CAMs. CCX832 administration suppresses MSC homing to OE21 + CAM tumours. Quantification of mean number of MSCs per section per tumour, results from 3-6 animals per group are shown.

5.4 Discussion

We have created subcutaneous xenografts using OE21 cells and shown that the addition of CAMs increases tumour yield. The use of 2 membrane dyes has allowed the identification of fluorescent MSCs in the tumour and in the spleen through increased FMT signal and in frozen sections. The addition of CAMs to OE21 tumours increased fluorescence in the tumour following MSC injection. Treatment with a ChemR23 antagonist decreased both fluorescence detected by FMT and areas of green fluorescence seen in frozen sections.

FMT's utilisation of the far-red part of the electromagnetic spectrum enables non-invasive fluorescent imaging with minimal loss of signal from tissue absorption and light scattering (280). FMT has been used to track fluorescently labelled cells in order to calculate tumour volume. Breast cancer cells stably transfected with the fluorescent protein dsRed have been used to monitor the response of the ensuing subcutaneous xenografts to chemotherapy by using measurements of tumour volume generated by FMT (281). FMT has also been used to study the migration of macrophages labelled with a fluorescent dye to a subcutaneous inflammatory stimulus (282). More recently, the recruitment of circulating fibrocytes to arthritic joints was investigated using a CellVue® Claret membrane label and visualisation by FMT (283). Alternative imaging methods have been used in tracking labelled cells following injection. Thus the recruitment of fibroblasts labelled with the lipophilic near infra-red fluorochrome CellTracker™ CM-DiI injected intraperitoneally was

followed in subcutaneous ovarian cancer xenografts using MRI (284). Iron oxide labelled MSCs were shown to home to pulmonary metastases from breast cancer xenografts using MRI (285). FMT is a safe, quick and non-invasive imaging method which is capable of detecting a variety of fluorescent molecular probes as well as fluorescent cells, making it more versatile than other imaging modalities. In future, FMT could provide a good method for examining cell migration or metastasis *in vivo*.

Our finding that OE21 cells established subcutaneous xenografts in nude mice is in keeping with other xenograft studies using these cells (286,287). Like AGS cells, few examples of xenografts using these cells exist in the literature, which might explain the lower tumour yield and longer growth time than in MKN45 cells, making this model less efficient. The histology of these tumours reflected the origin of these cells, showing a squamous cell carcinoma. The low tumour yield even when CAMs were co-injected suggests that future experiments should increase the number of mice injected at the start of the experiment. Nevertheless, it is clear that the addition of CAMs increased tumour yield substantially.

We have shown that systemically administered MSCs are capable of homing to OE21 xenografts, both through increased far red fluorescence measured by FMT and by examination of frozen tumour tissue sections for labelled MSCs. It has already been shown that MSCs, either from the bone marrow or injected into the circulation, home to tumours. GFP-labelled MSCs injected IV can later be identified in the subcutaneous breast cancer xenografts of those mice (288). Subcutaneously implanted human bone marrow-derived MSCs home to distant subcutaneous

xenografts, demonstrating that human MSCs can free themselves from local attachments, enter the circulation and establish themselves elsewhere (289).

A mechanism for the homing of MSCs remains uncertain. Unlike when leucocytes are recruited to tissues and the well-defined leucocyte adhesion cascade is activated, there is no consensus for a molecular mechanism of MSC homing. It has been speculated that specific recruitment to an organ is not occurring, but rather the cells are becoming trapped in the vasculature, a process known as 'passive engraftment' (290). This may explain why some studies show that MSCs become part of a tumour only when injected arterially into a vessel anatomically close to the tumour, but not when injected at a distant site or IV (291). However, there is also evidence that MSC recruitment occurs preferentially to sites of tumour or inflammation, suggesting specific molecular mechanisms are responsible. Moreover, MSC recruitment to ischaemic myocardium is dependent on integrin β1 (292). While in gastric cancer, bone marrow-derived MSCs contribute to the CAM population and recruitment of MSCs to the tumour is dependent on CXCR4/SDF-1 signalling (41). This pathway was previously identified as playing an important role in the promotion of an 'activated' myofibroblast state via autocrine signalling (33).

Our findings that successful *in vivo* MSC homing may require the ChemR23 receptor identify a novel signalling pathway which has not previously been associated with MSC recruitment. Proteomic data from our group identified chemerin as being expressed by oesophageal myofibroblasts (293). Further *in vitro* validation has confirmed this, and shown that MSCs express ChemR23. In Boyden chamber

migration assays, both chemerin and myofibroblast CM enhance MSC migration and both are suppressed by the addition of a chemerin neutralizing antibody or CCX832 (J. Dinesh Kumar, unpublished data). Taken together, these findings indicate that chemerin released by oesophageal CAMs acts as a chemoattractant to MSCs via the ChemR23 receptor.

In summary we have demonstrated homing of MSCs to oesophageal xenografts and examined the effect of a ChemR23 antagonist on this phenomenon. This novel use of FMT will permit future studies involving cell tracking. Further investigation of the mechanism of MSC homing will reveal precisely how chemerin-ChemR23 interaction leads to the recruitment of MSCs to tumours.

6.5 Conclusions

1. The addition of CAMs to OE21 cells increases the likelihood of producing a subcutaneous xenograft.
2. MSCs injected IV home to subcutaneous tumours (Figure 6.8).
3. Antagonism at the ChemR23 receptor inhibits MSC homing to OE21 xenografts containing CAMs.

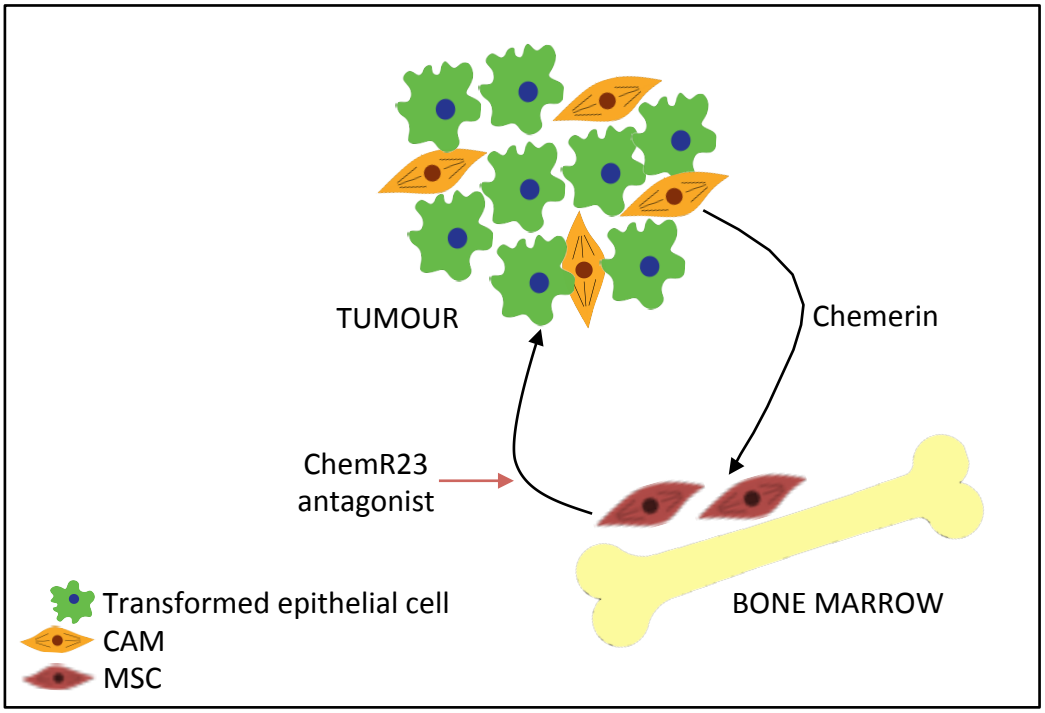

Figure 6.8. MSC homing requires chemerin signalling. Antagonism at the ChemR23 receptor suppresses MSC recruitment from the bone marrow, demonstrating that chemerin-ChemR23 signalling is necessary for MSC homing.

CHAPTER 7: GENERAL DISCUSSION

7.1 Main findings

This study has extended present understanding of the role of stroma-derived protease systems in tumour growth. PAI-1 overexpression in gastric cancer cells results in decreased *in vitro* cell adhesion and exerts a suppressive effect on tumour growth *in vivo*. Stromal myofibroblasts stimulate gastric tumour growth in a xenograft model and exert a systemic effect capable of affecting the growth of a distant tumour. Tumours seeded with myofibroblasts have increased MMP activity and MMP inhibition results in decreased tumour invasion in an organotypic model. Myofibroblasts play a role in the recruitment of MSCs from the bone marrow, a process which relies on chemerin signalling. FMT is a promising *in vivo* imaging technique, which is versatile, non-invasive and has the potential for imaging a wide variety of cellular processes.

7.2 Methodology

The present study relies on the use of cell lines, which are derived from a single population of cells and may not, therefore, reflect the heterogeneity of human gastric cancer. Having been maintained in culture for many years, these cells may acquire or lose characteristics through phenotypic drift (294). The use of early

passage primary cells, such as the gastric CAMs utilised in the present study, attempts to ensure that the characteristics of the cells still closely resemble those of the tissue of origin.

An insight into the role of stroma-derived PAI-1 in gastric cancer was provided by studying the effect of PAI-1 overexpression in cancer cells. This approach could have been complemented by the use of a knockdown system to decrease PAI-1 secreted by cancer cells and by myofibroblasts (295). For instance, siRNAs targeting PAI-1 mRNA could have been utilised to decrease PAI-1 expression. The growth of gastric cancer xenografts could have been studied in immunocompromised mice lacking the PAI-1 gene. The use of new PAI-1 inhibitors could also have provided insight into the effect of reducing extracellular PAI-1 (296).

The use of subcutaneous xenografts in immunosuppressed mice has the advantage of being simple and minimally invasive, and using cells of human origin. In the present study, this model permitted the manipulation of the myofibroblast component of the stroma, which was crucial to the investigation. However, the lack of a normal immune response to the tumour may compromise the accuracy of such models. In addition, subcutaneous xenografts have not proved to be reliable models of a tumour's response to treatment (297). Genetically modified mice prone to developing a tumour of interest can be useful in replicating the progression of human disease and have the advantage of a functioning immune component, but manipulation of the stromal component in these models is more difficult (298).

Organotypic cultures attempt to recreate the architectural arrangement of cells in a tumour and the resulting invasion pattern resembles those seen in human cancers (299). This approach enabled the use of specific MMP inhibitors and specifically examined the contribution of myofibroblasts. The *in vivo* xenograft system, although a good model incorporating most of the stromal features of a tumour, could not examine the specific contribution of CAMs to MMP activity.

The use of FMT, a novel imaging modality capable of visualising a variety of processes and molecules, enabled the tracking of cancer cells and MSCs and the assessment of protease activity *in vivo*. Alternative approaches to *in vivo* imaging include MRI, which has the advantage of giving simultaneous anatomical information (300). The identification of myofibroblasts in subcutaneous xenografts could have been improved using fluorescent tagging of primary myofibroblasts in combination with FMT.

7.3 Stromal PAI-1 in gastric cancer

This work has shown that in gastric cancer the myofibroblast is a rich source of PAI-1. This is in agreement with data from other cancers, where stromal contribution of PAI-1 has been characterised (211). In a recent study in colorectal cancer, MSCs were shown to produce PAI-1, with effects on cancer cell migration (301). In xenograft studies, PAI-1 secretion by host cells stimulates tumour growth and PAI-1 overexpression by cancer cells cannot overcome the absence of PAI-1 in the host,

emphasising the importance of the cellular origin of PAI-1 (302). It is clear that PAI-1 secretion by stromal cells forms an important component of the stromal-epithelial interactions in cancer.

The PAI-1 'paradox' in cancer refers to the ability of PAI-1 to stimulate tumour cell migration and invasion when its physiological function would suggest that by suppressing proteolysis it might suppress these processes and act to inhibit tumour growth. The present work has shown that in gastric cancer, PAI-1 can also have conflicting effects, as demonstrated by the finding that PAI-1 decreases cell adhesion *in vitro* but decreases *in vivo* xenograft growth. The 'paradox' of PAI-1 has been extended to other systems, as it seems that its role in the fibronolytic system extends wider than its ability to inhibit plasmin (303).

In gastric cancer, high PAI-1 expression is a marker of advanced stage and consequently of poor prognosis. In breast cancer, PAI-1 expression also denotes a poor prognosis and this has recently been used to identify patients most at risk of recurrence after surgery (304). Patients with tumours expressing PAI-1 are selected for chemotherapy and those negative for PAI-1 can avoid chemotherapy (and its toxic side effects) on the basis that they are at low risk of recurrence (305). Perhaps in future PAI-1 expression in gastric cancer might also provide a method for risk stratification in patients post gastrectomy.

7.4 The contribution of myofibroblasts to tumour growth

The present study has shown that primary gastric myofibroblasts stimulate the growth of gastric cancer subcutaneous xenografts. CAMs are known to differ from NTMs in the proteins they release and in their proliferation and migration *in vitro* (43). *In vivo*, however, this work has demonstrated that both CAMs and NTMs stimulate xenograft growth. This contrasts with data from other cancers where only CAMs stimulate xenograft growth (47). Future cancer therapies could be directed at myofibroblast-derived stimulators of tumour growth. Few molecular mechanisms promoting the recruitment of or activation of myofibroblasts have been identified although TGFβ is widely used to stimulate differentiation of fibroblasts into "activated fibroblasts" ie myofibroblasts (33).

Work from this group has identified TGFβIgh3 as a potential modulator of tumour growth. This protein is released by myofibroblasts and inhibits gastric cancer cell migration. Secretion of TGFβIgh3 is decreased in myofibroblasts from advanced cancer. Parenteral administration of TGFβIgh3 resulted in decreased tumour growth (43). The CXCR4-SDF-1 signalling pathway plays a role in the activation of myofibroblasts in breast cancer, and blockade of this pathway using a neutralising antibody suppressed tumour growth (48). These have not yet resulted in the development of any molecule suitable for use in the clinic. Inhibition of platelet-derived growth factor is also thought to inhibit tumour growth by affecting both cancer cells and stromal cells, but in spite of promising results in mouse models

(306), use of these compounds in the clinic has, again, not yet produced any survival benefit (307).

The addition of myofibroblasts to a xenograft resulted in the inhibition of the growth of a distant xenograft. Although it has long been known that tumours exert systemic effects, resulting in paraneoplastic syndromes (308), the mechanism for these has not been characterised. Using breast cancer cells, another group have shown that the growth of one xenograft can be potentiated by a distant xenograft composed of a more aggressive cell line. This is mediated by the release of osteopontin, which stimulates the recruitment of bone marrow cells (255). The present data add to this, as they demonstrate that a xenograft seeded with myofibroblasts is capable of affecting the growth of a distant xenograft without myofibroblasts. This confirms the existence of long-range signalling and implicates stromal-epithelial interactions in this process but further work is needed to elucidate a molecular mechanism for this not least because it might lead to a novel type of anti-cancer therapy.

7.5 Stroma-derived MMPs

MMP activation in a variety of cancers became a subject of interest some years ago and a number of MMP inhibitors were trialled. These did not, however, result in any clinically useful treatments for cancer and the reasons for this are complex (309). The trials only included patients with late stage disease and the measurements of the effect of MMP inhibitors may have been too simple. In addition, the inhibitors

used were not specific and there is growing evidence that different MMPs may have different roles in different cancers (257). The contribution of the stroma to MMP activity was not considered.

The present work has shown that MMP activity is increased in xenografts containing CAMs compared to those containing NTMs or no myofibroblasts. The identification of MMP-1, -1 and -3 as myofibroblast-derived stimulators of gastric cancer growth is encouraging for the development of specific MMP inhibitors (310). The increased MMP activity demonstrated in CAM-stimulated tumours may also be harnessed to activate drug molecules at the site of the cancer (311).

MMPs may also provide a source of biomarkers in gastric cancer. The elevated activation of MMPs demonstrated in gastric cancer is reflected in serum MMP concentrations and detection of these proteases could provide a useful marker for the diagnosis or monitoring of treatment response (312).

7.6 Recruitment of MSCs to oesophageal xenografts

Although the recruitment of MSCs to gastric tumours has previously been characterised (313), the finding that in oesophageal cancer, MSCs are recruited to the tumour is new. The data demonstrate that the presence of CAMs stimulates the recruitment of MSCs. In gastric cancer, MSC recruitment occurs through SDF-1 and hedgehog signalling (41,314). In oesophageal cancer, it seems that chemerin, a

novel chemoattractant, is important in recruiting MSCs (J. Dinesh Kumar, personal communication), as the administration of an antagonist to the chemerin receptor prevents MSC homing to an oesophageal subcutaneous xenograft.

A recent immunohistochemical study of samples of oesophageal mucosa taken from Barretts oesophagus and oesophageal cancer has shown increased chemerin expression in cancer (315). The pattern of staining was noted to include the stroma, which is consistent with the finding that oesophageal CAMs express chemerin, although epithelial expression of chemerin was also noted in this study. This work also postulated that chemerin expression stimulated the recruitment of dendritic cells; again this parallels the finding that chemerin release by CAMs results in MSC recruitment.

Further characterisation of this system may provide a novel approach to the development of cancer therapies directed at the stroma – rather than targeting the cells already within the tumour perhaps they could aim to prevent the recruitment of bone marrow-derived cells. CCX832 has been in a phase 1 trial for the treatment of psoriasis but its efficacy in human cancer has never been assessed.

This work emphasises the importance of assessing the contribution of specific proteases and their inhibitors in gastric cancer. The stroma is an important contributor to extracellular protease activity and myofibroblasts contribute both proteases and their inhibitors to the tumour microenvironment, resulting in the

modulation of tumour growth and cell adhesion. MSCs are recruited to oesophageal tumours via a novel signalling pathway (Figure 7.1).

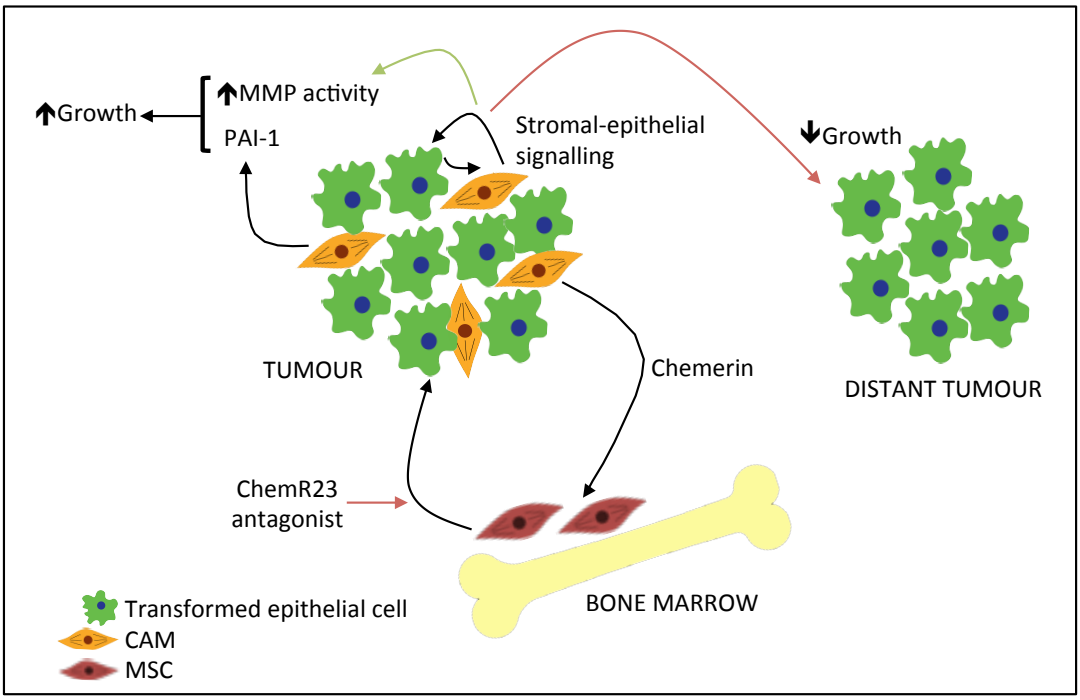

Figure 7.1 Short- and long- range signalling in upper gastrointestinal cancers. Within a solid tumour, signals between cell types modulate tumour growth and invasion. In gastric cancer, proteins from the uPA system and MMPs contribute to these signals. The addition of CAMs to gastric cancer cells potentiates tumour growth. Long-range signals occurring as a result of stromal-epithelial cell interactions are capable of modulating the growth of a distant tumour. In oesophageal cancer MSC recruitment is dependent on chemerin-ChemR23 signalling, a novel pathway involved in long-range signalling in cancer.

REFERENCES

1. Gross, C. G. Claude Bernard and the constancy of the internal environment. *Neuroscientist* **4,** 380–385 (1998).

2. Bayliss, W. M. & Starling, E. H. The mechanism of pancreatic secretion. *J. Physiol. (Lond.)* **28,** 325–353 (1902).

3. Paget, S. The distribution of secondary growths in cancer of the breast. 1889. *Cancer Metastasis Rev.* **8,** 98–101 (1989).

4. Mueller, M. M. & Fusenig, N. E. Friends or foes — bipolar effects of the tumour stroma in cancer. *Nat Rev Cancer* **4,** 839–849 (2004).

5. Nelson, C. M. & Bissell, M. J. Of extracellular matrix, scaffolds, and signaling: tissue architecture regulates development, homeostasis, and cancer. *Annu. Rev. Cell Dev. Biol.* **22,** 287–309 (2006).

6. Berenblum, I. & Shubik, P. An experimental study of the initiating stage of carcinogenesis, and a re-examination of the somatic cell mutation theory of cancer. *Br J Cancer* **3,** 109–118 (1949).

7. Mintz, B. & Illmensee, K. Normal genetically mosaic mice produced from malignant teratocarcinoma cells. *Proc. Natl. Acad. Sci. U.S.A.* **72,** 3585–3589 (1975).

8. Dvorak, H. F. Tumors: wounds that do not heal. Similarities between tumor stroma generation and wound healing. *N. Engl. J. Med.* **315,** 1650–1659 (1986).

9. Dingemans, K. P., Zeeman-Boeschoten, I. M., Keep, R. F. & Das, P. K. Transplantation of colon carcinoma into granulation tissue induces an invasive morphotype. *International Journal of Cancer* **54,** 1010–1016 (1993).

10. Hanahan, D. & Weinberg, R. A. Hallmarks of cancer: the next generation. *Cell* **144,** 646–674 (2011).

11. Tlsty, T. D. & Hein, P. W. Know thy neighbor: stromal cells can contribute oncogenic signals. *Current Opinion in Genetics & Development* **11,** 54–59 (2001).

12. Qian, B.-Z. & Pollard, J. W. Macrophage diversity enhances tumor progression and metastasis. *Cell* **141,** 39–51 (2010).

13. Murdoch, C., Muthana, M., Coffelt, S. B. & Lewis, C. E. The role of myeloid cells in the promotion of tumour angiogenesis. *Nat. Rev. Cancer* **8,** 618–631 (2008).

14. Carmeliet, P. & Jain, R. K. Angiogenesis in cancer and other diseases. *Nature* **407,** 249–257 (2000).

15. Tammela, T. & Alitalo, K. Lymphangiogenesis: Molecular mechanisms and future promise. *Cell* **140,** 460–476 (2010).

16. Aumailley, M. & Gayraud, B. Structure and biological activity of the extracellular matrix. *J. Mol. Med.* **76,** 253–265 (1998).

17. Howe, A., Aplin, A. E., Alahari, S. K. & Juliano, R. L. Integrin signaling and cell growth control. *Curr. Opin. Cell Biol.* **10,** 220–231 (1998).

18. Clarijs, R., Ruiter, D. J. & De Waal, R. M. W. Pathophysiological implications of stroma pattern formation in uveal melanoma. *J. Cell. Physiol.* **194,** 267–271 (2003).

19. Kalluri, R. Basement membranes: structure, assembly and role in tumour angiogenesis. *Nat. Rev. Cancer* **3,** 422–433 (2003).

20. Berndt, A., Borsi, L., Hyckel, P. & Kosmehl, H. Fibrillary co-deposition of laminin-5 and large unspliced tenascin-C in the invasive front of oral squamous cell carcinoma in vivo and in vitro. *J. Cancer Res. Clin. Oncol.* **127,** 286–292 (2001).

21. Gabbiani, G., Ryan, G. B. & Majno, G. Presence of modified fibroblasts in granulation tissue and their possible role in wound contraction. *Experientia* **27,** 549–550 (1971).

22. Sappino, A. P., Skalli, O., Jackson, B., Schürch, W. & Gabbiani, G. Smooth-muscle differentiation in stromal cells of malignant and non-malignant breast tissues. *Int. J. Cancer* **41,** 707–712 (1988).

23. Cardone, A., Tolino, A., Zarcone, R., Borruto Caracciolo, G. & Tartaglia, E. Prognostic value of desmoplastic reaction and lymphocytic infiltration in the management of breast cancer. *Panminerva Med* **39,** 174–177 (1997).

24. Maeshima, A. M. *et al.* Modified scar grade: a prognostic indicator in small peripheral lung adenocarcinoma. *Cancer* **95,** 2546–2554 (2002).

25. Powell, D. W. *et al.* Myofibroblasts. II. Intestinal subepithelial myofibroblasts. *Am J Physiol Cell Physiol* **277,** C183–C201 (1999).

26. Nakayama, H., Enzan, H., Miyazaki, E. & Toi, M. Alpha smooth muscle actin positive stromal cells in gastric carcinoma. *J. Clin. Pathol.* **55,** 741–744 (2002).

27. Fuyuhiro, Y. *et al.* Myofibroblasts are associated with the progression of scirrhous gastric carcinoma. *Exp Ther Med* **1,** 547–551 (2010).

28. Desmouliere, A., Guyot, C. & Gabbiani, G. The stroma reaction myofibroblast: a key player in the control of tumor cell behavior. *The International Journal of Developmental Biology* **48,** 509–517 (2004).

29. De Wever, O. *et al.* Tenascin-C and SF/HGF produced by myofibroblasts in vitro provide convergent pro-invasive signals to human colon cancer cells through RhoA and Rac. *FASEB J.* **18,** 1016–1018 (2004).

30. Sugimoto, H., Mundel, T. M., Kieran, M. W. & Kalluri, R. Identification of fibroblast heterogeneity in the tumor microenvironment. *Cancer Biol. Ther.* **5,** 1640–1646 (2006).

31. Kawase, A. *et al.* Podoplanin expression by cancer associated fibroblasts predicts poor prognosis of lung adenocarcinoma. *International Journal of Cancer* **123,** 1053–1059 (2008).

32. Kraman, M. *et al.* Suppression of antitumor immunity by stromal Cells expressing fibroblast activation protein. *Science* **330,** 827–830 (2010).

33. Kojima, Y. *et al.* Autocrine TGF-β and stromal cell-derived factor-1 (SDF-1) signaling drives the evolution of tumor-promoting mammary stromal myofibroblasts. *PNAS* **107,** 20009–20014 (2010).

34. De Wever, O., Demetter, P., Mareel, M. & Bracke, M. Stromal myofibroblasts are drivers of invasive cancer growth. *International Journal of Cancer* **123,** 2229–2238 (2008).

35. Hinz, B. Formation and function of the myofibroblast during tissue repair. *J Invest Dermatol* **127,** 526–537 (2007).

36. Eddy, A. A. The origin of scar-forming kidney myofibroblasts. *Nat Med* **19,** 964–966 (2013).

37. Rønnov-Jessen, L., Petersen, O. W., Koteliansky, V. E. & Bissell, M. J. The origin of the myofibroblasts in breast cancer. Recapitulation of tumor environment in culture unravels diversity and implicates converted fibroblasts and recruited smooth muscle cells. *J. Clin. Invest.* **95,** 859–873 (1995).

38. Radisky, D. C., Kenny, P. A. & Bissell, M. J. Fibrosis and cancer: do myofibroblasts come also from epithelial cells via EMT? *J. Cell. Biochem.* **101,** 830–839 (2007).

39. Kidd, S. *et al.* Origins of the tumor microenvironment: Quantitative assessment of adipose-derived and bone marrow–derived stroma. *PLoS ONE* **7,** e30563 (2012).

40. Direkze, N. C. *et al.* Bone marrow contribution to tumor-associated myofibroblasts and fibroblasts. *Cancer Res.* **64,** 8492–8495 (2004).

41. Quante, M. *et al.* Bone marrow-derived myofibroblasts contribute to the mesenchymal stem cell niche and promote tumor growth. *Cancer Cell* **19,** 257–272 (2011).

42. Krzysiek-Maczka, G. *et al.* Molecular alterations in fibroblasts exposed to Helicobacter pylori: a missing link in bacterial inflammation progressing into gastric carcinogenesis? *J. Physiol. Pharmacol.* **64,** 77–87 (2013).

43. Holmberg, C. *et al.* Release of TGFβig-h3 by gastric myofibroblasts slows tumor growth and is decreased with cancer progression. *Carcinogenesis* **33,** 1553–1562 (2012).

44. Hu, C. *et al.* Effects of cancer-associated fibroblasts on the migration and invasion abilities of SGC-7901 gastric cancer cells. *Oncol Lett* **5,** 609–612 (2013).

45. Fuyuhiro, Y. *et al.* Cancer-associated orthotopic myofibroblasts stimulates the motility of gastric carcinoma cells. *Cancer Sci.* **103,** 797–805 (2012).

46. Shan, L.-H. *et al.* Roles of fibroblasts from the interface zone in invasion, migration, proliferation and apoptosis of gastric adenocarcinoma. *J. Clin. Pathol.* **65,** 888–895 (2012).

47. Olumi, A. F. *et al.* Carcinoma-associated fibroblasts direct tumor progression of initiated human prostatic epithelium. *Cancer Res.* **59,** 5002–5011 (1999).

48. Orimo, A. *et al.* Stromal fibroblasts present in invasive human breast carcinomas promote tumor growth and angiogenesis through elevated SDF-1/CXCL12 secretion. *Cell* **121,** 335–348 (2005).

49. Guo, X., Oshima, H., Kitmura, T., Taketo, M. M. & Oshima, M. Stromal fibroblasts activated by tumor cells promote angiogenesis in mouse gastric cancer. *J. Biol. Chem.* **283,** 19864–19871 (2008).

50. Noma, K. *et al.* The essential role of fibroblasts in esophageal squamous cell carcinoma-induced angiogenesis. *Gastroenterology* **134,** 1981–1993 (2008).

51. Kellermann, M. G. *et al.* Mutual paracrine effects of oral squamous cell carcinoma cells and normal oral fibroblasts: induction of fibroblast to myofibroblast transdifferentiation and modulation of tumor cell proliferation. *Oral Oncol.* **44,** 509–517 (2008).

52. Calon, A. *et al.* Dependency of colorectal cancer on a TGF-β-driven program in stromal cells for metastasis initiation. *Cancer Cell* **22,** 571–584 (2012).

53. Goetz, J. G. *et al.* Biomechanical remodeling of the microenvironment by stromal caveolin-1 favors tumor invasion and metastasis. *Cell* **146,** 148–163 (2011).

54. Moinfar, F. *et al.* Concurrent and independent genetic alterations in the stromal and epithelial cells of mammary carcinoma: Implications for tumorigenesis. *Cancer Res* **60,** 2562–2566 (2000).

55. Qiu, W. *et al.* No evidence of clonal somatic genetic alterations in cancer-associated fibroblasts from human breast and ovarian carcinomas. *Nat. Genet.* **40,** 650–655 (2008).

56. Walter, K., Omura, N., Hong, S.-M., Griffith, M. & Goggins, M. Pancreatic cancer associated fibroblasts display normal allelotypes. *Cancer Biology & Therapy* **7,** 882–888 (2008).

57. Hosein, A. N. *et al.* Breast carcinoma–associated fibroblasts rarely contain p53 mutations or chromosomal aberrations. *Cancer Res* **70,** 5770–5777 (2010).

58. Wu, Y. *et al.* Comprehensive genomic meta-analysis identifies intra-tumoural stroma as a predictor of survival in patients with gastric cancer. *Gut* **62,** 1100–1111 (2013).

59. Jiang, L. *et al.* Global hypomethylation of genomic DNA in cancer-associated myofibroblasts. *Cancer Res.* **68,** 9900–9908 (2008).

60. Yu, J. *et al.* Unlike pancreatic cancer cells pancreatic cancer associated fibroblasts display minimal gene induction after 5-aza-2′-deoxycytidine. *PLoS ONE* **7,** e43456 (2012).

61. Spaeth, E. L. *et al.* Mesenchymal stem cell transition to tumor-associated fibroblasts contributes to fibrovascular network expansion and tumor progression. *PLoS ONE* **4,** e4992 (2009).

62. Worthley, D. L., Si, Y., Quante, M., Churchill, M. & Mukherjee, S. Bone marrow cells as precursors of the tumor stroma. *Exp. Cell Res.* (2013).

63. Friedenstein, A. J., Chailakhyan, R. K., Latsinik, N. V., Panasyuk, A. F. & Keiliss-Borok, I. V. Stromal cells responsible for transferring the microenvironment of the hemopoietic tissues. Cloning in vitro and retransplantation in vivo. *Transplantation* **17,** 331–340 (1974).

64. Caplan, A. I. Mesenchymal stem cells. *J. Orthop. Res.* **9,** 641–650 (1991).

65. Sacchetti, B. *et al.* Self-renewing osteoprogenitors in bone marrow sinusoids can organize a hematopoietic microenvironment. *Cell* **131,** 324–336 (2007).

66. Da Silva Meirelles, L., Chagastelles, P. C. & Nardi, N. B. Mesenchymal stem cells reside in virtually all post-natal organs and tissues. *J. Cell. Sci.* **119,** 2204–2213 (2006).

67. Muguruma, Y. *et al.* Reconstitution of the functional human hematopoietic microenvironment derived from human mesenchymal stem cells in the murine bone marrow compartment. *Blood* **107,** 1878–1887 (2006).

68. Dominici, M. *et al.* Minimal criteria for defining multipotent mesenchymal stromal cells. The International Society for Cellular Therapy position statement. *Cytotherapy* **8,** 315–317 (2006).

69. Ranganath, S. H., Levy, O., Inamdar, M. S. & Karp, J. M. Harnessing the mesenchymal stem cell secretome for the treatment of cardiovascular disease. *Cell Stem Cell* **10,** 244–258 (2012).

70. Nagpal, S. *et al.* Tazarotene-induced gene 2 (TIG2), a novel retinoid-responsive gene in skin. *J. Invest. Dermatol.* **109,** 91–95 (1997).

71. Wittamer, V. *et al.* Specific recruitment of antigen-presenting cells by chemerin, a novel processed ligand from human inflammatory fluids. *J. Exp. Med.* **198,** 977–985 (2003).

72. Meder, W. *et al.* Characterization of human circulating TIG2 as a ligand for the orphan receptor ChemR23. *FEBS Lett.* **555,** 495–499 (2003).

73. Roh, S. *et al.* Chemerin—A new adipokine that modulates adipogenesis via its own receptor. *Biochemical and Biophysical Research Communications* **362,** 1013–1018 (2007).

74. Bondue, B., Wittamer, V. & Parmentier, M. Chemerin and its receptors in leukocyte trafficking, inflammation and metabolism. *Cytokine Growth Factor Rev.* **22,** 331–338 (2011).

75. Weigert, J. *et al.* Systemic chemerin is related to inflammation rather than obesity in type 2 diabetes. *Clinical Endocrinology* **72,** 342–348 (2010).

76. Bozaoglu, K. *et al.* Chemerin is a novel adipokine associated with obesity and metabolic syndrome. *Endocrinology* **148,** 4687–4694 (2007).

77. Wang, N., Wang, Q.-J., Feng, Y.-Y., Shang, W. & Cai, M. Overexpression of chemerin was associated with tumor angiogenesis and poor clinical outcome in squamous cell carcinoma of the oral tongue. *Clin Oral Investig* (2013). doi:10.1007/s00784-013-1046-8

78. Pachynski, R. K. *et al.* The chemoattractant chemerin suppresses melanoma by recruiting natural killer cell antitumor defenses. *J. Exp. Med.* **209,** 1427–1435 (2012).

79. Fukumura, D. *et al.* Tumor induction of VEGF promoter activity in stromal cells. *Cell* **94,** 715–725 (1998).

80. Grivennikov, S. I., Greten, F. R. & Karin, M. Immunity, inflammation, and cancer. *Cell* **140,** 883–899 (2010).

81. Rawlings, N. D., Morton, F. R. & Barrett, A. J. MEROPS: the peptidase database. *Nucleic Acids Res.* **34,** D270–272 (2006).

82. Estreicher, A., Mühlhauser, J., Carpentier, J. L., Orci, L. & Vassalli, J. D. The receptor for urokinase type plasminogen activator polarizes expression of the protease to the leading edge of migrating monocytes and promotes degradation of enzyme inhibitor complexes. *J. Cell Biol.* **111,** 783–792 (1990).

83. Webb, D. J., Nguyen, D. H., Sankovic, M. & Gonias, S. L. The very low density lipoprotein receptor regulates urokinase receptor catabolism and breast cancer cell motility in vitro. *J. Biol. Chem.* **274,** 7412–7420 (1999).

84. Loskutoff, D. J., Van Mourik, J. A., Erickson, L. A. & Lawrence, D. Detection of an unusually stable fibrinolytic inhibitor produced by bovine endothelial cells. *Proc. Natl. Acad. Sci. U.S.A.* **80,** 2956–2960 (1983).

85. Simpson, A. J., Booth, N. A., Moore, N. R. & Bennett, B. Distribution of plasminogen activator inhibitor (PAI-1) in tissues. *J. Clin. Pathol.* **44,** 139–143 (1991).

86. Hekman, C. M. & Loskutoff, D. J. Endothelial cells produce a latent inhibitor of plasminogen activators that can be activated by denaturants. *J. Biol. Chem.* **260,** 11581–11587 (1985).

87. Prendergast, G. C., Diamond, L. E., Dahl, D. & Cole, M. D. The c-myc-regulated gene mrl encodes plasminogen activator inhibitor 1. *Mol. Cell. Biol.* **10,** 1265–1269 (1990).

88. Dewilde, M. *et al.* Subtle structural differences between human and mouse PAI-1 reveal the basis for biochemical differences. *J. Struct. Biol.* **171,** 95–101 (2010).

89. Carmeliet, P. *et al.* Plasminogen activator inhibitor-1 gene-deficient mice. II. Effects on hemostasis, thrombosis, and thrombolysis. *J. Clin. Invest.* **92,** 2756–2760 (1993).

90. Kenny, S. *et al.* The role of plasminogen activator inhibitor-1 in gastric mucosal protection. *Am. J. Physiol. Gastrointest. Liver Physiol.* **304,** G814–822 (2013).

91. Iwaki, T. *et al.* Life-threatening hemorrhage and prolonged wound healing are remarkable phenotypes manifested by complete plasminogen activator inhibitor-1 deficiency in humans. *J. Thromb. Haemost.* **9,** 1200–1206 (2011).

92. Deng, G., Curriden, S. A., Hu, G., Czekay, R. P. & Loskutoff, D. J. Plasminogen activator inhibitor-1 regulates cell adhesion by binding to the somatomedin B domain of vitronectin. *J. Cell. Physiol.* **189,** 23–33 (2001).

93. Kjøller, L. *et al.* Plasminogen activator inhibitor-1 represses integrin- and vitronectin-mediated cell migration independently of its function as an inhibitor of plasminogen activation. *Exp. Cell Res.* **232,** 420–429 (1997).

94. Stahl, A. & Mueller, B. M. Melanoma cell migration on vitronectin: regulation by components of the plasminogen activation system. *Int. J. Cancer* **71,** 116–122 (1997).

95. López-Alemany, R., Redondo, J. M., Nagamine, Y. & Muñoz-Cánoves, P. Plasminogen activator inhibitor type-1 inhibits insulin signaling by competing with alphavbeta3 integrin for vitronectin binding. *Eur. J. Biochem.* **270,** 814–821 (2003).

96. Degryse, B. *et al.* The low density lipoprotein receptor-related protein is a motogenic receptor for plasminogen activator inhibitor-1. *J. Biol. Chem.* **279,** 22595–22604 (2004).

97. Zhang, Y.-P. *et al.* Plasminogen activator inhibitor-1 promotes the proliferation and inhibits the apoptosis of pulmonary fibroblasts by Ca(2+) signaling. *Thromb. Res.* **131,** 64–71 (2013).

98. Bruckner, A., Filderman, A. E., Kirchheimer, J. C., Binder, B. R. & Remold, H. G. Endogenous receptor-bound urokinase mediates tissue invasion of the human lung carcinoma cell lines A549 and Calu-1. *Cancer Res.* **52,** 3043–3047 (1992).

99. Planus, E. *et al.* Binding of urokinase to plasminogen activator inhibitor type-1 mediates cell adhesion and spreading. *J. Cell. Sci.* **110 (Pt 9),** 1091–1098 (1997).

100. Praus, M., Collen, D. & Gerard, R. D. Both u-PA inhibition and vitronectin binding by plasminogen activator inhibitor 1 regulate HT1080 fibrosarcoma cell metastasis. *Int. J. Cancer* **102,** 584–591 (2002).

101. Kwaan, H. C., Wang, J., Svoboda, K. & Declerck, P. J. Plasminogen activator inhibitor 1 may promote tumour growth through inhibition of apoptosis. *Br. J. Cancer* **82,** 1702–1708 (2000).

102. Beyer, B. C. M. *et al.* Urokinase system expression in gastric carcinoma: prognostic impact in an independent patient series and first evidence of

predictive value in preoperative biopsy and intestinal metaplasia specimens. *Cancer* **106,** 1026–1035 (2006).

103. Sakakibara, T. *et al.* Plasminogen activator inhibitor-1 as a potential marker for the malignancy of gastric cancer. *Cancer Sci.* **97,** 395–399 (2006).

104. Kaneko, T., Konno, H., Baba, M., Tanaka, T. & Nakamura, S. Urokinase-type plasminogen activator expression correlates with tumor angiogenesis and poor outcome in gastric cancer. *Cancer Sci.* **94,** 43–49 (2003).

105. Nishioka, N. *et al.* Plasminogen activator inhibitor 1 RNAi suppresses gastric cancer metastasis in vivo. *Cancer Sci.* **103,** 228–232 (2012).

106. Gross, J. & Lapiere, C. M. Collagenolytic activity in amphibian tissues: A tissue culture assay. *PNAS* **48,** 1014–1022 (1962).

107 . Werb, Z. & Chin, J. R. Extracellular matrix remodeling during morphogenesis. *Ann. N. Y. Acad. Sci.* **857,** 110–118 (1998).

108. Lund, L. R. *et al.* Functional overlap between two classes of matrix-degrading proteases in wound healing. *EMBO J.* **18,** 4645–4656 (1999).

109. Pepper, M. S. Role of the matrix metalloproteinase and plasminogen activator-plasmin systems in angiogenesis. *Arterioscler. Thromb. Vasc. Biol.* **21,** 1104–1117 (2001).

110. Murphy, G. Tissue inhibitors of metalloproteinases. *Genome Biol.* **12,** 233 (2011).

111. Sottrup-Jensen, L. & Birkedal-Hansen, H. Human fibroblast collagenase-alpha-macroglobulin interactions. Localization of cleavage sites in the bait regions of five mammalian alpha-macroglobulins. *J. Biol. Chem.* **264,** 393–401 (1989).

112. Liotta, L. A. *et al.* Metastatic potential correlates with enzymatic degradation of basement membrane collagen. *Nature* **284,** 67–68 (1980).

113. Sternlicht, M. D. *et al.* The stromal proteinase MMP3/stromelysin-1 promotes mammary carcinogenesis. *Cell* **98,** 137–146 (1999).

114. Sympson, C. J., Bissell, M. J. & Werb, Z. Mammary gland tumor formation in transgenic mice overexpressing stromelysin-1. *Semin. Cancer Biol.* **6,** 159–163 (1995).

115. Rudolph-Owen, L. A., Chan, R., Muller, W. J. & Matrisian, L. M. The matrix metalloproteinase matrilysin influences early-stage mammary tumorigenesis. *Cancer Res.* **58,** 5500–5506 (1998).

116. Wroblewski, L. E. *et al.* Stimulation of MMP-7 (matrilysin) by Helicobacter pylori in human gastric epithelial cells: role in epithelial cell migration. *J. Cell. Sci.* **116,** 3017–3026 (2003).

117. Wilson, C. L., Heppner, K. J., Labosky, P. A., Hogan, B. L. & Matrisian, L. M. Intestinal tumorigenesis is suppressed in mice lacking the metalloproteinase matrilysin. *Proc. Natl. Acad. Sci. U.S.A.* **94,** 1402–1407 (1997).

118. Coussens, L. M., Fingleton, B. & Matrisian, L. M. Matrix metalloproteinase inhibitors and cancer: trials and tribulations. *Science* **295,** 2387–2392 (2002).

119. Bramhall, S. R. *et al.* Marimastat as maintenance therapy for patients with advanced gastric cancer: a randomised trial. *Br. J. Cancer* **86,** 1864–1870 (2002).

120. Dahl, K. D. C. *et al.* Matrix metalloproteinase 9 is a mediator of epidermal growth factor–dependent E-cadherin loss in ovarian carcinoma cells. *Cancer Res* **68,** 4606–4613 (2008).

121. Mitsiades, N., Yu, W. H., Poulaki, V., Tsokos, M. & Stamenkovic, I. Matrix metalloproteinase-7-mediated cleavage of Fas ligand protects tumor cells from chemotherapeutic drug cytotoxicity. *Cancer Res.* **61,** 577–581 (2001).

122. Dufour, A., Sampson, N. S., Zucker, S. & Cao, J. Role of the hemopexin domain of matrix metalloproteinases in cell migration. *Journal of Cellular Physiology* **217,** 643–651 (2008).

123. Houghton, A. M., Hartzell, W. O., Robbins, C. S., Gomis-Rüth, F. X. & Shapiro, S. D. Macrophage elastase kills bacteria within murine macrophages. *Nature* **460,** 637–641 (2009).

124. López-Boado, Y. S. *et al.* Bacterial exposure induces and activates matrilysin in mucosal epithelial cells. *J Cell Biol* **148,** 1305–1315 (2000).

125. Ala-aho Risto & Kähäri, V.-M. Collagenases in cancer. *Biochimie* **87,** 273–286 (2005).

126. Sternlicht, M. D. & Werb, Z. How matrix metalloproteinases regulate cell behavior. *Annual Review of Cell and Developmental Biology* **17,** 463–516 (2001).

127. Robinson, S. C., Scott, K. A. & Balkwill, F. R. Chemokine stimulation of monocyte matrix metalloproteinase-9 requires endogenous TNF-α. *European Journal of Immunology* **32,** 404–412 (2002).

128. Fang, K. C. *et al.* Mast cell expression of gelatinases A and B is regulated by kit ligand and TGF-β. *J Immunol* **162,** 5528–5535 (1999).

129. Roche, W. R. The nature and significance of tumour-associated mast cells. *J. Pathol.* **148,** 175–182 (1986).

130. Van Lint, P. & Libert, C. Matrix metalloproteinase-8: cleavage can be decisive. *Cytokine Growth Factor Rev.* **17,** 217–223 (2006).

131.Rundhaug, J. E. Matrix metalloproteinases and angiogenesis. *J. Cell. Mol. Med.* **9,** 267–285 (2005).

132. Nielsen, B. S. *et al.* Collagenase-3 expression in breast myofibroblasts as a molecular marker of transition of ductal carcinoma in situ lesions to invasive ductal carcinomas. *Cancer Res.* **61,** 7091–7100 (2001).

133. Noël, A. *et al.* Inhibition of stromal matrix metalloproteases: effects on breast-tumor promotion by fibroblasts. *Int. J. Cancer* **76,** 267–273 (1998).

134. Chu, D. *et al.* Matrix metalloproteinase-9 is associated with disease-free survival and overall survival in patients with gastric cancer. *Int. J. Cancer* **129,** 887–895 (2011).

135. Al-Batran, S.-E. *et al.* The validation of matrix metalloproteinase-9 mRNA gene expression as a predictor of outcome in patients with metastatic gastric cancer. *Ann. Oncol.* **23,** 1699–1705 (2012).

136. Wroblewski, L. E., Pritchard, D. M., Carter, S. & Varro, A. Gastrin-stimulated gastric epithelial cell invasion: the role and mechanism of increased matrix metalloproteinase 9 expression. *Biochem. J.* **365,** 873–879 (2002).

137. Cai, Q.-W., Li, J., Li, X.-Q., Wang, J.-Q. & Huang, Y. Expression of STAT3, MMP-1 and TIMP-1 in gastric cancer and correlation with pathological features. *Mol Med Rep* **5,** 1438–1442 (2012).

138. Inoue, T. *et al.* Matrix metalloproteinase-1 expression is a prognostic factor for patients with advanced gastric cancer. *Int. J. Mol. Med.* **4,** 73–77 (1999).

139. Koskensalo, S. *et al.* MMP-7 overexpression is an independent prognostic marker in gastric cancer. *Tumour Biol.* **31,** 149–155 (2010).

140. McDonnell, S., Navre, M., Coffey, R. J., Jr & Matrisian, L. M. Expression and localization of the matrix metalloproteinase pump-1 (MMP-7) in human gastric and colon carcinomas. *Mol. Carcinog.* **4,** 527–533 (1991).

141. Ohtani, H., Motohashi, H., Sato, H., Seiki, M. & Nagura, H. Dual over-expression pattern of membrane-type metalloproteinase-1 in cancer and stromal cells in human gastrointestinal carcinoma revealed by in situ hybridization and immunoelectron microscopy. *Int. J. Cancer* **68,** 565–570 (1996).

142. Grigioni, W. F. *et al.* Gelatinase A (MMP-2) and its mRNA detected in both neoplastic and stromal cells of tumors with different invasive and metastatic properties. *Diagn. Mol. Pathol.* **3,** 163–169 (1994).

143. Shen, K. H. *et al.* Serum matrix metalloproteinase-9 level associated with stromal reaction in patients with gastric cancer. *Anticancer Res.* **20,** 1307–1310 (2000).

144. Sakurai, Y. *et al.* The role of stromal cells in the expression of interstitial collagenase (matrix metalloproteinase-1) in the invasion of gastric cancer. *J Surg Oncol* **66,** 168–172 (1997).

145. Varro, A. *et al.* Increased gastric expression of MMP-7 in hypergastrinemia and significance for epithelial-mesenchymal signaling. *Am. J. Physiol. Gastrointest. Liver Physiol.* **292,** G1133–1140 (2007).

146. Bergin, P. J. *et al.* Increased production of matrix metalloproteinases in Helicobacter pylori-associated human gastritis. *Helicobacter* **9,** 201–210 (2004).

147. McCaig, C. *et al.* The role of matrix metalloproteinase-7 in redefining the gastric microenvironment in response to Helicobacter pylori. *Gastroenterology* **130,** 1754–1763 (2006).

148. Bremer, C., Tung, C.-H. & Weissleder, R. In vivo molecular target assessment of matrix metalloproteinase inhibition. *Nat Med* **7,** 743–748 (2001).

149 . Furumoto, S. *et al.* Tumor detection using 18F-labeled matrix metalloproteinase-2 inhibitor. *Nucl. Med. Biol.* **30,** 119–125 (2003).

150. Jastrzębska, B. *et al.* New enzyme-activated solubility-switchable contrast agent for magnetic resonance imaging: From synthesis to in vivo imaging. *J. Med. Chem.* **52,** 1576–1581 (2009).

151. Turk, D. & Guncar, G. Lysosomal cysteine proteases (cathepsins): promising drug targets. *Acta Crystallogr. D Biol. Crystallogr.* **59,** 203–213 (2003).

152. Jedeszko, C. & Sloane, B. F. Cysteine cathepsins in human cancer. *Biol. Chem.* **385,** 1017–1027 (2004).

153. Joyce, J. A. *et al.* Cathepsin cysteine proteases are effectors of invasive growth and angiogenesis during multistage tumorigenesis. *Cancer Cell* **5,** 443–453 (2004).

154. Konno-Shimizu, M. *et al.* Cathepsin E is a marker of gastric differentiation and signet-ring cell carcinoma of stomach: a novel suggestion on gastric tumorigenesis. *PLoS ONE* **8,** e56766 (2013).

155. Ding, S. *et al.* Molecular imaging of gastric neoplasia with near-infrared fluorescent activatable probes. *Mol Imaging* **11,** 507–515 (2012).

156. Yang, Y. *et al.* Cathepsin S mediates gastric cancer cell migration and invasion via a putative network of metastasis-associated proteins. *J. Proteome Res.* **9,** 4767–4778 (2010).

157. Lijnen, H. R. Matrix metalloproteinases and cellular fibrinolytic activity. *Biochemistry Mosc.* **67,** 92–98 (2002).

158. Menshikov, M. *et al.* Urokinase upregulates matrix metalloproteinase-9 expression in THP-1 monocytes via gene transcription and protein synthesis. *Biochem. J.* **367,** 833–839 (2002).

159. Skrzydlewska, E., Sulkowska, M., Koda, M. & Sulkowski, S. Proteolytic-antiproteolytic balance and its regulation in carcinogenesis. *World J. Gastroenterol.* **11,** 1251–1266 (2005).

160. Karam, S. M. & Leblond, C. P. Dynamics of epithelial cells in the corpus of the mouse stomach. I. Identification of proliferative cell types and pinpointing of the stem cell. *Anat. Rec.* **236,** 259–279 (1993).

161. Stange, D. E. *et al.* Differentiated Troy+ chief cells act as reserve stem cells to generate all lineages of the stomach epithelium. *Cell* **155,** 357–368 (2013).

162. Singh, S. R. Gastric cancer stem cells: a novel therapeutic target. *Cancer Lett.* **338,** 110–119 (2013).

163. Office for National Statistics, Cancer Statistics registrations: Registrations of cancer diagnosed in 2008, England. Series MB1 no.39. 2010, National Statistics: London.

164. Blot, W. J., Devesa, S. S., Kneller, R. W. & Fraumeni, J. F., Jr. Rising incidence of adenocarcinoma of the esophagus and gastric cardia. *JAMA* **265,** 1287–1289 (1991).

165. Office for National Statistics (ONS). Cancer survival in England: Patients diagnosed 2005-2009 and followed up to 2010. London: ONS; 2011

166. Ferlay J, Shin HR, Bray F, Forman D, Mathers C, Parkin DM, GLOBOCAN 2008 v1.2, Cancer incidence and mortality worldwide: IARC CancerBase No.10 [Internet]. Lyon, France: International Agency for Research on Cancer, 2010. Available from http://globocan.iarc.fr

167. Ferlay, J. *et al.* Estimates of worldwide burden of cancer in 2008: GLOBOCAN 2008. *Int. J. Cancer* **127,** 2893–2917 (2010).

168. Lauren, P. The two histological main types of gastric carcinoma: diffuse and so-called intestinal-type carcinoma. An attempt at a histo-clinical classification. *Acta Pathol Microbiol Scand* **64,** 31–49 (1965).

169. Washington, K. 7th edition of the AJCC cancer staging manual: stomach. *Ann. Surg. Oncol.* **17,** 3077–3079 (2010).

170. Ott, K., Lordick, F., Blank, S. & Büchler, M. Gastric cancer: surgery in 2011. *Langenbecks Arch Surg* **396,** 743–758 (2011).

171. Thompson, G. B., Van Heerden, J. A. & Sarr, M. G. Adenocarcinoma of the stomach: are we making progress? *Lancet* **342,** 713–718 (1993).

172. Pasini, F., Fraccon, A. P. & DE Manzoni, G. The role of chemotherapy in metastatic gastric cancer. *Anticancer Res.* **31,** 3543–3554 (2011).

173. Correa, P., Haenszel, W., Cuello, C., Tannenbaum, S. & Archer, M. A model for gastric cancer epidemiology. *Lancet* **2,** 58–60 (1975).

174. Marshall, B. J. & Warren, J. R. Unidentified curved bacilli in the stomach of patients with gastritis and peptic ulceration. *Lancet* **1,** 1311–1315 (1984).

175. Eslick, G. D., Lim, L. L., Byles, J. E., Xia, H. H. & Talley, N. J. Association of Helicobacter pylori infection with gastric carcinoma: a meta-analysis. *Am. J. Gastroenterol.* **94,** 2373–2379 (1999).

176. Jönsson, K. A., Ström, M., Bodemar, G. & Norrby, K. Histologic changes in the gastroduodenal mucosa after long-term medical treatment with cimetidine or parietal cell vagotomy in patients with juxtapyloric ulcer disease. *Scand. J. Gastroenterol.* **23,** 433–441 (1988).

177. Bryan, N. S., Alexander, D. D., Coughlin, J. R., Milkowski, A. L. & Boffetta, P. Ingested nitrate and nitrite and stomach cancer risk: an updated review. *Food Chem. Toxicol.* **50,** 3646–3665 (2012).

178. González, C. A. *et al.* Smoking and the risk of gastric cancer in the European Prospective Investigation Into Cancer and Nutrition (EPIC). *Int. J. Cancer* **107,** 629–634 (2003).

179. Fearon, E. R. & Vogelstein, B. A genetic model for colorectal tumorigenesis. *Cell* **61,** 759–767 (1990).

180. Boussioutas, A. & Taupin, D. Towards a molecular approach to gastric cancer management. *Intern Med J* **31,** 296–303 (2001).

181. Milne, A. N., Carneiro, F., O'Morain, C. & Offerhaus, G. J. A. Nature meets nurture: molecular genetics of gastric cancer. *Hum. Genet.* **126,** 615–628 (2009).

182. Li, Q. L. *et al.* Causal relationship between the loss of RUNX3 expression and gastric cancer. *Cell* **109,** 113–124 (2002).

183. Fenoglio-Preiser, C. M., Wang, J., Stemmermann, G. N. & Noffsinger, A. TP53 and gastric carcinoma: a review. *Hum. Mutat.* **21,** 258–270 (2003).

184. Parsonnet, J., Friedman, G. D., Orentreich, N. & Vogelman, H. Risk for gastric cancer in people with CagA positive or CagA negative Helicobacter pylori infection. *Gut* **40,** 297–301 (1997).

185. Taketo, M. M. Wnt signaling and gastrointestinal tumorigenesis in mouse models. *Oncogene* **25,** 7522–7530 (2006).

186. Kenny, S. *et al.* Increased expression of the urokinase plasminogen activator system by Helicobacter pylori in gastric epithelial cells. *Am. J. Physiol. Gastrointest. Liver Physiol.* **295,** G431–441 (2008).

187. Tatematsu, M. *et al.* Induction of adenocarcinomas in the glandular stomach of BALB/c mice treated with N-methyl-N-nitrosourea. *Jpn. J. Cancer Res.* **83,** 915–918 (1992).

188. Fox, J. G. *et al.* Germ-line p53-targeted disruption inhibits helicobacter-induced premalignant lesions and invasive gastric carcinoma through down-regulation of Th1 proinflammatory responses. *Cancer Res.* **62,** 696–702 (2002).

189. Fanning, E. & Knippers, R. Structure and function of simian virus 40 large tumor antigen. *Annu. Rev. Biochem.* **61,** 55–85 (1992).

190. Wang, T. C. *et al.* Synergistic interaction between hypergastrinemia and Helicobacter infection in a mouse model of gastric cancer. *Gastroenterology* **118,** 36–47 (2000).

191. El-Omar, E. M. *et al.* The role of interleukin-1 polymorphisms in the pathogenesis of gastric cancer. *Nature* **412,** 99 (2001).

192. Kerbel, R. S. Human tumor xenografts as predictive preclinical models for anticancer drug activity in humans: better than commonly perceived-but they can be improved. *Cancer Biol. Ther.* **2,** S134–139 (2003).

193. Johnson, J. I. *et al.* Relationships between drug activity in NCI preclinical in vitro and in vivo models and early clinical trials. *Br. J. Cancer* **84,** 1424–1431 (2001).

194. Cunha, G. R., Chung, L. W. K., Shannon, J. M. & Reese, B. A. Stromal-epithelial interactions in sex differentiation. *Biology of Reproduction* **22,** 19–42 (1980).

195. Schor, S. L., Schor, A. M. & Rushton, G. Fibroblasts from cancer patients display a mixture of both foetal and adult-like phenotypic characteristics. *J. Cell. Sci.* **90 (Pt 3),** 401–407 (1988).

196. Wilens, S. The Ross Granville Harrison papers. *Mendel Newsl* 1–5 (1980).

197. http://www2.brc.riken.jp/lab/cell/detail.cgi?cell_no=RCB1001

198. http://www.lgcstandards-atcc.org/products/all/CRL-1739.aspx?geo_country=gb

199. Yamada, K. M. & Cukierman, E. Modeling tissue morphogenesis and cancer in 3D. *Cell* **130,** 601–610 (2007).

200. Bell, E., Ehrlich, H. P., Buttle, D. J. & Nakatsuji, T. Living tissue formed in vitro and accepted as skin-equivalent tissue of full thickness. *Science* **211,** 1052–1054 (1981).

201. Benbrook, D. M. Organotypic cultures represent tumor microenvironment for drug testing. *Drug Discovery Today: Disease Models* **3,** 143–148 (2006).

202. Bhowmick, N. A. *et al.* TGF-ß Signaling in fibroblasts modulates the oncogenic potential of adjacent epithelia. *Science* **303,** 848–851 (2004).

203. Beauvoit, B., Evans, S. M., Jenkins, T. W., Miller, E. E. & Chance, B. Correlation between the light scattering and the mitochondrial content of normal tissues and transplantable rodent tumors. *Analytical Biochemistry* **226,** 167–174 (1995).

204. Webb, R. H. Theoretical basis of confocal microscopy. *Meth. Enzymol.* **307,** 3–20 (1999).

205. Stephens, D. J. & Allan, V. J. Light microscopy techniques for live cell imaging. *Science* **300,** 82–86 (2003).

206. Sharpe, J. *et al.* Optical projection tomography as a tool for 3D microscopy and gene expression studies. *Science* **296,** 541–545 (2002).

207. Ntziachristos, V. & Weissleder, R. Experimental three-dimensional fluorescence reconstruction of diffuse media by use of a normalized Born approximation. *Opt Lett* **26,** 893–895 (2001).

208. Ntziachristos, V., Tung, C.-H., Bremer, C. & Weissleder, R. Fluorescence molecular tomography resolves protease activity in vivo. *Nat. Med.* **8,** 757–760 (2002).

209. Hyde, D. *et al.* Hybrid FMT-CT imaging of amyloid-beta plaques in a murine Alzheimer's disease model. *Neuroimage* **44,** 1304–1311 (2009).

210. Brooksby, B. *et al.* Imaging breast adipose and fibroglandular tissue molecular signatures by using hybrid MRI-guided near-infrared spectral tomography. *Proc. Natl. Acad. Sci. U.S.A.* **103,** 8828–8833 (2006).

211. Shcherbo, D. *et al.* Far-red fluorescent tags for protein imaging in living tissues. *Biochem. J.* **418,** 567–574 (2009).

212. Strack, R. L. *et al.* A rapidly maturing far-red derivative of dsred-Express2 for whole-cell labeling. *Biochemistry* **48,** 8279–8281 (2009).

213. Sevick-Muraca, E. M. Translation of near-infrared fluorescence imaging technologies: emerging clinical applications. *Annu. Rev. Med.* **63,** 217–231 (2012).

214. Offersen, B. V. *et al.* The myofibroblast is the predominant plasminogen activator inhibitor-1-expressing cell type in human breast carcinomas. *Am J Pathol* **163,** 1887–1899 (2003).

215. Holmberg, C. *et al.* Mapping proteolytic processing in the secretome of gastric cancer-associated myofibroblasts reveals activation of MMP-1, MMP-2 and MMP-3. *J. Proteome Res.* (2013). doi:10.1021/pr400270q

216. Workman, P. *et al.* Guidelines for the welfare and use of animals in cancer research. *Br. J. Cancer* **102,** 1555–1577 (2010).

217. Nyström, M. L. *et al.* Development of a quantitative method to analyse tumour cell invasion in organotypic culture. *J. Pathol.* **205,** 468–475 (2005).

218. Peraldi, M. N. *et al.* Cell-specific regulation of plasminogen activator inhibitor 1 and tissue type plasminogen activator release by human kidney mesangial cells. *Biochim. Biophys. Acta* **1134,** 189–196 (1992).

219. Andreasen, P. A., Egelund, R. & Petersen, H. H. The plasminogen activation system in tumor growth, invasion, and metastasis. *Cell. Mol. Life Sci.* **57,** 25–40 (2000).

220. Binder, B. R. & Mihaly, J. The plasminogen activator inhibitor 'paradox' in cancer. *Immunol. Lett.* **118,** 116–124 (2008).

221. Cho, J. Y. *et al.* High level of urokinase-type plasminogen activator is a new prognostic marker in patients with gastric carcinoma. *Cancer* **79,** 878–883 (1997).

222. Nørsett, K. G. *et al.* Gastrin stimulates expression of plasminogen activator inhibitor-1 in gastric epithelial cells. *Am. J. Physiol. Gastrointest. Liver Physiol.* **301,** G446–453 (2011).

223. Luebke, T. *et al.* Is the urokinase-type plasminogen activator system a reliable prognostic factor in gastric cancer? *Int. J. Biol. Markers* **21,** 162–169 (2006).

224. Ito, H. *et al.* Prognostic relevance of urokinase-type plasminogen activator (uPA) and plasminogen activator inhibitors PAI-1 and PAI-2 in gastric cancer. *Virchows Arch.* **427,** 487–496 (1996).

225. Sordat, I. *et al.* In situ stromal expression of the urokinase/plasmin system correlates with epithelial dysplasia in colorectal adenomas. *Am. J. Pathol.* **150,** 283–295 (1997).

226. Gillespie, E. *et al.* Plasminogen activator inhibitor-1 is increased in colonic epithelial cells from patients with colitis-associated cancer. *J Crohns Colitis* **7,** 403–411 (2013).

227. Christensen, L. *et al.* Immunohistochemical localization of urokinase-type plasminogen activator, type-1 plasminogen-activator inhibitor, urokinase receptor and alpha(2)-macroglobulin receptor in human breast carcinomas. *Int. J. Cancer* **66,** 441–452 (1996).

228. Smith, H. W. & Marshall, C. J. Regulation of cell signalling by uPAR. *Nat. Rev. Mol. Cell Biol.* **11,** 23–36 (2010).

229. Danø, K. *et al.* Plasminogen activators, tissue degradation, and cancer. *Adv. Cancer Res.* **44,** 139–266 (1985).

230. Czekay, R.-P. *et al.* PAI-1: An integrator of cell signaling and migration. *Int J Cell Biol* **2011,** 562481 (2011).

231. Brooks, T. D. *et al.* Antibodies to PAI-1 alter the invasive and migratory properties of human tumour cells in vitro. *Clin. Exp. Metastasis* **18,** 445–453 (2000).

232. Surnamehogan, G. M. *et al.* Impact of mesenchymal stem cell secreted PAI-1 on colon cancer cell migration and proliferation. *Biochem. Biophys. Res. Commun.* (2013). doi:10.1016/j.bbrc.2013.05.013

233. Stefansson, S. & Lawrence, D. A. The serpin PAI-1 inhibits cell migration by blocking integrin alpha V beta 3 binding to vitronectin. *Nature* **383,** 441–443 (1996).

234. Madsen, C. D., Ferraris, G. M. S., Andolfo, A., Cunningham, O. & Sidenius, N. uPAR-induced cell adhesion and migration: vitronectin provides the key. *J. Cell Biol.* **177,** 927–939 (2007).

235. Palmieri, D., Lee, J. W., Juliano, R. L. & Church, F. C. Plasminogen activator inhibitor-1 and -3 increase cell adhesion and motility of MDA-MB-435 breast cancer cells. *J. Biol. Chem.* **277,** 40950–40957 (2002).

236. Czekay, R.-P., Aertgeerts, K., Curriden, S. A. & Loskutoff, D. J. Plasminogen activator inhibitor-1 detaches cells from extracellular matrices by inactivating integrins. *J. Cell Biol.* **160,** 781–791 (2003).

237. Polanska, U. M. & Orimo, A. Carcinoma-associated fibroblasts: non-neoplastic tumour-promoting mesenchymal cells. *J. Cell. Physiol.* **228,** 1651–1657 (2013).

238. Hiratsuka, S. *et al.* MMP9 induction by vascular endothelial growth factor receptor-1 is involved in lung-specific metastasis. *Cancer Cell* **2,** 289–300 (2002).

239. Direkze, N. C. & Alison, M. R. Bone marrow and tumour stroma: an intimate relationship. *Hematological Oncology* **24,** 189–195 (2006).

240. Franke WW, Schmid E, Osborn M, Weber K. Intermediate-sized filaments of human endothelial cells. J Cell Biol. 1979 Jun 1;81(3):570–80.

241. Rønnov-Jessen L, Petersen OW, Bissell MJ. Cellular changes involved in conversion of normal to malignant breast: importance of the stromal reaction. Physiol. Rev. 1996 Jan;76(1):69–125.

242. Bertotti, A. *et al.* Inhibition of Src impairs the growth of met-addicted gastric tumors. *Clin. Cancer Res.* **16,** 3933–3943 (2010).

243. Sawaoka, H. *et al.* Cyclooxygenase-2 inhibitors suppress the growth of gastric cancer xenografts via induction of apoptosis in nude mice. *Am. J. Physiol.* **274,** G1061–1067 (1998).

244. Liu, S. H. *et al.* Honokiol inhibits gastric tumourigenesis by activation of 15-lipoxygenase-1 and consequent inhibition of peroxisome proliferator-activated receptor-gamma and COX-2-dependent signals. *Br. J. Pharmacol.* **160,** 1963–1972 (2010).

245. Zhang, C. *et al.* Small molecule R1498 as a well-tolerated and orally active kinase inhibitor for hepatocellular carcinoma and gastric cancer treatment via targeting angiogenesis and mitosis pathways. *PLoS One* **8,** (2013).

246. Yoon, Y.-K. *et al.* Combination of EGFR and MEK1/2 inhibitor shows synergistic effects by suppressing EGFR/HER3-dependent AKT activation in human gastric cancer cells. *Mol. Cancer Ther.* **8,** 2526–2536 (2009).

247. Serini, G. & Gabbiani, G. Mechanisms of myofibroblast activity and phenotypic modulation. *Exp. Cell Res.* **250,** 273–283 (1999).

248. Nakamura, M. *et al.* Fluorescent histochemical study on the localization of myofibroblasts in the healing of acetic acid-induced gastric ulcers in the rat. *Scand. J. Gastroenterol. Suppl.* **162,** 150–153 (1989).

249. Bhattacharya, S. D. *et al.* Osteopontin regulates epithelial mesenchymal transition-associated growth of hepatocellular cancer in a mouse xenograft model. *Annals of Surgery* **255,** 319–325 (2012).

250. Chang, Q., Foltz, W. D., Chaudary, N., Hill, R. P. & Hedley, D. W. Tumor-stroma interaction in orthotopic primary pancreatic cancer xenografts during hedgehog pathway inhibition. *International Journal of Cancer* **133,** 225–234 (2013).

251. Jacobsen, B. M. *et al.* Spontaneous fusion with, and transformation of mouse stroma by malignant human breast cancer epithelium. *Cancer Res* **66,** 8274–8279 (2006).

252. Duda DG, Fukumura D, Munn LL, Booth MF, Brown EB, Huang P, et al. Differential transplantability of tumor-associated stromal cells. Cancer Res. 2004 Sep 1;64(17):5920–4.

253. Suetsugu, A. *et al.* Multi-color palette of fluorescent proteins for imaging the tumor microenvironment of orthotopic tumorgraft mouse models of clinical pancreatic cancer specimens. *J. Cell. Biochem.* **113,** 2290–2295 (2012).

254 . Worthley, D. L. *et al.* Human gastrointestinal neoplasia-associated myofibroblasts can develop from bone marrow-derived cells following allogeneic stem cell transplantation. *Stem Cells* **27,** 1463–1468 (2009).

255. Petersen OW, Nielsen HL, Gudjonsson T, Villadsen R, Rank F, Niebuhr E, et al. Epithelial to mesenchymal transition in human breast cancer can provide a nonmalignant stroma. Am. J. Pathol. 2003 Feb;162(2):391–402.

256. Rønnov-Jessen L, Petersen OW. Induction of alpha-smooth muscle actin by transforming growth factor-beta 1 in quiescent human breast gland fibroblasts. Implications for myofibroblast generation in breast neoplasia. Lab. Invest. 1993 Jun;68(6):696–707.

257. McAllister, S. S. *et al.* Systemic endocrine instigation of indolent tumor growth requires osteopontin. *Cell* **133,** 994–1005 (2008).

258. Kim, M.-Y. *et al.* Tumor self-seeding by circulating cancer cells. *Cell* **139,** 1315–1326 (2009).

259. Bauvois, B. New facets of matrix metalloproteinases MMP-2 and MMP-9 as cell surface transducers: outside-in signaling and relationship to tumor progression. *Biochim. Biophys. Acta* **1825,** 29–36 (2012).

260. Gondi, C. S. & Rao, J. S. Cathepsin B as a cancer target. *Expert Opin. Ther. Targets* **17,** 281–291 (2013).

261. Moutasim, K. A., Nystrom, M. L. & Thomas, G. J. Cell migration and invasion assays. *Methods Mol. Biol.* **731,** 333–343 (2011).

262. Zheng, Q.-H. *et al.* Synthesis, biodistribution and micro-PET imaging of a potential cancer biomarker carbon-11 labeled MMP inhibitor (2R)-2-[[4-(6-fluorohex-1-ynyl)phenyl]sulfonylamino]-3-methylbutyric acid [11C]methyl ester. *Nucl. Med. Biol.* **30,** 753–760 (2003).

263. Lepage, M. *et al.* Noninvasive detection of matrix metalloproteinase activity in vivo using a novel magnetic resonance imaging contrast agent with a solubility switch. *Mol Imaging* **6,** 393–403 (2007).

264 . Scherer, R. L., McIntyre, J. O. & Matrisian, L. M. Imaging matrix metalloproteinases in cancer. *Cancer Metastasis Rev.* **27,** 679–690 (2008).

265. Jodele, S., Blavier, L., Yoon, J. M. & DeClerck, Y. A. Modifying the soil to affect the seed: role of stromal-derived matrix metalloproteinases in cancer progression. *Cancer Metastasis Rev.* **25,** 35–43 (2006).

266. Zigrino, P. *et al.* Stromal expression of MMP-13 is required for melanoma invasion and metastasis. *J. Invest. Dermatol.* **129,** 2686–2693 (2009).

267. Zhou, L., El-Deiry, W., Wang, W., Ingram, M. E. & Katz, S. I. Extracellular protease imaging for cell mass tracking of xenografted human malignant pleural mesothelioma. *Oncol. Rep.* **28,** 883–888 (2012).

268. Hensley, H. H. *et al.* Combined in vivo molecular and anatomic imaging for detection of ovarian carcinoma-associated protease activity and integrin expression in mice. *Neoplasia* **14,** 451–462 (2012).

269 . Podgorski, I. & Sloane, B. F. Cathepsin B and its role(s) in cancer progression. *Biochem. Soc. Symp.* 263–276 (2003).

270. Mullins, S. R. *et al.* Three-dimensional cultures modeling premalignant progression of human breast epithelial cells: role of cysteine cathepsins. *Biol. Chem.* **393,** 1405–1416 (2012).

271 . Chen, X. *et al.* Increased plasma MMP9 in integrin alpha1-null mice enhances lung metastasis of colon carcinoma cells. *Int. J. Cancer* **116,** 52–61 (2005).

272. Pozzi, A. *et al.* Elevated matrix metalloprotease and angiostatin levels in integrin alpha 1 knockout mice cause reduced tumor vascularization. *Proc. Natl. Acad. Sci. U.S.A.* **97,** 2202–2207 (2000).

273. Sadlonova, A. *et al.* Breast fibroblasts modulate epithelial cell proliferation in three-dimensional in vitro co-culture. *Breast Cancer Res.* **7,** R46–59 (2005).

274. Olsen, C. J., Moreira, J., Lukanidin, E. M. & Ambartsumian, N. S. Human mammary fibroblasts stimulate invasion of breast cancer cells in a three-dimensional culture and increase stroma development in mouse xenografts. *BMC Cancer* **10,** 444 (2010).

275. Woenne, E. C. *et al.* MMP inhibition blocks fibroblast-dependent skin cancer invasion, reduces vascularization and alters VEGF-A and PDGF-BB expression. *Anticancer Res.* **30,** 703–711 (2010).

276. Lagergren, J. & Lagergren, P. Oesophageal cancer. *BMJ* **341,** c6280–c6280 (2010).

277. Courrech Staal, E. F. W. *et al.* The stromal part of adenocarcinomas of the oesophagus: does it conceal targets for therapy? *Eur. J. Cancer* **46,** 720–728 (2010).

278. Liu, J., Li, Z., Cui, J., Xu, G. & Cui, G. Cellular changes in the tumor microenvironment of human esophageal squamous cell carcinomas. *Tumour Biol.* **33,** 495–505 (2012).

279. http://www.chemocentryx.com/product/working.html

280. Ntziachristos, V., Bremer, C. & Weissleder, R. Fluorescence imaging with near-infrared light: new technological advances that enable in vivo molecular imaging. *Eur Radiol* **13,** 195–208 (2003).

281. Liu, F. *et al.* Monitoring of tumor response to cisplatin by subsurface fluorescence molecular tomography. *J Biomed Opt* **17,** 040504 (2012).

282. Eisenblätter M, Ehrchen J, Varga G, Sunderkötter C, Heindel W, Roth J, et al. In vivo optical imaging of cellular inflammatory response in granuloma formation using fluorescence-labeled macrophages. J. Nucl. Med. 2009 Oct;50(10):1676–82.

283. Galligan, C. L. & Fish, E. N. Circulating fibrocytes contribute to the pathogenesis of collagen antibody–induced arthritis. *Arthritis & Rheumatism* **64,** 3583–3593 (2012).

284. Granot D, Addadi Y, Kalchenko V, Harmelin A, Kunz-Schughart LA, Neeman M. In vivo imaging of the systemic recruitment of fibroblasts to the angiogenic rim of ovarian carcinoma tumors. Cancer Res. 2007 Oct 1;67(19):9180–9.

285. Loebinger, M. R. *et al.* Magnetic resonance imaging of mesenchymal stem cells homing to pulmonary metastases using biocompatible magnetic nanoparticles. *Cancer Res.* **69,** 8862–8867 (2009).

286. Bruyère, C. *et al.* Considering temozolomide as a novel potential treatment for esophageal cancer. *Cancer* **117,** 2004–2016 (2011).

287. Ford, S. J. *et al.* Deferasirox (ICL670A) effectively inhibits oesophageal cancer growth in vitro and in vivo. *Br. J. Pharmacol.* **168,** 1316–1328 (2013).

288. Karnoub, A. E. *et al.* Mesenchymal stem cells within tumour stroma promote breast cancer metastasis. *Nature* **449,** 557–563 (2007).

289. Goldstein, R. H., Reagan, M. R., Anderson, K., Kaplan, D. L. & Rosenblatt, M. Human bone marrow-derived MSCs can home to orthotopic breast cancer tumors and promote bone metastasis. *Cancer Res.* **70,** 10044–10050 (2010).

290. Walczak, P. *et al.* Dual-modality monitoring of targeted intraarterial delivery of mesenchymal stem cells after transient ischemia. *Stroke* **39,** 1569–1574 (2008).

291. Doucette, T. *et al.* Mesenchymal stem cells display tumor-specific tropism in an RCAS/Ntv-a glioma model. *Neoplasia* **13,** 716–725 (2011).

292. Ip, J. E. *et al.* Mesenchymal stem cells use integrin β1 not CXC chemokine receptor 4 for myocardial migration and engraftment. *Mol. Biol. Cell* **18,** 2873–2882 (2007).

293. Holmberg, C. (2009) *The secretome of myofibroblasts and its significance in gastric cancer.* PhD Thesis. University of Liverpool, UK

294. Welch, D. R., Krizman, D. B. & Nicolson, G. L. Multiple phenotypic divergence of mammary adenocarcinoma cell clones. I. In vitro and in vivo properties. *Clin. Exp. Metastasis* **2,** 333–355 (1984).

295. Hazra, S. *et al.* Enhancing the function of CD34+ cells by targeting plasminogen activator inhibitor-1. *PLoS ONE* **8,** e79067 (2013).

296. Fjellström, O. *et al.* Characterization of a small molecule inhibitor of plasminogen activator inhibitor type 1 that accelerates the transition into the latent conformation. *J. Biol. Chem.* **288,** 873–885 (2013).

297. Sausville, E. A. & Burger, A. M. Contributions of human tumor xenografts to anticancer drug development. *Cancer Res.* **66,** 3351–3354, discussion 3354 (2006).

298. Richmond, A. & Su, Y. Mouse xenograft models vs GEM models for human cancer therapeutics. *Dis Model Mech* **1,** 78–82 (2008).

299. Zimmermann, M., Box, C. & Eccles, S. A. Two-dimensional vs. three-dimensional in vitro tumor migration and invasion assays. *Methods Mol. Biol.* **986,** 227–252 (2013).

300. Vandsburger, M. H. *et al.* Ovarian carcinoma: quantitative biexponential MR imaging relaxometry reveals the dynamic recruitment of ferritin-expressing fibroblasts to the angiogenic rim of tumors. *Radiology* **268,** 790–801 (2013).

301. Hogan, N. M. *et al.* Impact of mesenchymal stem cell secreted PAI-1 on colon cancer cell migration and proliferation. *Biochem. Biophys. Res. Commun.* **435,** 574–579 (2013).

302. Bajou, K. *et al.* Host-derived plasminogen activator inhibitor-1 (PAI-1) concentration is critical for in vivo tumoral angiogenesis and growth. *Oncogene* **23,** 6986–6990 (2004).

303. Diebold, I., Kraicun, D., Bonello, S. & Görlach, A. The 'PAI-1 paradox' in vascular remodeling. *Thromb. Haemost.* **100,** 984–991 (2008).

304. Harbeck, N. *et al.* Ten-year analysis of the prospective multicentre Chemo-N0 trial validates American Society of Clinical Oncology (ASCO)-recommended biomarkers uPA and PAI-1 for therapy decision making in node-negative breast cancer patients. *Eur. J. Cancer* **49,** 1825–1835 (2013).

305. Jacobs, V. R. *et al.* Prospective multi-center study for quantification of chemotherapies and CTX-related direct medication costs avoided by use of biomarkers uPA and PAI-1 in primary breast cancer. *Breast* **22,** 436–443 (2013).

306. Kitadai, Y., Kodama, M. & Shinagawa, K. Stroma-directed molecular targeted therapy in gastric cancer. *Cancers (Basel)* **3,** 4245–4257 (2011).

307. Ohtsu, A. *et al.* Bevacizumab in combination with chemotherapy as first-line therapy in advanced gastric cancer: a randomized, double-blind, placebo-controlled phase III study. *J. Clin. Oncol.* **29,** 3968–3976 (2011).

308. Pelosof, L. C. & Gerber, D. E. Paraneoplastic Syndromes: An Approach to Diagnosis and Treatment. *Mayo Clin Proc* **85,** 838–854 (2010).

309. Dufour, A. & Overall, C. M. Missing the target: matrix metalloproteinase antitargets in inflammation and cancer. *Trends Pharmacol. Sci.* **34,** 233–242 (2013).

310. Cuniasse, P. *et al.* Future challenges facing the development of specific active-site-directed synthetic inhibitors of MMPs. *Biochimie* **87,** 393–402 (2005).

311. Liu, S. *et al.* Matrix metalloproteinase-activated anthrax lethal toxin demonstrates high potency in targeting tumor vasculature. *J. Biol. Chem.* **283,** 529–540 (2008).

312. Sampieri, C. L., León-Córdoba, K. & Remes-Troche, J. M. Matrix metalloproteinases and their tissue inhibitors in gastric cancer as molecular markers. *J Cancer Res Ther* **9,** 356–363 (2013).

313. Quante, M. *et al.* Bone marrow-derived myofibroblasts contribute to the mesenchymal stem cell niche and promote tumor growth. *Cancer Cell* **19,** 257–272 (2011).

314. Donnelly, J. M., Chawla, A., Houghton, J. & Zavros, Y. Sonic hedgehog mediates the proliferation and recruitment of transformed mesenchymal stem cells to the stomach. *PLoS ONE* **8,** e75225 (2013).

315. Somja, J. *et al.* Dendritic cells in Barrett's esophagus carcinogenesis: an inadequate microenvironment for antitumor immunity? *Am. J. Pathol.* **182,** 2168–2179 (2013).